Size related processes in phytoplankton

Dissertation

zur Erlangung des Doktorgrades

der Mathematisch-Naturwissenschaftlichen Fakultät

der Christian-Albrechts-Universität

zu Kiel

vorgelegt von

Marcel Sandow

Kiel

2004

Referent: Prof. Dr. U. Sommer

Korreferent: Priv. Doz. Dr. A. Oschlies

Tag der mündlichen Prüfung: 03.06.2004

Zum Druck genehmigt: Kiel, 09.06.2004

Dekan gez. Prof. W. Depmeier

Contents

List of Figures

List of Tables

Zusammenfassung

Wachstum, Sterben (einschliesslich Grazing), Respiration, Exkretion und Sedimentation beschreiben die hauptsächlichen Umsatzprozesse des Phytoplanktons. Die mit diesen Prozessen gekoppelten Umsatzraten sind oft allometrisch skaliert ($Rate = a \cdot Biomasse^{\beta_{rs}+1}$). Der Allometriekoeffizient β_{rs} bechreibt die Abweichung der Größenskalierung von einer linearen ($\beta_{rs} = 0$) Rate-Biomasse-Funktion. Literaturwerte des Allometriekoeffizienten reichen von -0.48 bis -0.1. Diese Werte wurden entweder aus Kulturexperimenten oder aus Experimenten mit natürlichem Phytoplankton unter künstlichen Bedingungen abgeleitet. Deshalb war nicht klar, ob größenskalierte Prozesse in natürlichen Systemen vorkommen und wenn wie stark ihr Einfluß ist.

Daten einer Forschungsfahrt im Subtropenwirbel des Nordatlantiks zeigen deutlich eine Abhängigkeit der Kohlenstoffaufnahmerate von der jeweiligen Zellgröße. Der konservativste Ansatz ergab für die nördlichste Station (28.6^{o}N 30^{o}W) eine dreimal höhere spezifische Kohlenstoffaufnahmerate für die kleinen Phytoplankter gegenüber den großen Phytoplanktern. An den zwei südlichen Stationen (18^{o}N 30^{o}W; 22.9^{o}N 30^{o}W) ist die spezifische Aufnahmerate der kleinen Phytoplankter sogar fünfmal höher.

Niedrige δ^{15}N Werte der mittleren Größenklasse ($< 5\mu$m) in den oberflächen nahen Proben von Station 148 und Station 159 sind ein Indiz für Stickstoffixierung durch einzellige Stickstoffixierer. Wegen der Hintergrundsbedingungen und der Daten aus dem ^{14}C Experiment wurde Station 159 als typisch für ein stabiles oligotrophes System eingestuft.

Die Daten zur Kohlenstoffaufnahme aus dem ^{14}C Experiment von Station 159 konnten gut von einem Dreikomponentenmodell (N:gel. Nährstoffe(Stickstoff); P:Phytoplankton; R:Recyclingpool) mit zwei unabhängigen Phytoplanktongrößenklassen simuliert werden. Eine hohe Stickstoffremineralisierungsrate ($\xi_{Ps,N}$=0.5) und eine hohe realisierte Wach-

stumsrate (μ_r ≈3.4) waren notwendig, um in dem Modell eine Kohlenstoffaufnahme zu erreichen, die mit den Beobachtungswerten übereinstimmt. Es wird angenommen, daß die Kopplung der Kohlenstoff- und Stickstoffaufnahme für diese hohen Parameterwerte verantwortlich ist. Die größenabhängige Skalierung der Aufnahme- und Verlustraten der zwei Größenklassen wurde durch die folgende Formel berechnet: $Rate_{groß} = Rate_{Klein} \cdot (Biomasseverh.)^{\beta rs}$. Deshalb hängt die größenabhängige Skalierung sowohl vom Allometriekoeffizienten β_{rs} als auch von dem Biomasseverhältnis ab. Das Biomasseverhältnis ist der Quotient aus der mittleren spezifischen Biomasse einer großen Phytoplanktonzelle und einer kleinen Phytoplanktonzelle. Eine Modelloptimierung mit einem vorher festgelegten Biomasseverhältnis von 10 ergab für einen Allometriekoeffizienten von -0.88 bis -0.6 die besten Übereinstimmungen der Kohlenstoffaufnahme von Modell und Beobachtungen. Ein höheres Biomasseverhältnis der zwei Phytoplankter von 66 (mittlere Algengröße: $\approx 0.2\mu$m und 7μm) verringert den aus der Modelloptimierung abgeleiteten Bereich des Allometriekoeffizienten auf -0.48 bis -0.32.

Die Metabolismusexperimente, die mit natürlichem Phytoplankton der Ostsee durchgeführt wurden, ergaben einen allgemeinen Allometriekoeffizienten von -0.71 (Datenaufnahme über neuen Monate). Die Koeffizienten der einzelen Messtage zeigten einen zeitlichen Trend mit den höchsten Allometriekoeffizienten (-0.62) im späten Frühjahr und den niedrigsten Koeffizienten im späten Herbst (-0.8). Dieser Gradient scheint mit der Ressourcenverteilung und der Konkurrenz im System korreliert zu sein. Ein Kulturexperiment, dass mit derselben Methode durchgeführt wurde, ergab einen Allometriekoeffizienten von -0.52, was mit der unteren Grenze der in der Literatur beschriebenen Werte übereinstimmt.

Abschätzungen des Allometriekoeffizienten aus Freilandproben zeigten, daß grössenabhängige Umsatzprozesse beobachtet werden können und daß diese sowohl in oligotrophen als auch in eutrophen Ökosystemen stärker ausgeprägt sind als bisher angenommen.

Abstract

Growth, death (incl. grazing), respiration, excretion and sedimentation describe the major rate processes of phytoplankton. These rates often scale allometrically ($rate = a \cdot mass^{\beta_{rs}+1}$). The allometric coefficient β_{rs} describes the deviation of the size scaling from a linear ($\beta_{rs} = 0$) rate mass relationship. Values of the allometric coefficient published in the literature range from -0.48 to -0.1. All the data that were used to calculate these allometric coefficients were derived from culture experiments or from incubation of natural phytoplankton under unnatural conditions. Therefore, it was not clear if any size scaling can be observed in natural systems.

Data from a cruise to the subtropical North Atlantic gyre clearly showed a size scaling for the carbon uptake measured by ^{14}C assimilation. The most conservative approach revealed that the specific carbon assimilation rate of the smaller phytoplankton was 3 (at the northern station (28.6^{o}N 30^{o}W)) to 5 (at the two southern stations (18^{o}N 30^{o}W; 22.9^{o}N 30^{o}W)) times higher than of the larger phytoplankton. Low δ^{15}N values of the intermediate size class ($< 5\mu$m) indicated nitrogen fixation by unicellular nitrogen fixers in the subsurface samples of St.148 and St.159. From the background conditions and the carbon uptake experiment, St.159 (22.9^{o}N 30^{o}W) was classified as most representative of the stable oligotrophic ecosystem of the eastern subtropical North Atlantic.

A three compartment model (N:nitrogen (dissolved); P:phytoplankton; R:recycling pool) with two distinct phytoplankton size classes, that is based on the data from St.159, could reasonably well describe the carbon uptake that was measured in the ^{14}C assimilation experiment. High nitrogen remineralisation ($\xi_{Ps,N}$=0.5) and a high realised growth rate ($\mu_r \approx$3.4) were necessary to achieve carbon assimilation values in the model, that corresponds to the observations. It is assumed that the coupling of the carbon and nitrogen

uptake is responsible for these high parameter values. The size scaling of the uptake and loss rates of the two size classes are calculated by: $rate_{large} = rate_{small} \cdot (mass\ ratio)^{\beta rs}$. Therefore, the size scaling depends on the allometric coefficient β_{rs} and the preselected mass ratio. The mass ratio describes the quotient of the averaged cell mass from the large size class divided by the averaged cell mass from the small size class. A model optimization setup with a mass ratio of 10 revealed an allometric coefficient range of -0.88 to -0.6 to best describe the observations of the carbon assimilation experiment at St.159. A higher preselected mass ratio of 66 (algae mean size: $\approx 0.2\mu$m and 7μm) decreased the derived allometric coefficient range to -0.48/-0.32.

The metabolic turnover experiments conducted with natural phytoplankton from the Baltic showed a general allometric coefficient of -0.71 (data collected over nine months). The single day data revealed a time dependency with the highest allometric coefficients (-0.62) in late spring and the lowest allometric coefficients in late autumn (-0.8). This gradient seems to be correlated with the ressource (nutrients,light) and competition status of the natural system. Culture experiments conducted with the same method exhibited an allometric coefficient of -0.52 which corresponds to the lower boundary values reported in literature.

Estimates of the allometric coefficient of field samples indicate that size scaling of rate processes occurs and is even more pronounced than previously thought in oligotrophic and eutrophic marine ecosystems.

General introduction

Phytoplankton organisms are the major primary producers of the marine pelagic ecosystem. They are responsible for the transfer of dissolved inorganic carbon and nitrogen into particles. This particle formation is important for biogeochemical and ecological studies, because these biological particles can move relative to the water in contrast to their dissolved counterparts and beacuse they form one part of the base of the foodweb. Therefore, all trophic relations and the productivity of an ecosystem are related to the primary production of phytoplankton. But it is not the absolute primary production alone that determines the biogeochemical or ecological effect. The size of the producing phytoplankton organism is one additional crucial factor. It determines for example the growth rate, the sedimentation rate and the link to the food web. Eutrophic areas of the ocean are generally dominated by larger phytoplankton like diatoms. They can reach sizes of 70 μm to several hundred μm cell diameter. These species show sinking rates of more than 9 m$\cdot$d^{-1} Sommer (1998) and growth rates of 0.72 d^{-1} Blasco et al. (1982). Less eutrophic areas and beginning spring blooms are dominated by small diatoms (10μm) which show sinking rates of about 1 m$\cdot$d^{-1} and growth rates of 1.92 d^{-1}. In oligotrophic areas picoplankton ($< 2\mu$m) are the dominant size fraction. These cell do not sink and their growth rates can be even higher than 2 d^{-1}. Besides these observed patterns the influence of size on rate processes is controversially discussed (Chrisholm, 1992). The most simple approach assumes that the growth rate of differently sized cells increases linearly with bodymass (the specific rate ist constant). More sophisticated approaches assume a power function like: $rate = a \cdot mass^{\beta_{rs}+1}$. In this function the allometric coefficient β_{rs} (index $_{rs}$ indicates the coefficient of the specific rate) is responsible for the deviation from the linear correlation ($\beta_{rs} = 0$). Low allometric coefficients result in a decrease of rate processes of larger cells.

For an allometric coefficient of -0.15 a larger cell ($\text{mass}_{large} = 10^3 \cdot \text{mass}_{small}$) will only grow with a rate of 35%, compared with the small cell. For an allometric coefficient of -0.5 the growth rate is further reduced to 3% of the small cell. Measurements from incubations of field samples and culture experiements revealed allometric coefficients in the range of -0.48 (Finkel (2001), Raven and Kübler (2002)) to -0.1 (Banse (1976), Sommer (1989)). The lower boundary was derived from culture experiments with light limitation. The upper boundary down to -0.33 was derived from incubation experiments under ideal growth conditions. These incubations necessarily modify the growth conditions and therefore do not represent the natural conditions.

The studies presented here are conducted to examine the occurence and shape of size related processes in natural phytoplankton communities. The first chapter describes size fractionated standing stock and carbon uptake data which were collected at the eastern part of the subtropical gyre of the North Atlantic. From these data the background conditions and the occurence of size scaling of carbon uptake were extracted. These data were used in chapter two to set up a model which simulated the carbon uptake observed at the cruise. The modelling approach helps to estimate the value of the allometric coefficient which is necessary to explain the observed size fractionated carbon uptake data. Chapter three describes several experiments using a method to estimate the allometric coefficients directly from instantaneous metabolic turnover of differently sized phytoplankton in one sample. These experiments were conducted with phytoplankton from the Baltic in order to have estimates of the allometric coefficient from two different ecosystems. The experiments were conducted over a time period of nine months to examine the influence of different ecosystem conditions on the allometric coefficient .

1. Observations of size class distribution and turnover processes of the subtropical gyre of the Atlantic Ocean

1.1. Introduction

The size distribution and size dependent turnover processes of the open ocean phytoplankton determine the productivity and the carbon export of marine pelagic food-webs (Moloney and Field (1991), Boyd and Newton (1995), Hurtt and Armstrong (1996), Boyd and Newton (1999), Hurtt and Armstrong (1999)). Depending on the size of the major primary producer the newly fixed inorganic carbon is channeled into recycling processes of the microbial loop, into direct sedimentation to the ocean interior or into higher trophic levels. One major factor controlling the size of the major primary producer of the ocean is the spatial and temporal nutrient supply to the specific ecosystem. In eutrophic areas the major primary producers are generally larger than in oligotrophic areas. Especially the subtropical gyres are known for their permanent oligotrophic conditions. These conditions result in pronounced influence of the microbial loop to the overall carbon turnover (Roman et al., 1995). The carbon fixation in the microbial loop is mainly accompanied by the assimilation of ammonia. Therefore, it is classified as regenerated production. The contribution of nitrate driven "new" production (export production) to the overall carbon turnover is thought to be small, because the nitrate fluxes into the euphotic zone are remarkably low (0.01-0.1 mol N $\cdot m^{-2} \cdot y^{-1}$ Oschlies (2002)). Pronounced research ef-

forts focus on the contribution of nitrogen fixation as an additional source of nitrogen in the subtropical areas of the world ocean (reviewed in Capone and Carpenter (1999)). The amount of nitrogen fixation is of great interest, because any nitrogen input (nitrate and dinitrogen) into the euphotic zone must be accompanied by a corresponding export of particles. For *Trichodesmium* sp., the assumed major nitrogen fixer, fixation rates of about 0.05 mol N $\cdot m^{-2} \cdot y^{-1}$ have been estimated (Karl, 1997). Besides *Trichodesmium* sp., the occurence of unicellular nitrogen fixers could be shown in recent years(Zehr et al. (1998), Zehr et al. (2000)). Because of their high cell densitites and wide dispersal, these unicellular nitrogen fixers can contribute the same amount of nitrogen as the nitrate fluxes from the deep ocean or the fixation of *Trichodesmium* sp. (Zehr et al. (2001), Wasmund et al. (2001)). The size of these unicellulars allows direct grazing by micro- and mesozooplankton (like salps and appendicullariens). Therefore, the nitrogen introduced by these small nitrogen fixers can be directly transferred to higher trophic levels or to the deep ocean by forming fecal pellets.

One open question which is of remarkable importance for carbon turnover processes is the influence of the cell size on the turnover rate of the individual cell. From laboratory experiments and theoretical approaches it can be assumed that smaller cells have higher specific turnover rates than larger cells (Raven (1999)). But this pattern is not that clear (Chrisholm, 1992). In the oligotrophic ocean, higher turnover rates of smaller cells will even enhance the regenerative part of the food-web and therefore alter the carbon export. Although the absolute amount of carbon and nitrogen export does not change, because of the long term steady state, this enhanced recycling can result in a spatial averaging or in an amplification of the small cell based food-web structures.

Size turnover rate relationships can be extracted from size fractionated biomass and turnover rate data. When assuming equal specific turnover rates for all phytoplankton size classes, the biomass and turnover rate proportions should be equal for one specific size class at one specific site. Such patterns were observed by Bury et al. (2001) (biomass and production of the $< 5\mu$m size class: 75% of the total) at the JGOFS 47^{o}N, 20^{o}W site. For the subtropical gyre of the North Atlantic Jochem and Zeitschel (1993) showed that picoplankton contribute more to production (83-98%) than to biomass (78-90%). Therefore, the picoplankton had a higher specific production rate than the larger phyto-

plankton. Contrarily, Marañón et al. (2001) reported a biomass proportion of about 80% and a production proportion of 40% to 80% for the picoplankton at a 21^{o}W transect of the subtropical gyre of the eastern North Atlantic Ocean. Fernández et al. (2003) published similar proportions leading to a biomass to production ratio of about 1.33 derived from several AMT (Atlantic Meridional Transect) cruises conducted at the same transect described from Marañón et al. (2001). At two sites (14^{o}N,28^{o}W and 23^{o}N,28^{o}W) Fernández et al. (2003) additionally found the same production biomass ratios than at more eastern transects. Therefore, it is not clear whether picoplankton grows faster than the larger phytoplankton or even slower.

This chapter describes data of a cruise that was conducted in the eastern subtropical North Atlantic Ocean to examine the contribution of the different size classes to the overall biomass and carbon turnover. Background and size fractionated biomass data were collected to distinguish the conditions that predominate at the single stations. Besides the carbon and nitrogen content of the differently sized organisms the δ^{15}N values were estimated to distinguish the growth status, the trophic position and the potential occurence of nitrogen fixation in the size classes. Long term size fractionated ^{14}C assimilation experiments were additionally performed to estimate the contribution of the different size classes to the overall carbon assimilation and turnover. From the size fractionated biomass and production data it was estimated whether the picoplankton in the subtropical gyre shows increased carbon turnover compared with larger size classes.

1.2. Material and methods

1.2.1. Cruise track

The data were collected during the RV Poseidon cruise 284 in March 2002. The first section of the cruise started west of the Canary Islands heading southwest (see figure 1.1. The second section consisted of several small (1-4h) and three large (24h) stations. All data presented in this chapter were derived from samples of these three large stations. In the map these stations are marked with multiple station numbers. The first large station (148-154; hereafter St.148) was located at 18^{o}N, 30^{o}W, the second station (159-165; hereafter St.159) was located at 23^{o}N, 30^{o}W and the third station (173-180; hereafter

St.173) was located at 28,6°N, 30°W.

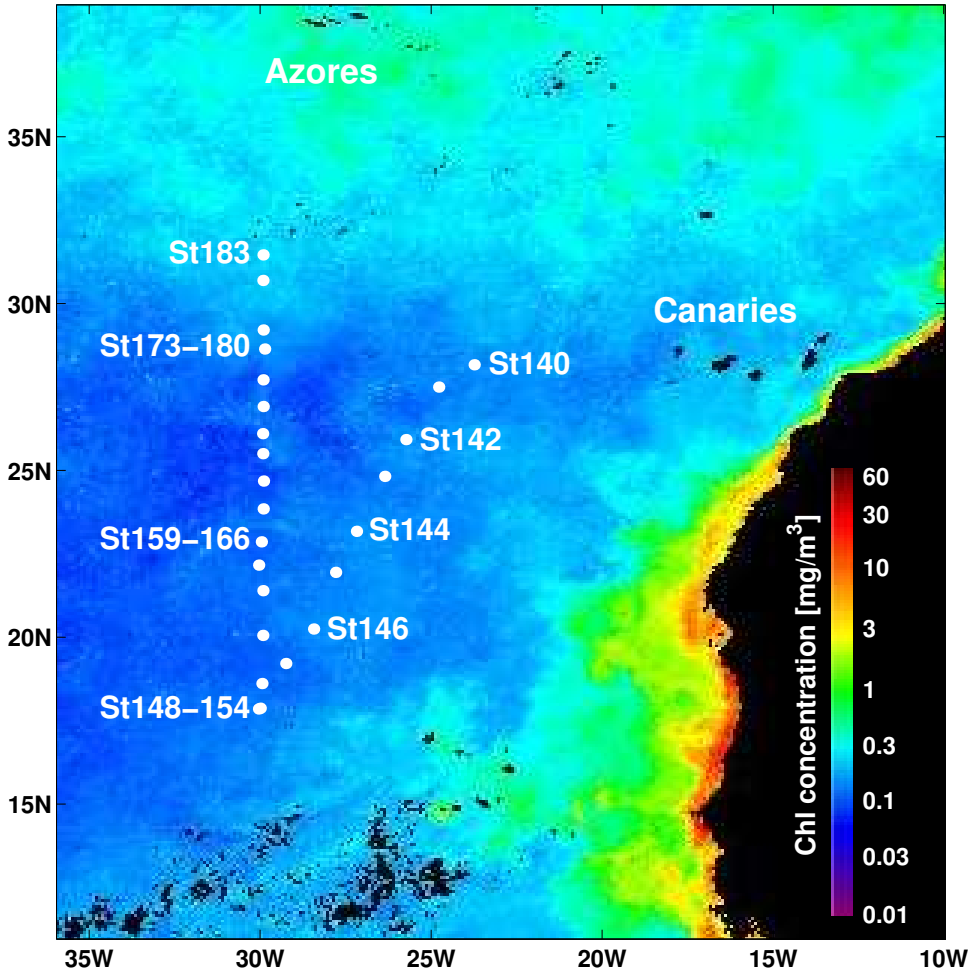

Figure 1.1.: Track of the Poseidon 284 cruise; the three large stations are marked with multiple station numbers; the background picture and color scale (chlorophyll concentration) were contributed by the SEAWIFS project

1.2.2. Sample collection and parameter analysis

Sampling procedure

Samples for the main stations were taken at 4 AM local time. This sampling time was chosen to have enough time to prepare all incubation experiments before sunrise at 7:30 AM. All water samples were collected with a CTD multisampler fitted with 24 black 10 liter NISKIN type water bottles. The CTD was equipped with sensors for pressure, salinity, temperature, oxygen and fluorescence.

Parameter analysis

Nutrients All samples were collected directly from the CTD rosette and analysed by using an onboard autanalyser system processing the samples following the protocols of Grasshoff et al. (1983).

Chlorophyll The fluorimeter setup onboard did not fit the needs because of high background concentration of phaeopigments. Therefore, the CTD fluorimeter (arbitrary units) was used as an indicator of the phytoplankton pigment distribution.

Flow cytometry From every bottle a 2 ml subsample was fixed with formalin to a final concentration of 2%. These samples were immediately frozen at -80°C. They were stored at -20°C until being processed in the laboratory. The samples were gently thawed and resuspended directly before the measurement. From each sample a 1 ml subsample was filtered through a 50μm syringe prefilter to prevent the flow cytometer mess cuvette from becoming clogged up by larger particles. The samples were processed in a Becton Dickinson FACSCalibur flow cytometer. The setup of the flow cytometer which is used for these acquisitions offers the possiblity to monitor cells in the size range of 0.5μm to about 10μm. Larger cells are also acquired but they can not be separated that well from each other. This limitation was of minor significance, because only very few cells could be observed in the $> 10\mu$m size class.

From each sample either 20000 events were aquired or the whole subsample was measured. To estimate the correct volume measured, the three sample flow velocities defined by the user panel of the flow cytometer were calibrated with a numerically predefined bead suspension (TRUCOUNT BEADS; MOLECULAR PROBES). Based on the estimated sample flow speeds the measured subsample volume could be calculated from the measurement time. The collected data were analysed with the WINMDI 2.8 software. Species or group clusters were defined using forward or side scatter (FSC: size, SSC: granularity) versus red (FL3:chlorophyll) or orange (Fl2:phycoerythrin) fluorescence dotplots. From these dotplots cell counts per measured sample volume were extracted. Afterwards the derived cell density was normalized to one ml sample volume.

Particulate organic carbon/nitrogen (POC/N) and δ^{15}N For particle component analysis a 4 liter water sample was filtered with a pressure filtration unit. Samples were filtered separatly for three size classes. Material of all three fractions was collected on acidified GFF filters (WHATMAN) for later analysis. For the total fraction the GFF filter (0.7μm) was used solely. For the smaller fractions prefilters were used leading to size class data of $<2\mu$m and $<5\mu$m. The GFF filters were dried at 50^{o}C in a drying oven and stored in a desiccator. At the institute laboratory the filters were rolled into tin foil and analysed with a ThermoFinnigan Elemental Analyser (Fisons, 1500N) connected to a Finnigan Delta Plus Mass Spectrometer. The mass spectrometer not only delivers the isotopic data but also the absolute carbon and nitrogen biomass data. The analysis of blank filters and tin foil showed detectable backround only for carbon. This background was subtracted from the measured POC data.

The δ^{15}N signatures were calculated from equation 1.1:

$$\delta^{15}N[‰] = \left[\frac{\left(\frac{^{15}N}{^{14}N}\right)_{sample}}{\left(\frac{^{15}N}{^{14}N}\right)_{standard}} - 1 \right] \cdot 1000 \tag{1.1}$$

N_2 gas was used as a primary standard, which was calibrated against IAEA standards (N1, N2, N3, NBS22). An internal standard (acetanilide) was included every sixth sample to ensure correct data acquisition. From different runs of the mass spectrometer the precision of the δ^{15}N acquisition was calculated to be ± 0.2‰.

For the biomass distribution the larger size class was calculated as $POC_{>5\mu m} = POC_{total} - POC_{<5\mu m}$. A corresponding calculation of the $2-5\mu$m size class was skipped, because the biomass of the intermediate size class was very low. Therefore, sampling variance resulted in negative biomass for some samples.

^{14}C incubation experiments The maximum incubation time of the ^{14}C experiments described in this chapter was 48 hours. During that period short (6 hours), intermediate (12 hours) and long term (24 and 48 hours) estimates of the carbon assimilation were achieved. In general, the correct correlation of the estimated carbon assimilation to distinct processes is quite difficult.

For the oligotrophic ocean a comparison of different methods ($^{18}O_2$ production, O_2 light/dark bottles and ^{14}C uptake) published by Grande et al. (1989) revealed that the 12

hour onboard incubations of the ^{14}C method always better represented the net production measured by the O_2 light/dark method than gross production measured by $^{18}O_2$ production. In samples from greater depth the results of the ^{14}C method were much closer to the gross production. So it seems to be more reasonable to follow the carbon assimilation over several hours to get an insight into the short and long term dynamics.

The water samples of the ^{14}C incubation experiments were collected at depths which correspond to the 0.3%, 1%, 6%, 20% and 50% light level. 250 ml subsamples were filled in polycarbonate bottles spiked with 25 to 50 μCi ^{14}C-bicarbonate and placed in on-deck incubators. The incubators were equipped with a water circulation and a color neutral screen on top representing the light percentage of the corresponding water sample collection depth. After 6h, 12h, 24h and 48h a subset of bottles for each light level was filtered on parallel mounted filters with 0.2μm, 2μm and 5μm pore size. The two larger filters were polycarbonate filters. The smallest filter was a polyethersulfone membrane. This membrane was chosen because the water passage is faster and the holes do not have sharp edges, which reduces cell damage during the filtration. For the 12h and 24h filtration three replicates were prepared. The filters were smoked in a HCl chamber for 6 to 12 hours to eliminate ^{14}C-bicarbonate from the filters. In the laboratory 10 to 20 ml Scintillationcocktail (Lumagel SB; Packard) was added. The samples were measured in a liquid scintillation counter (Liquid Scintillation Analyser, Modell Tri-Carb 2100 TR, Packard). The external standard method was applied as quench correction.

The conversion of radioactive counts to carbon turnover followed the method described by Steemann Nielsen (1952):

$$Carbon\ uptake\left[\frac{mmol\ C}{m^3 \cdot d}\right] = \frac{dpm_f \cdot C_e \cdot 1.06}{dpm_a \cdot t} \tag{1.2}$$

C_e	total dissolved inorganic carbon in the environment: here 2142 $\frac{mmolC}{m^3}$ (JGOFS protocol)
dpm_f	decays per minute measured on filter
dpm_a	decays per minute added (^{14}C-bicarbonate)
t	incubation time (days)
1.06	^{12}C:^{14}C fractionation factor

Dark samples were incubated for the 24h filtrations. An analysis showed remarkable scatter of the values. A comparison to the corresponding light bottles showed higher values for the dark bottles in some cases. I assume that the darkening and maybe the temperature conditions were not ideal for the dark bottles. Therefore, it was not reasonable to subtract any dark uptake values from the light uptake values. Threshold values of dark uptake from the publication of Markager (1997) were added to the figures to show critical light uptake values.

1.3. Results

1.3.1. Density

The distribution of σ_0 showed a pycnocline at 100 m depth in the southern part of the section (18^{o}N to 22^{o}N). North of 22^{o}N the pycnocline is much less pronounced at about 150 m depths (see figure 1.2). The σ_0 isoclines rise north of 30^{o}N. At station 169 and 182 signatures of cold core eddies could be observed.

1.3.2. Nutrients

The nutrient distribution showed similar patterns for all macronutrients. Therefore, I included the nitrate distribution as an example. In general, the nutricline can be located at a depth of 100 to 150 m (see figure 1.3). Above this nutricline, nitrate and phosphate

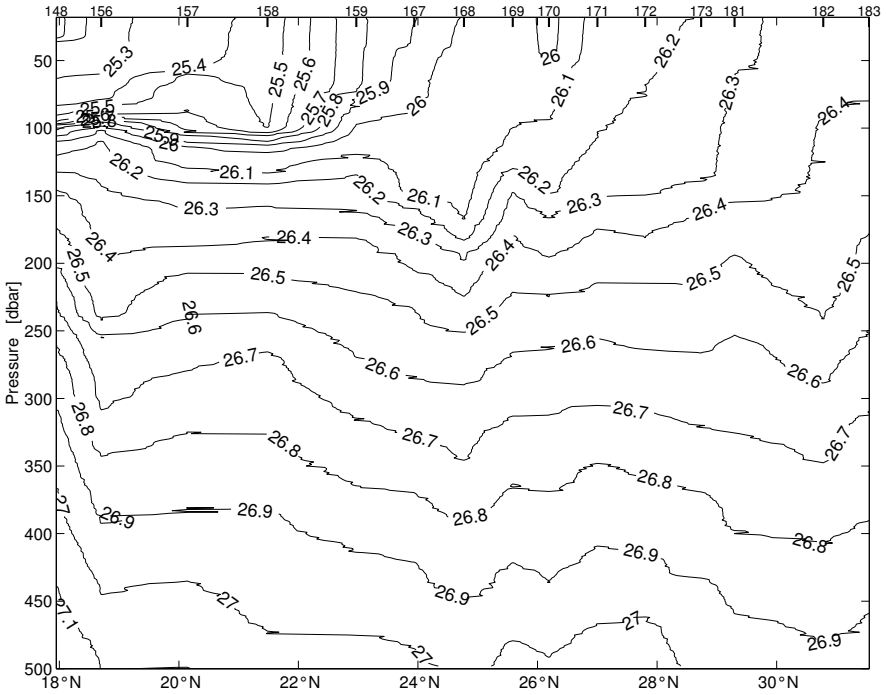

Figure 1.2.: Density (σ_0) depth distribution at section II (30^oW) of the Poseidon 284 cruise; station numbers are given at the top; position north is given at the bottom; isolines indicate equal σ_0; units: kg $\cdot$ m^{-3} $-$ 1000

were undetectable. Only silicate showed background concentrations of about 0.5 mmol Si $\cdot$ m^{-3} above the general nutricline. In the southern part of the section the nutrient isolines rise above the still persisting pycnocline. In the northern part the nutrient isolines also rise, but more slightly. At station 181 a dome like cold core eddy structure could be observed.

1.3.3. Fluorescence

The fluorescence maximum could be observed at 100 m depth for the southern part of section II of the Poseidon 284 cruise (see figure 1.4). Only at station 158 and 169 increased fluorescence was detected at lower depth. In the northern part (north of station 172) the fluorescence maximum was located at more and more shallow depths. At station 182 the highest fluorescence was observed at the surface, decreasing down to 150 m.

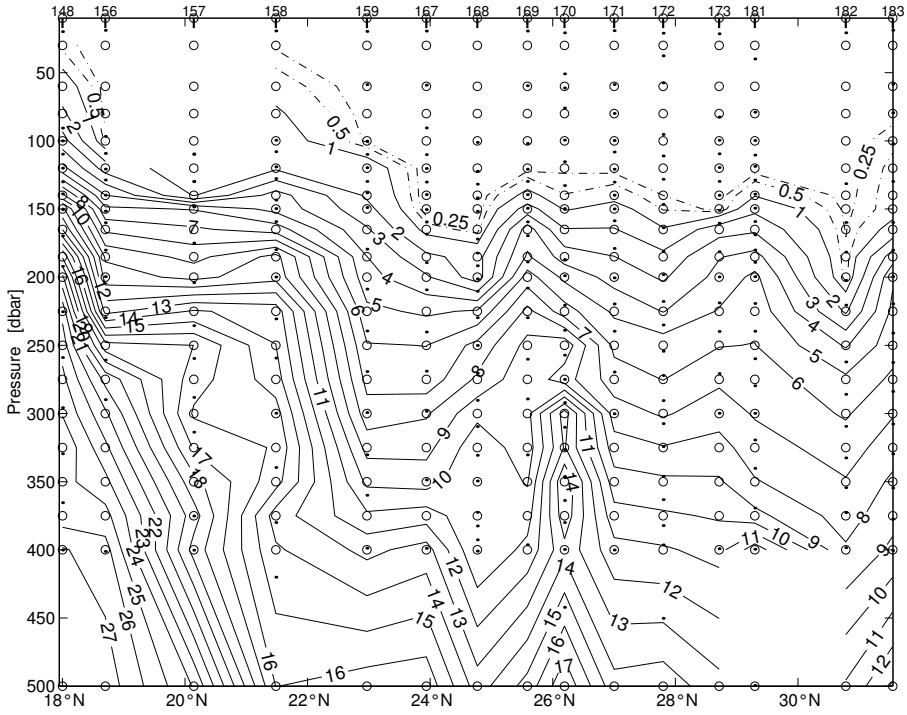

Figure 1.3.: Nitrate depth distribution at section II (30^{o}W) of the Poseidon 284 cruise; station numbers are given at the top; position north is given at the bottom; isolines indicate equal nitrate concentrations; units: mmol $NO_3 \cdot m^{-3}$

1.3.4. Picoplankton distribution

The flow cytometric analysis of the small phytoplankton revealed three major groups. The smallest (*Prochlorococcus* sp.) showed the highest cell densities of all three groups (up to 90000 cells $\cdot$ ml^{-1}). The background cell density of *Prochlorococcus* sp. was quite homogeneous (about 40000 cells $\cdot$ ml^{-1}) above the pycnocline. Below the pycnocline the cell density decreased rapidly, but *Prochlorococcus* sp. was still detectable down to 170 m. Only at 60 m depth of station 148 and at 20 m depth of station 157 the cell density increased to twice the background value. At station 159 and 169 a very slight cell density increase could be observed at 100 m. At station 173 the *Prochlorococcus* sp. cell denstiy was generally enhanced to about 60000 cells $\cdot$ ml^{-1}. Only at station 182 *Prochlorococcus* sp. showed cell densities below the general backgound value (10000-30000 cells $\cdot$ ml^{-1}).

Synechococcus sp. background cell densities were much lower (2000 cells $\cdot$ ml^{-1}). At the southern part of the section only at station 158 an increase of *Synechococcus* sp. cell

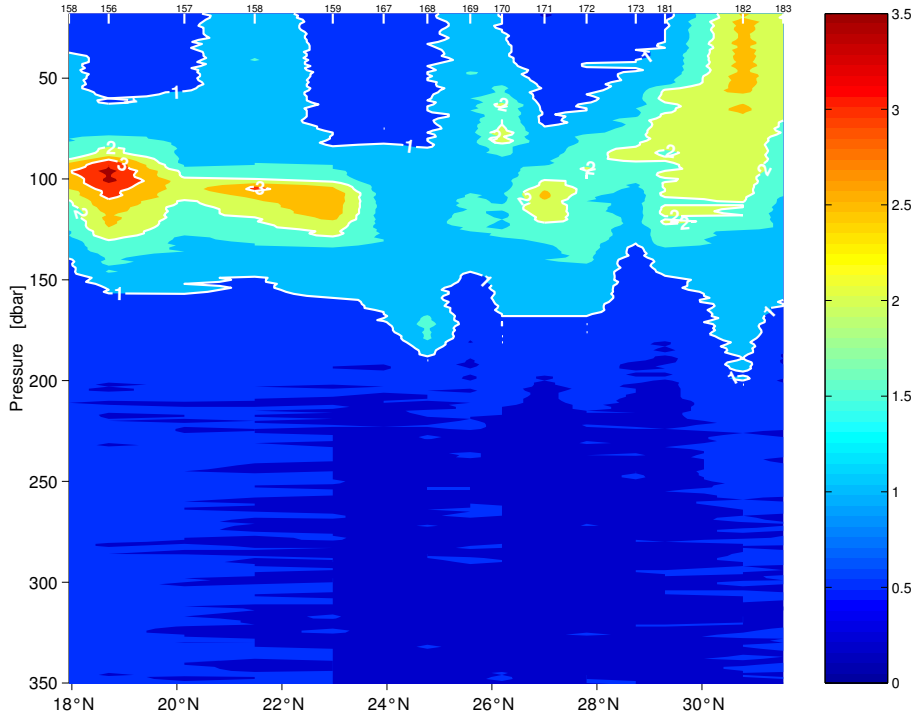

Figure 1.4.: CTD fluorescence at section II (30°W) of the Poseidon 284 cruise; station numbers are given at the top; position north is given at the bottom; isolines indicate equal fluorescence; colorbar: arbitrary fluorescence units

density could be observed (2 fold of the background). North of station 171 the cell density increased to the 5 and 7 fold of the background. In the southern part *Synechococcus* sp. was only detectable down to 100 to 120 m. In the northern part it was detectable down to 200 m.

The picoeucaryotic flagellates were even less adundant than the two other groups. Their backgound value of about 250 cells $\cdot$ ml^{-1} were found quite homogeneously down to 170 m. At station 148 a very slight increase at 100 m depth was estimated. At station 158 a general increase to the 4 fold of the background was observed. The highest cell densities were observed at station 182 with about 2500 cells $\cdot$ ml^{-1} (10 fold of the backgound).

1.3.5. Biomass distribution

Vertical profiles of particulate organic carbon (POC) of the eastern subtropical North Atlantic showed biomass maxima at variable depths in the upper 50 m. At St.148 and St.159 the biomass maximum was found at 40 m depth with 1.9 and 2.1 mmol C $\cdot$ m^{-3}

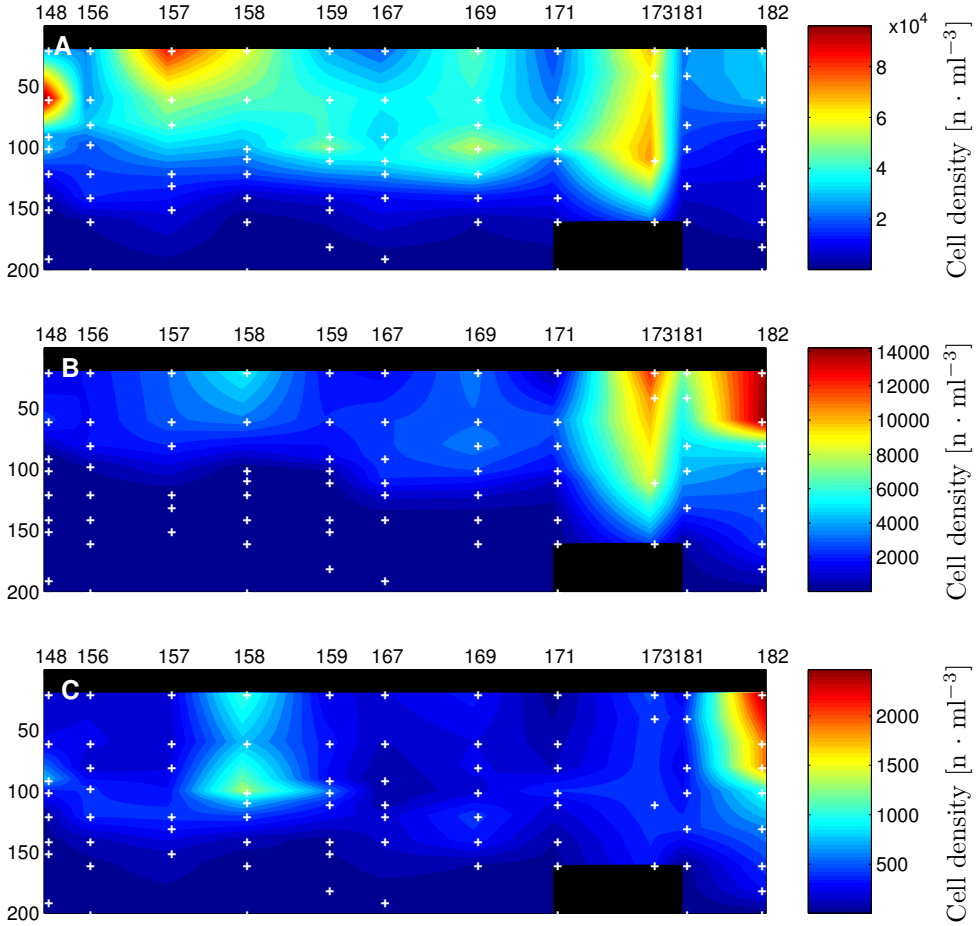

Figure 1.5.: Cell densities of *Prochlorococcus* sp. (A), *Synechococcus* sp. (B) and picoeucaryotic flagellates (C) from the 30°W transect of the Poseidon 284 cruise; x-axis: Station number; y-axis: Depth [m]; the color bar indicates cell densities in $n \cdot ml^{-3}$; white crosses mark the sample depths

(see figure 1.6). POC decreased to about 50% of the maximum values at 100 m depth. For both stations POC of the most shallow depth decreased to 5 and 25% of the maximum value. At St.173 the maximum (2.1 mmol $C \cdot m^{-3}$) was found at 20 m depth. The average POC decrease with depth was about 25% of the maximum value. The profile showed quite heterogeneous structures.

POC fractionation data revealed difficulties in separating the $< 2\mu$m and $< 5\mu$m size fractions. Generally, it was assumed that the $< 5\mu$m fraction contributes higher biomass values to the total POC than the $< 2\mu$m size fraction. From the left hand side of figure 1.6 it is obvious that the filtration and filter processing led to alternating higher values

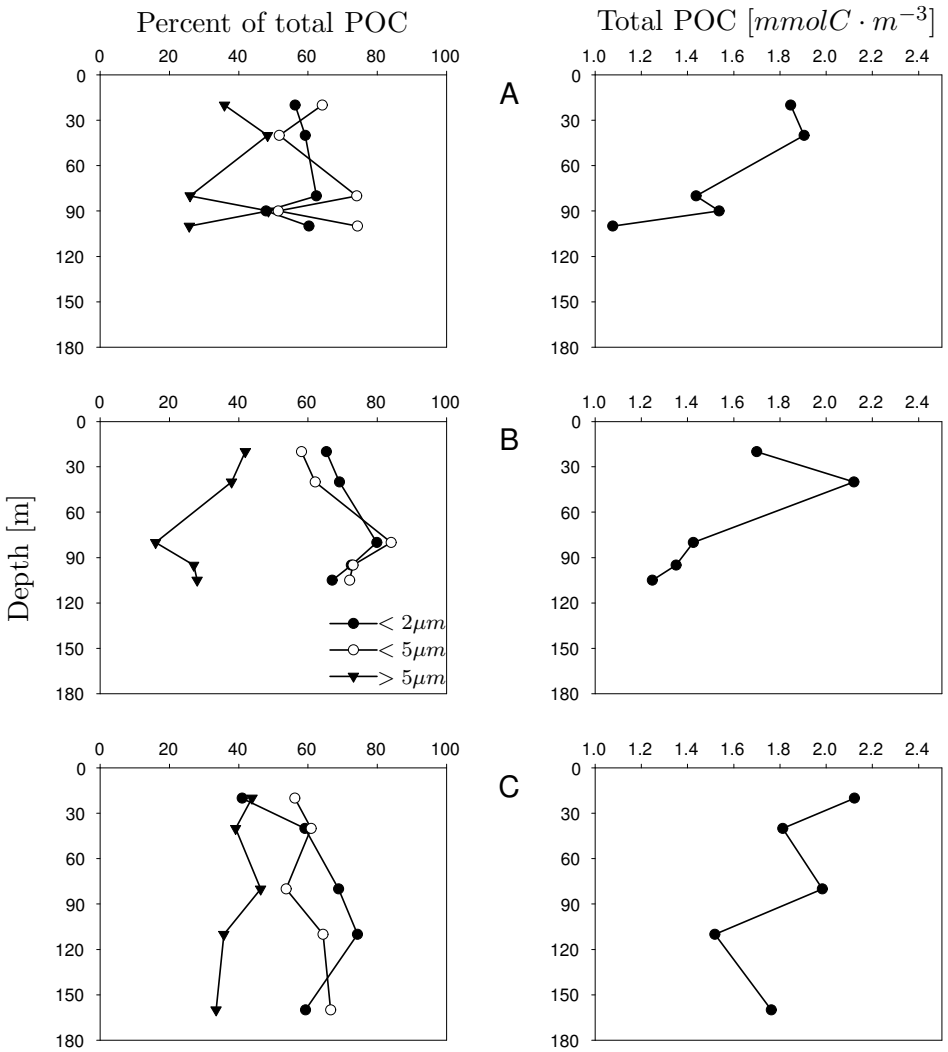

Figure 1.6.: Particulate organic carbon (POC) profiles from the eastern subtropical Atlantic; left hand side shows the biomass proportion of the three size classes $< 2\mu m$, $< 5\mu m$ and $> 5\mu m$ of the total particulate organic carbon (POC, right hand side); A: Station 148 (18^oN, 30^oW), B: Station 159 (23^oN, 30^oW), C: Station 173 ($28{,}6^oN$, 30^oW)

of these two size fractions. The calculation of intermediate size fractions will lead to negative biomass contribution. Therefore, intermediate values are not reasonable but the $< 2\mu$m and $< 5\mu$m fraction difference can be interpreted as an estimate of error of the data collection procedure for the smaller size fraction. Here I present the average of the $< 2\mu$m and $< 5\mu$m fraction proportion as the $< 5\mu$m fraction value and the corresponding

value (total-$< 5\mu$m) as the $> 5\mu$m fraction.

From the data presented on the left hand side of figure 1.6 two patterns can be extracted. At St.148 and St.173 the smaller size fractions showed higher variability (20% error) which made all possible depth dependent gradients undetectable. The average POC proportion of the $< 5\mu$m and $> 5\mu$m fraction was 60% and 40% for both stations. At St.159 the error range was much smaller ($< 10\%$). Therefore, a proportion maximum of the smaller size class was observed at 85 m. At 20 m depth the proportions were 60% and 40% for the $< 5\mu$m and $> 5\mu$m fraction like at the two other stations. At 85 m depth the POC proportions increased to 80% for the $< 5\mu$m fraction and decreased to 20% for the $> 5\mu$m fraction. At 100 m depth this proportion difference decreased to 70% and 30% for the two fractions. The average POC proportion for St.159 was 68% and 32% for the $< 5\mu$m and $> 5\mu$m fraction.

1.3.6. Chemical particle composition

Carbon to nitrogen ratio

The profiles of the carbon to nitrogen ratio (C:N) of the total particulate organic matter showed little variation with depth for all three stations (see figure 1.7). At St.148 and St.159 the average C:N was estimated to be 7. The range at St.148 was 6.7 to 7.1 in the upper depths. At 100 m the total POM C:N value increased to 8. At St.159 the range was 6.5 to 7.5. At St.173 the total C:N showed an average value of 7.8, with a range of 7.1 to 8.5. At St.148 the different size classes showed parallel profiles for all depths. At the two northern stations (159, 173) at intermediate depths the total fraction showed lowest C:N values, followed by the $< 5\mu$m (St.159: 6.9-7.2; St.173: 8-8-5)) fraction. The smallest size fraction ($< 2\mu$m) showed the highest C:N values (St.159: 7.5-8; St.173: 8.5-9) at both stations. These general patterns are only altered at 20 m. At this depth at St.159 both small fractions revealed lower C:N values than the total, but the $< 5\mu$m was still lower than $< 2\mu$m fraction. At St.173 the C:N value of only the smallest fraction decreased to a C:N value of 7.

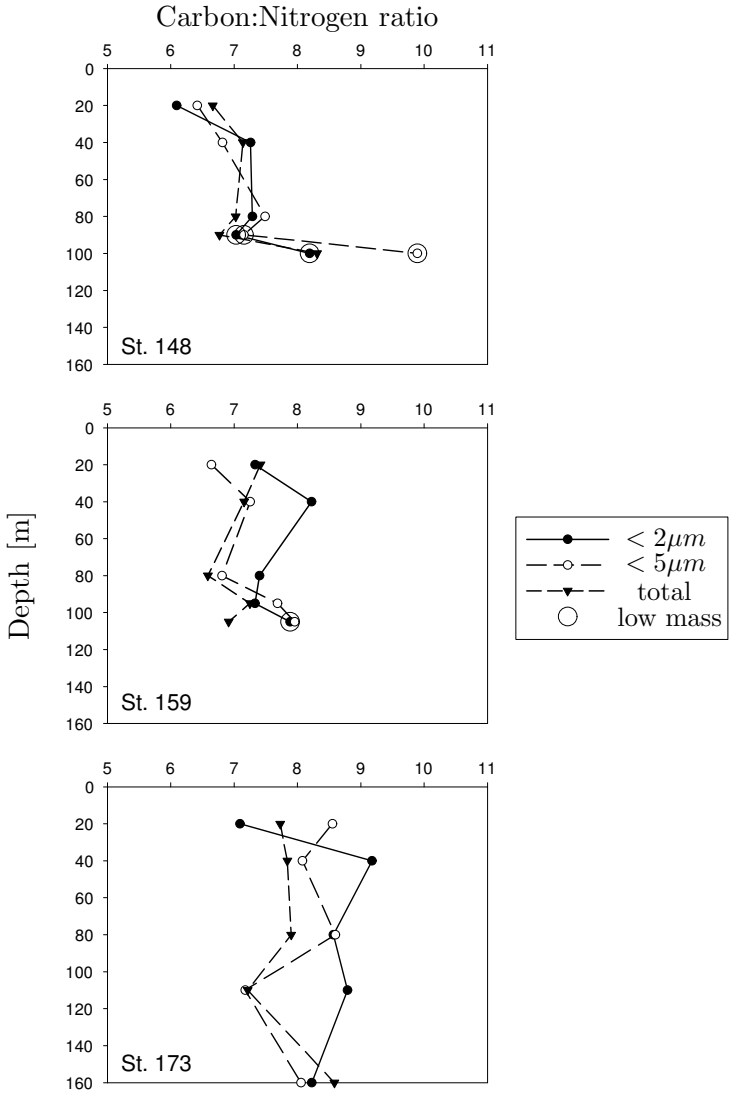

Figure 1.7.: Carbon:Nitrogen ratios of particulate organic matter (POM) from the eastern subtropical Atlantic of the three size classes $< 2\mu m$, $< 5\mu m$ and total; the low mass indicator marks individual measurements which were lower than the calibration range of the mass spectrometer and can therefore be erroneous

Particulate organic matter (POM) δ^{15}N isotopic signature

The δ^{15}N isotopic signatures were very different for all three stations. Generally, the total fraction had the highest δ^{15}N values (see figure 1.8). At St.148 the total fraction increased from about 2.2‰ in the upper layers to 4.5 at 90 m depth. At 100 m the δ^{15}N still decreased to 2.5‰. The smaller size fractions always showed smaller δ^{15}N values at

all depths. In the upper layers the smallest size class ($< 2\mu$m) revealed values in the range of 1 to 2‰. The $< 5\mu$m fraction showed even smaller values with 0.5‰ for the upper two depths. At 80 m it reached the same value (1.8‰) as the $< 2\mu$m fraction.

At St.159 the total fraction increased from 1 to 4.3‰ in the upper 40 m. Below this maximum it decreased again to 1‰ at 95 m. The size fractions follow this pattern quite parallel with reduced values of about 1‰ for the $< 2\mu$m and 1.5‰ for the $< 5\mu$m fraction.

At St.173 the total POM showed a slight decrease of the δ^{15}N value from 4‰ at 20 m depth to 2.8‰ at 160 m depth. The smaller fractions showed reduced δ^{15}N values of 1.5 to 2‰ at larger depths. At the subsurface the δ^{15}N values of the smaller fractions is even further reduced from 2.5 to 3.5‰. At this depth the smallest fraction ($< 2\mu$m) revealed the lowest δ^{15}N value of 0.5‰.

1.3.7. Carbon turnover

The comparison of the total carbon uptake rates for the different incubation times for each station revealed that in most cases the 6 hour incubation showed four times the carbon uptake rates of the 24 incubation. The 12 hour incubation showed the 2-2.5 fold of the 24 hour incubation value, and the 48 hour incubation resulted in identical carbon uptake values than the 24 hour incubation (see figure 1.9, 1.10 and 1.11). This pattern is best observed at St.173 where all four incubation times fit into this pattern (subsurface: 6h: 1; 12h: 0.7; 24h: 0.27; 48h: 0.3 mmol C $\cdot$ m$^{-3}\cdot$ d^{-1}). This can be observed for all depths at St.173. For the surface samples of St.159 this pattern held only for the 12, 24 and 48h incubation, because the surface sample of the 6 hour incubation showed a very high carbon uptake of 3.8 mmol C $\cdot$ m$^{-3}\cdot$ d^{-1}), compared to values of 0.5 to 0.72 for the long term incubations. The deeper samples reproduced this pattern entirely. At St.148 this pattern is approximately maintained for depths below 30 m. Deviations from the pattern can be observed for the subsurface(20m) samples of the 6 and 24 hour incubation which were remarkably higher (6h: 15.3; 24h: 6.3 mmol C $\cdot$ m$^{-3}\cdot$ d^{-1}) than expected.

The following data descriptions are based on the 24 hour incubations of the three stations. A general pattern that can be observed at every station was the highest total carbon uptake rate in the subsurface sample at 20 m depth. At St.148 the highest overall carbon

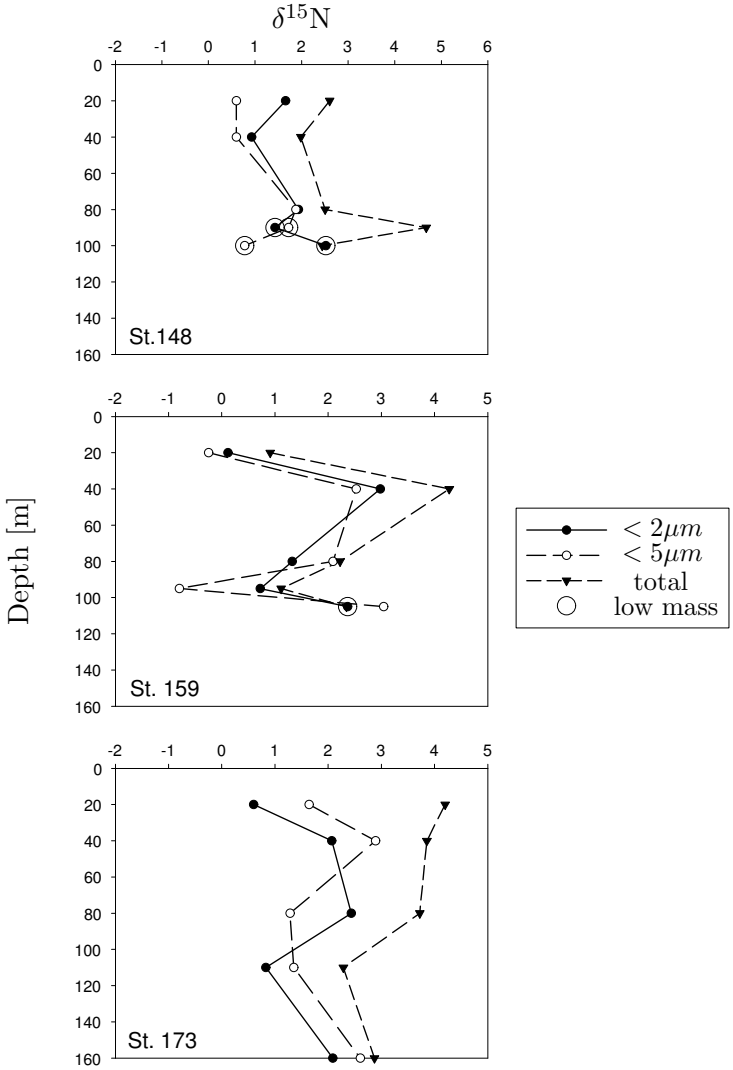

Figure 1.8.: δ^{15}N signal of particulate organic matter (POM) from the eastern subtropical Atlantic of the three size classes $< 2\mu m$, $< 5\mu m$ and total; the low mass indicator marks individual measurements which were lower than the calibration range of the mass spectrometer and can therefore be erroneous

uptake rate was observed. As mentioned before, the subsurface showed an uptake rate of about 6.3±4.5 mmol C $\cdot$ m$^{-3}\cdot$ d^{-1}. The large error indicates a remarkable heterogeneity of the three replicates. I suggest that the real carbon uptake rate would be ≈1 mmol C $\cdot$ m$^{-3}\cdot$ d^{-1} for the subsurface sample, because at the other stations I observed that the 24 and 48 hour incubations revealed nearly the same carbon uptake rates. The total carbon uptake rate decreased to an averaged rate of 0.25 mmol C $\cdot$ m$^{-3}\cdot$ d^{-1} at intermediate

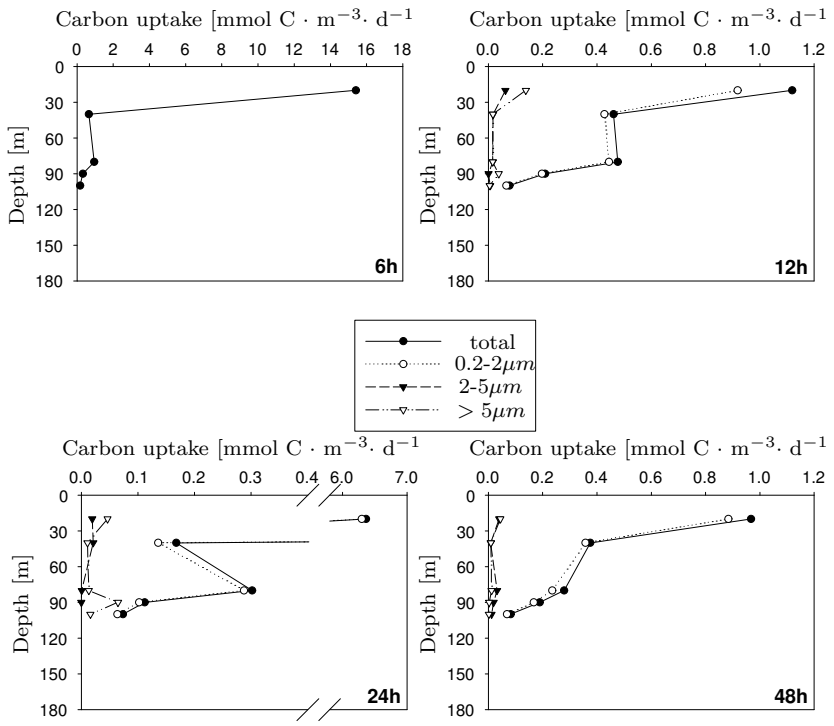

Figure 1.9.: Time course of the fractionated carbon uptake at St.148 (18^{o}N, 30^{o}W); values show light bottle values without dark bottle correction, Markager (1997) published dark uptake values of 0.001 to 0.02 mmol C · m^{-3}· d^{-1} for the oligotrophic subtropical gyre of the North Atlantic

depths and to 0.06 at 100 m. More than 90% of this carbon uptake rate are contributed by the smallest size fraction (0.2-2μm) at all depths. The 2-5μm and > 5μm fraction showed nearly the same carbon uptake values for all depths (subsurface: 0.03; deep: 0.01 mmol C · m^{-3}· d^{-1}). Only at the subsurface sample the > 5μm fraction increased slightly to 0.05.

The maximum total carbon uptake rate at St.159 was estimated to be 0.5 mmol C · m^{-3}· d^{-1} at the subsurface. This value decreased to 0.28 at 40 m, 0.36 at 85 m, 0.14 at 95 m and 0.08 mmol C · m^{-3}· d^{-1} at 105 m depth. With increasing depths the 0.2-2μm fractions contribute higher proportions to the total carbon uptake rate (20m: 80%; 40m: 76%; >80m: >90%). The remaining carbon turnover was equally distributed to the 2-5μm and > 5μm fraction.

At St.173 the maximum total carbon uptake rate was 0.27 at 20 m depth. It decreased linearly to 0.02 at 160 m depth. The contribution of the smallest size class was lowest at

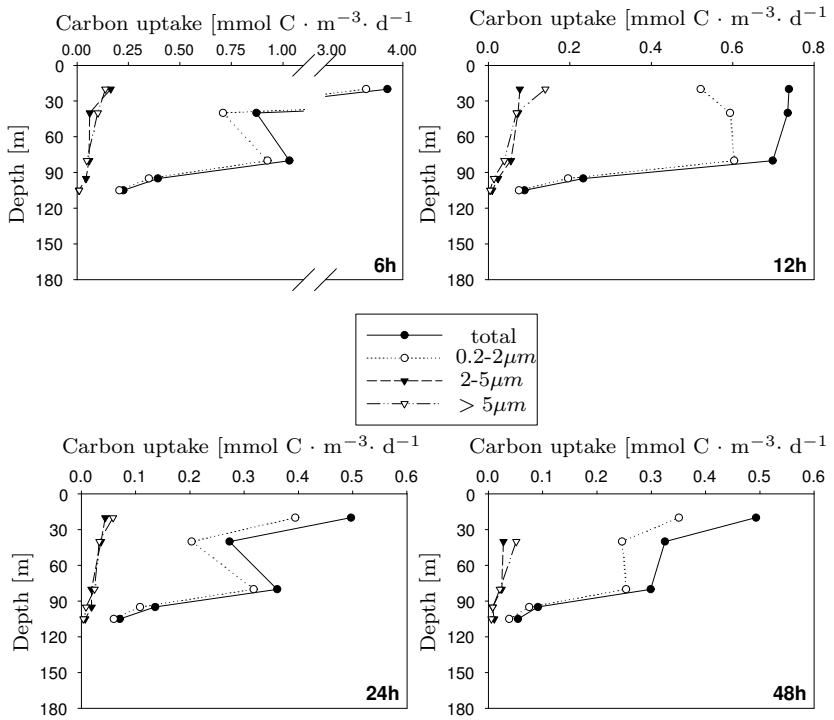

Figure 1.10.: Time course of the fractionated carbon uptake at St.159 (23^{o}N, 30^{o}W); values show light bottle values without dark bottle correction, Markager (1997) published dark uptake values of 0.001 to 0.02 mmol C · m^{-3}· d^{-1} for the oligotrophic subtropical gyre of the North Atlantic

this station. At 40 m depth the 0.2-2μm accounted for 44% of the total carbon uptake rate. This proportion is further decreased to 30% at greater depths. The 2-5μm and $> 5\mu m$ fraction split the remaining carbon uptake rate equally.

1.4. Discussion

The subtropical gyres of the world ocean are generally distinguished from other ocean provinces by their pronounced oligotrophic conditions, resulting in deep chlorophyll maxima (DCM) at the nutricline. For the North Atlantic this pattern is best observed in the western part of the subtropical gyre. At our cruise in the eastern North Atlantic a DCM could also be detected. From the chlorophyll background of the cruise it is obvious that the sampled region was more heterogenous than the western part of the gyre. The southern stations are influenced by offshoots of the upwelling at the African coast and by

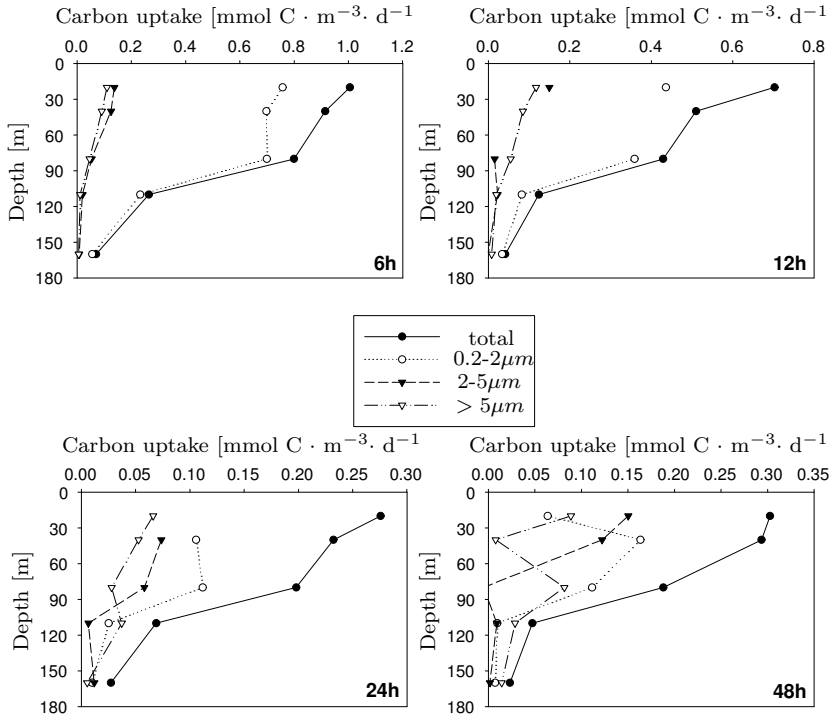

Figure 1.11.: Time course of the fractionated carbon uptake at St.173 (28.6^{o}N, 30^{o}W); values show light bottle values without dark bottle correction, Markager (1997) published dark uptake values of 0.001 to 0.02 mmol C · m^{-3}· d^{-1} for the oligotrophic subtropical gyre of the North Atlantic

the underlying nutrient rich antarctic intermediate water (AAIW) (Dietrich et al. (1975), Brown et al. (1989)). The upwelling influence results in more spatial patchiness. The underlying nutrient rich water enhances the nutrient gradients in the southern part and therefore the nutrient fluxes into the euphotic zone. A model study revealed that mainly horizontal advection can transport up to 0.5 mol N · m^{-2}· y−1 into the southern part of the study area (Oschlies, 2002). The nitrate input into the euphotic zone was estimated to be 0.1 mol N · m^{-2}· y−1 (Oschlies, 2002). The northern part of the cruise is characterized by spatial heterogeneity induced by hydrographic processes in the Azores Front zone, which is located between 32^{o}N and 37^{o}N (Sy (1988), Klein and Siedler (1989)). At the Azores Front the nutricline and pycnocline can be found in more shallow depths. Furthermore, cold core nutrient rich eddies south of the Azores current system (Alves and de Verdière (1999)) enhance the nitrate input into the euphotic zone (Oschlies and Garcon, 1998). Total horizontal advective nitrogen input reached the same values than

in the southern part of the study area (Oschlies, 2002).

1.4.1. Distribution and composition of particulate organic matter

A general pattern of the oligotrophic ocean is the DCM. As observed during the cruise several authors stated that the subsurface fluorescence and chlorophyll maximum does not necessarily correspond to the biomass maximum of the depth profiles (Beers et al. (1975), Cullen and Eppley (1981), Kimor et al. (1987), Tagushi et al. (1988)). This discrepancy could either be caused by photoadaptation of the phytoplankton cells at greater depths or by higher amounts of non phototrophic particles at the biomass maximum. In contrast to my results, Jochem (1990) and Jochem and Zeitschel (1993) reported quite good agreement of chorophyll and biomass maximum which was estimated by microscopic counts and POC/PON measurements for two stations of the southern JGOFS NABE experiment at 18^oN, 30^oW and 33^oN, 21^oW. It seems that no general pattern exist for the oligotrophic North Atlantic and that chlorophyll is an improper biomass estimator in that area. Therefore, it is necessary to examine the individual patterns for each station. The biomass range that was achieved at the cruise (1 to 2.2 mmol $C \cdot m^{-3}$) correspond to POC data at the Bermuda Atlantic Time series Study (BATS) site published by Roman et al. (1995) (1.4 to 2.4 mmol $C \cdot m^{-3}$). They showed that in March 1990 in the upper layer nearly 50% of the biomass could be assigned to the phototrophic and 50% to the heterotrophic organisms. In the deep layers only 30% of the biomass consisted of phototrophic organisms.

From the flow cytometry analysis (see figure 1.5) it is obvious that the POC peak at St.148 was caused by a high *Prochlorococcus* sp. cell density. The individual cell fluorescence signature of *Prochlorococcus* sp. showed weak fluorescence at shallow depth, compared with deep samples. Therefore, I suggest that photoadaptation is the main reason for the DCM at St.148. The biomass distribtuion is accompanied by a homogenous C:N ratio near Redfield proportion at layers deeper than 40 m, indicating that the present particles wre built under conditions of sufficient nutrient supply. This fits into the description given above of enhanced horizontal nutrient fluxes at the southern border of the study area. The lowered C:N ratios of the subsurface samples are of special interest. They are accompanied by lower $\delta^{15}N$ values of the $< 5\mu m$ size class. This size class

sum the C:N and the δ^{15}N values of the $< 2\mu$m and the 2-5μm size class. Because the intermediate size class has very low biomass values it must have very low δ^{15}N values to achieve a summed value ($< 5\mu$m size class) being 1 ‰ smaller than the $< 2\mu$m size class. Because the biomasses were so small it is not possible to calculate the δ^{15}N value of the intermediate size class. Two explanations are possible for these low δ^{15}N values. First, the intermediate size class assimilates ammonia with low δ^{15}N values much more efficient than the smaller size fraction and the cells fractionate for the lighter isotope. Second, the intermediate size class fixes nitrogen. The processes described in the first explanation would not change the C:N ratio of all three groups but if the imtermediate size class fixes nitrogen, the C:N ratio of the fixing cells could be decreased (lowered C:N ratios ($\approx$4) are known from actively fixing *Trichodesmium* sp., (Breitbarth pers. commm.). Released light dissolved organic nitrogen (DON) could also significantly decrease the C:N ratio of the other size fractions. The interpretation of the low δ^{15}N values of the intermediate size class as an indication of nitrogen fixation correspond to the findings of Zehr et al. (2001) from the subtropical North Pacific Ocean. In general, nitrogen fixation occurs if the nitrogen to phosphorus ratio of the ressource tends to decrease below the Redfield ratio (N:P=16)(Falkowski et al. (1998), Karl et al. (2001), Sterner and Elser (2002)), a pattern that can be observed in the upper layers of the study area (N:P$\approx$10).

At St.159 the biomass peak is even more pronounced at 40 m depth. Flow cytometry data showed no peak for any of the photoautotrophs in the upper 90 m (especially in the smaller size fractions). A comparison of the biomass proportions in and below the biomass maximum revealed that the overall biomass reduction is mainly caused by the decrease of the $> 5\mu$m size fraction. This larger size fraction additionally showed low C:N ratios and high δ^{15}N values. Therefore, I conclude that this larger fraction mainly consists of heterotrophs (Sterner and Elser (2002), DeNiro and Epstein (1981), Owens (1987), Wada et al. (1987), Fry (1988), Rau et al. (1990), Hansson et al. (1997), Sommer (2003)).

Generally, the $< 2\mu$m size class consists of heterotrophic and autotrophic procaryotes. Heterotrophic procaryotes have higher nitrogen content and therefore lower C:N ratios. In contrast, the C:N ratio of the phototrophic procaryote *Prochlorococcus* sp. showed the same patterns like other photoautotrophs. At St.159 the larger size classes showed C:N ratios of $\approx$7 quite near the Redfield ratio. The C:N ratios of the smaller size class instead

increased at the biomass maximum. Increased C:N ratios by carbon overconsumption are published for phytoplankton with reduced specific growth rate under nutrient limitation (Goldman et al., 1979) or in combination of nutrient limitation and high light conditions (Healey, 1985). I assume that the combined effect of nutrient limitation and high light is responsible for the decreasing C:N ratio profile with depth.

The decrease of the C:N ratio in the subsurface sample of the $< 2\mu$m and $< 5\mu$m size fraction could also be explained by nitrogen fixation of the intermediate size class like at St.148. Correspondingly the δ^{15}N value of the intermediate size class was reduced in the subsurface sample and the δ^{15}N value sequence $((< 5\mu m) < (< 2\mu m) < total)$ is identical to the St.148 subsurface δ^{15}N value sequence.

At St.173 the biomass peak found in the subsurface sample did not correspond to the DCM. As for St.148 I assume that the DCM is mainly caused by photoadaptation of the phytoplankton cells. The higher amounts of total biomass were combined with a slight increase of the larger size fraction biomass. The large size fraction was identified as heterotrophic organisms, because of the low C:N ratio and the high δ^{15}N value. These patterns are comparable to St.159. Although the maximum observed biomass was comparable to the two other stations, the depth integrated biomass was nearly twice as high. The hydrographic, fluorescence and cell density patterns indicate that St.173 is influenced by offshoots of the Azores front. The generally higher C:N ratios, depleted nutrients at isopycnals and the higher overall biomass indicate late bloom conditions at St.173.

1.4.2. Carbon turnover

The correction of light incubation carbon uptake by dark bootle incubation values is recommended especially for samples originating from low light conditions (Steemann Nielsen (1952), Markager (1997)). This correction was skipped for my samples, because the dark uptake estimates were erroneous. Markager (1997) published a linear increase of the dark uptake values with an increasing maximum photosynthetic rate. Assuming that the dark uptake values of Markager (1997) hold for the incubations of this cruise, a dark correction of 0.01 mmol C $\cdot$ m$^{-3}\cdot$ d^{-1} should be subtracted from low carbon turnover values, and 0.02 mmol C $\cdot$ m$^{-3}\cdot$ d^{-1} should be subtracted from high carbon turnover values. Especially for these low carbon uptake values the dark correction could contribute more than 50%

to the total carbon uptake. Therefore, the carbon uptake rates presented here could be an overestimation of the real carbon uptake rates. Especially for the carbon uptake proportions a dark correction of about 50% of the low uptake values can shift the proportion of the smallest size class towards higher percentages.

The large range of carbon estimates of the replicates in the subsurface samples is mainly due to sampling error. First, in low biomass water the use of small (250 ml) bottles can lead to heterogenous distribution of the organisms. Second, the randomized filtration results in higher error values when the turnover is high. Both sources of error can not be distinguished. A general correction can not be applied, because the first error source is caused by system patterns being amplified by the method.

The general pattern described in the results means that the total carbon uptake (mmol $C \cdot m^{-3}$) after 6 hours, 12 hours and 24 hours is nearly identical. In some cases the 12 hour carbon uptake is slightly higher than the 6 hour and 24 hour value. Eppley and Sharp (1975) were the first to publish such patterns of carbon uptake. They assumed that the difference between the expected carbon uptake that would result from linear extrapolation of the 6 hour incubation is due to respiration (factor of 3-4). This interpretation is discussed controversely in the literature. Grande et al. (1989) estimated a factor of 2 to 3 for the conversion of production estimates by the ^{14}C assimilation method, to estimates derived from gross O_2 production measured by the turnover of $H_2{}^{18}O_2$ in onboard incubators. Sheldon and Sutcliffe (1978) stated that this pattern of carbon uptake in long term incubations described by Eppley and Sharp (1975) is mainly due to reaching the isotope equilibrium in the particles than to physiological processes. Different conditions have to be distinguished to interprete the 24 and 48 hour incubation results. When assuming a steady state system which reached the $^{14}C/^{12}C$ isotopic equilibrium, the carbon uptake derived from ^{14}C measurements represents the standing stock. In this case no further increase of the carbon uptake over time should be observed and the corresponding carbon uptake rate after 48 hours should be half of the 24 hour value. If the system did not reach the isotopic equilibrium the measured carbon uptake estimate represents the net carbon turnover of the system. This net carbon turnover should be quite stable from 24 to 48 hours. It should steadily decrease depending on the relative amount of the net carbon turnover of the overall biomass. I suggest that the total carbon uptake values observed at

the cruise fit into the steady state non-equilibrium situation, because the carbon uptake increased linearly (the carbon uptake rate was nearly constant) from the 24 to the 48 hour incubation. The alternative, a linear biomass increase, can not be excluded, because no biomass patterns were observed in the incubations, but a linear biomass increase over 48 hours at different depths seems to be implausible. The observed decrease (≈30%) of the carbon uptake from the 12 hour to the 24 hour incubations especially in the subsurface samples at St.173 corresponds to estimates of night losses from the North Pacific gyre (33%; Grande et al. (1989)).

The total carbon uptake rates which were estimated at the cruise (0.7 to 1 mmol C · m^{-3}· d^{-1}) fell into the range published by Jochem and Zeitschel (1993) (0.8 to 1.4 mmol C · m^{-3}· d^{-1} at the beginning of the experiment at 18^{o}N; 3.4 mmol C · m^{-3}· d^{-1} after crossing a front; the same range at 33^{o}N). Grande et al. (1989) reported carbon uptake rates for the North Pacific gyre of 0.4 to 0.74 mmol C · m^{-3}· d^{-1} for 12 hour incubations, and 0.3 to 0.55 mmol C · m^{-3}· d^{-1} for the 24 hour incubation. The difference marks the 33% loss mentioned above. At the NABE site at 47^{o}N 20^{o}W maximum carbon turnover rates of 4 mmol C · m^{-3}· d^{-1} have been reported (Lochte et al., 1993). The range estimated by the different teams onboard of three ships was 2.6 to 6.4 mmol C · m^{-3}· d^{-1}. For the Celtic Sea Joint and Pomroy (1983) published values of about 2.7 mmol C · m^{-3}· d^{-1} from 24 hour incubations. The authors also stated that 75% of the total production was contributed by organisms in the $< 5\mu$m size class. These proportions correspond to the lower boundary I observed in the production estimates of the oligotrophic stations.

The size fractionated production showed a decreasing proportion of the 0.2-2μm size class ($< 2\mu$m) with decreasing maximum total carbon uptake rate. The maximum values of about 90 to 95% were observed at St.148 which fit into the range published by Jochem and Zeitschel (1993) (83-98%). The high carbon turnover of ≈ 50% of the total biomass per day (≈300% if based on the measured carbon uptake rate 6.3 mmol C · m^{-3}· d^{-1}) indicates either very high carbon recycling or a pre-bloom situation. The exact reason for this high carbon turnover remains "enigmatic", as stated by Jochem and Zeitschel (1993) who also reported high and heterogenous carbon turnover at the 18^{o}N study site.

St.159 is characterized by half the carbon uptake measured at St.148. Therefore, the daily carbon pool turnover is reduced to ≈ 25%. This means that the total carbon pool

is completely recycled in about 4 days. This estimate is quite reasonable for oligotrophic oceans with high nutrient and carbon recycling. The amount of carbon uptake of the larger size fractions is equal at St.148 and St.159. The reduction of carbon uptake mainly took place in the smaller size fraction.

At the northern station (St.173) the maximum total carbon uptake is further reduced. I suggest that this low carbon turnover ($\approx$ 15% daily carbon pool turnover) is due to the late bloom conditions which are indicated by the biomass signatures. A late bloom condition will also explain the higher carbon turnover (about 50% to 100%) in the larger fractions. These higher value are caused by increased growth of phytoplankton in the large size fraction due to higher nutrient supply during the bloom and by delayed growth of heterotrophic organisms in the larger size fraction. In general, the organisms at St.173 must have higher carbon retention than the organisms at St.159.

1.4.3. Summary and conclusion

The biomass distribution, stoichiometric composition of the particles and the production values indicate that the three stations described in this chapter represent different conditions of the eastern oligotrophic North Atlantic subtropical gyre.

The conditions of the southern station (St.148) are not that clear. Hydrographic patterns and satellite data reveal influences of high nutrient supply caused by pronounced nutrient gradients and casual offshoots of the African coastal upwelling system. These influences could be observed in the generally low C:N values and the high production values in comparison to the more northern stations.

St.159 shows the typically more stable oligotrophic conditions expected for the subtropical gyre. It is characterized by lower production than at St.148, by higher proportions of smaller cells and by enhanced C:N values.

The northern station (St.173) shows typical patterns of late bloom conditions induced by hydrographic influences of the Azores front. Typical patterns are the doubled depth integrated biomass in comparison to the other two stations and the increased C:N ratios. Increased δ^{15}N values imply the consumption of isotopically heavier nitrate which could not be detected any more in the nutrient profiles.

δ^{15}N values at the two southern stations indicate that nitrogen fixation could be a source

of new nitrogen, especially in the subsurface samples. Lowest δ^{15}N values are observed in the intermediate size class (2-5μm). This implies that unicellular nitrogen fixers and not *Trichodesmium* sp. trichomes or colonies are responsible for the nitrogen fixation. Therefore, the estimates of nitrogen input into the euphotic zone by nitrogen fixation of *Trichodesmium* sp. blooms in the western subtropical gyre are missing the potentially more widespread nitrogen input caused by unicellular nitrogen fixers.

The long term carbon uptake experiments reveal that the 24 hour values are a good estimate of the net carbon turnover of the system. But the different ecosystem status at the three stations and the observed heterogeneity of small volume incubations can disturb these general patterns.

In general, the total carbon turnover in the system is dominated by picoplankton. For the southern stations about 70 to 95% of the total carbon turnover is performed by picoplankton. Only at St.173 the late bloom conditions reduce this amount to about 50%. This pattern is of interest concerning size related processes in the ocean. When assuming no size related scaling of turnover processes, the specific carbon turnover of autotrophs should be equal for all size classes. This implies that the biomass ratio ($Mass_{small} \cdot Mass_{large}{}^{-1}$) and the carbon uptake ratio should be equal. The biomass ratio of the $< 5\mu$m to the $> 5\mu$m size class was in the range of 1 to 1.8 for the three stations. This ratio is calculated from the total biomass values, but the biomass ratio of the autotrophs would have been in the same range (Roman et al., 1995). The corresponding carbon uptake ratio derived from the 24 hour incubation was in the range of 3 to 10. The biomass and turnover ratios presented above are derived from net carbon turnover of the system. The autotrophic turnover is more pronounced in data of the short (6 and 12 hour) incubations. Even using a conservative approach (replacing the very high 6 hour incubation values by extrapolation of the longer incubations), the carbon turnover ratio is further increased to a range of 10 to 20. The upper boundary of the ranges correspond to the southern stations. At these stations the carbon turnover is approximately 5 to 10 times faster in the smaller cells than in the larger cells. At St.173 the turnover of the smaller cells is still 3 to 10 times faster. Therefore, size scaling is crucial for the comparison or calculation of gross and net turnover estimates, because all loss terms are also more pronounced in systems dominated by smaller cells. This is important for models which should adequately describe

biogeochemical processes in different oceanic regions (Hurtt and Armstrong (1996), Hurtt and Armstrong (1999)). But it is also important for ecologists because the size scaling and the more pronounced cycling in the smaller fractions is responsible for shifts in the species composition and secondary production. The shape of the size scaling is subject of the next chapter.

2. Simulated distribution of assimilated carbon in different phytoplankton size classes

2.1. Introduction

In the last decades considerable research activities developed to understand the role of the ocean as a sink for anthropogenic CO_2 (Sarmiento and Toggweiler (1984), Sarmiento and Siegenthaler (1992), Siegenthaler and Sarmiento (1993)). The biological fixation of dissolved inorganic carbon in the upper layers of the ocean is the major process which is responsible for carbon fluxes to the deep ocean ("biological pump"; Volk and Hoffert (1985), Berger et al. (1989)). The amount of this particle flux to the deep ocean ("export production") is mainly controlled by the fixation of carbon into the particles (primary production; pump input) and by biological, chemical and physical processes that control the degradation and sinking of the produced particles (pump efficiency, Berger et al. (1989)). Although some studies show direct correlations of primary production to particle flux (Eppley and Peterson (1979), Süss (1980), Betzer et al. (1984), McCave (1984), Asper et al. (1992), Lohrenz et al. (1992)), this pattern is not generally observed (Martin et al. (1987), Boyd and Newton (1995)). Abiotic processes like particle aggregation (Kriest and Evans, 1999) and the contribution of different plankton community structures (Michaels and Silver (1988)) are explanations for the observed decoupling of primary production and particle fluxes to the deep ocean. The modelling approach of Boyd and Newton (1999) could reasonably well explain particle fluxes by splitting the producer compartment into several size classes with different sinking rates (50% loss from the largest algal size class).

The authors used empirical data to distinguish the biomass and flux distribution of the different food web components. The theoretical approach of Moloney and Field (1991) to explain food web dynamics also consisted of distinct predefined size classes. The rate parameters for each size class with mass W was computed from the allometric equation $rate = a \cdot W^{\beta_{rs}+1}$. They used the general allometric coefficient $\beta_{rs} = -0.25$ (allometric coefficient for the specific rate) which they extracted from publications (Moloney and Field, 1989). Hurtt and Armstrong (1996) showed that the integration of size related processes into biogeochemical models can significantly improve model fits to BATS (Bermuda Atlantic Time series Study) and OWSI (Ocean Wheather Ship India) data (Hurtt and Armstrong (1999)). In contrast to Moloney and Field (1991) the authors did not use single size classes for their approach. To keep the model simple, they integrated the rate derived from the allometric relationship over all size classes. The parameter optimization routine they used estimated the allometric coefficient β_{rs} to be in the range of -0.44 to -0.33, which is significantly lower than the value assumed by Moloney and Field (1989) and Moloney and Field (1991).

The model framework of this study is set up to investigate the influence of the phytoplankton size structure on the carbon assimilation of phytoplankton. The phytoplankton compartment is split into two distinct size classes. Rate process scaling of the size classes is performed using the allometric equation presented above. The model should describe the carbon assimilation measured as size fractionated primary production on a cruise to the oligotrophic subtropical North Atlantic Ocean. An optimization of the model parameters should investigate whether the general allometric coefficient (β_{rs}=-0.25) holds for the carbon assimilation turnover processes or not.

2.2. Background data

The ship experiment performed at Station 159 onboard RV Poseidon (March 2002) served as data basis for the modelling approach. Water samples were taken from five depths which were determined by the fraction of surface light reaching the specific depth (50%, 20%, 11%, 6% and 0.3%). After addition of radioactive ^{14}C-bicarbonate to each sample the bottles were placed in onboard incubators simulating the original light distribution.

The experiments started at 7:30 AM and lasted for 48 hours. After 6, 12, 24 and 48 hours subsamples were filtered on 0.2, 2 and 5 μm filters.

The biomass data (POC/PON) were collected using a size fractionated filtration on GFF filters with the same pore size filters used in the ^{14}C experiment. The samples were dried and measured with a Finnigan elemental analyser (EA-MS).

The background nutrient data were measured onboard using an autanalyser. The system collects data for nitrite, nitrate and ammonium separately. For the modelling experiment these three values were summed to get the total dissolved inorganic nitrogen (DIN).

A detailled description of the experiment and the background data collection is included in chapter 1.2 on page 17.

2.3. Model description

2.3.1. Physical model setup

The model uses five discrete depth levels defined by the ambient light quantity as described for the ship experiment above. Light at sea surface was computed from the astronomic equations of Brock (1981) using direct and indirect irradiance without clouds. The irradiance was calculated for the specific latitude (22.965), day (76) and hour (actual timestep) of the modelling experiment. The depth specific light intensity was computed by multiplying the surface irradiance with the according light percent factor (0.5, 0.2, 0.11, 0.06, 0.003).

A temperature compensation was excluded from these model experiments, because the incubation temperature was equal for all bottles in the ship experiment.

The first tests of the basic model were performed using a time resolution of one minute. To reduce computing time especially for the optimization procedure this resolution was reduced to five minutes. A comparison of the model results revealed no differences for the time resolutions.

2.3.2. Biological model

The model is a simple NPR (Nitrogen/Phytoplankton/Recycling pool) model with a set of state variables representing nitrogen content and a set of state variables representing assimilated carbon which is traced by ^{14}C in the field experiments (figure 2.1). The state variables of the nitrogen variables are named N for dissolved inorganic nitrogen, $P_{s,N}$ for small phytoplankton nitrogen, $P_{l,N}$ for large phytoplankton nitrogen and R_N for recycling pool nitrogen. For carbon the state variables are named accordingly C, P_{s,C_a}, P_{l,C_a} and R_{C_a}. All the state variables are expressed in [mmol $\cdot$ m^{-3}].

Phytoplankton equation

The phytoplankton compartment was divided into two size groups (0.2-5μm and >5μm). Processes which are size dependent are marked with an indexed s for *small* and l for *large* phytoplankton. The nitrogen state equation for the small phytoplankton group is:

$$\frac{\mathrm{d}P_{s,N}}{\mathrm{d}t} = \underbrace{\mu_{Ps}(I,N)\cdot P_{s,N}}_{phytopl.\ growth} - \underbrace{\xi_{Ps,N}\cdot P_{s,N}}_{direct\ remin.} - \underbrace{\omega_{Ps}\cdot P_{s,N}}_{part.trans.P_s\rightarrow R} \tag{2.1}$$

where $\mu_{Ps}(I,N)$ represents the light (I=irradiance) and nutrient (N) dependent growth function which is calculated using equation 2.2. The direct remineralization $\xi_{Ps,N}$ includes processes like passive and active exsudation, losses of dissolved substances by sloppy feeding and viral lysis of entire cells. It is assumed that all of the substances which contribute to these losses can be used for phytoplankton growth. Sedimentation losses are not included into my model formulations, because in the closed incubation bottles no sedimentation losses are expected.

$$\mu_{Ps}(I,N) = \mu_{max}\cdot\min\left(\frac{\alpha\cdot I}{\sqrt{\mu_{max}^2+\alpha^2\cdot I^2}}\ ;\ \frac{N}{k_N+N}\right) \tag{2.2}$$

I used the Liebig minimum approach for determining the resource which is limiting the phytoplankton growth rate for the actual growth conditions. The light limited growth function is derived from Smith (1936). The nutrient limited growth function is derived from Monod (1950). The parameters used in the equations are summarized in table 2.1. The state equation for the larger phytoplankton group looks quite similar than the state equation of the small phytoplankton:

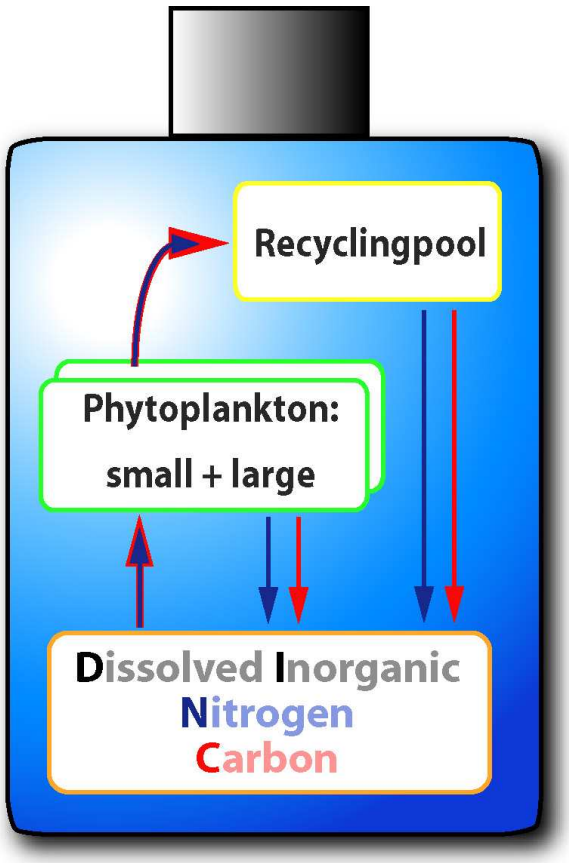

Figure 2.1.: **Model diagram**: The phytoplankton small compartment (in the front) is independent of the phytoplankton large compartment (in the background). The structures of the transfer to and from the phytoplankton are identical for both phytoplankton compartments. For simplification only the fluxes of one phytoplankton compartment are shown. Blue arrows indicate nitrogen and red arrows indicate carbon fluxes. Overlapping arrows show Redfield ratio coupled nitrogen and carbon uptake

$$\frac{\mathrm{d}P_{l,N}}{\mathrm{d}t} = \underbrace{\mu_{Pl}(I,N)\cdot P_{l,N}}_{phytopl.\ growth} - \underbrace{\xi_{Pl,N}\cdot P_{l,N}}_{direct\ remin.} - \underbrace{\omega_{Pl}\cdot P_{l,N}}_{part.trans.P_l\to R} \tag{2.3}$$

Allometry From table 2.1 it is obvious that I do not use a complete parameter set for the larger phytoplankton. I decided to derive the parameters for the larger phytoplankton from the parameters of the smaller phytoplankton. This approach has the advantage that the number of parameters is reduced to get better statistical analysis. All terms which

Table 2.1.: Biological parameters of the model

Parameter	Description	Unit
μ_{max}	maximum phytoplankton growth (small)	day^{-1}
α	initial slope of P–I curve	$(Wm^{-2})^{-1}day^{-1}$
k_N	nutrient half saturation coefficient	mmol N m^{-3}
$\xi_{Ps,N}$	remin. rate of phytoplankton nitrogen (small)	day^{-1}
ξ_{Ps,C_a}	remin. rate of phytoplankton carbon (small)	day^{-1}
$\xi_{R,N}$	remin. rate of recycling pool nitrogen	day^{-1}
$\xi_{R,C}$	remin. rate of recycling pool carbon	day^{-1}
ω_{Ps}	transfer rate from phytopl. small to the recyc.pool	day^{-1}
β_{rs}	allometric coefficient	

have to be scaled are rate processes. All scalings that were performed are based on the general allometric equation $rate = a \cdot mass^b$. Hurtt and Armstrong (1996) modified this general equation to calculate a rate (r_{Cx}) of a specific size class (Cx) from the highest rate (r_{max}) observed (in size class $Crmax$):

$$r_{Cx} = r_{max} \cdot \left(\frac{mass_{Cx}}{mass_{Crmax}} \right)^{\beta_{rs}} \tag{2.4}$$

For the rate processes in my equation: growth rate ($\mu_{Pl}(I, N)$) and remineralisation rate ($\xi_{Pl,N}$) the highest rate is usually observed in the smaller phytoplankton group. Therefore the parameters in table 2.1 are assigned to this group. The according specific mass ratio of the allometric equation is $\frac{mass_{Pl}}{mass_{Ps}}$. From the data I could not fix the correct mass ratio of the two phytoplankton size classes, especially because the larger size class had no upper limit. For the model runs that are present here the specific mass ratio was assigned to a value of 10. This value indicates that the cell diameter of the larger phytoplankton will be about the 2.1 fold of the cell diameter of the small phytoplankton. This factor could be too small. Therefore, the influence of larger mass ratios on the allometric coefficient is discussed in an extra paragraph.

The growth rate was first calculated for the small phytoplankton group using equation 2.2. From these results and the predefined remineralisation rate parameter the according rates for the larger phytoplankton group were calculated using:

$$\mu_{Pl}(I,N) = \mu_{Ps}(I,N) \cdot \left(\frac{mass_{Pl}}{mass_{Ps}}\right)^{\beta_{rs}} \quad (2.5)$$

$$\xi_{Pl,N} = \xi_{Ps,N} \cdot \left(\frac{mass_{Pl}}{mass_{Ps}}\right)^{\beta_{rs}} \quad (2.6)$$

$$\omega_{Pl} = \omega_{Ps} \cdot \left(\frac{mass_{Pl}}{mass_{Ps}}\right)^{\beta_{rs}} \quad (2.7)$$

Recycling Pool equation

The recycling pool is a heterogenous compartment which consists of detritus and zooplankton. Bacteria are not included in this model. Their function and contribution to the carbon turnover is not adequatly represented by any of the pools and the corresponding turnover processes. The recycling pool formulation and the according transfer functions are kept simple to reduce the number of parameters. In my study the recycling pool serves as a phytoplankton loss pool with reduced and delayed remineralisation.

The state equation is:

$$\frac{\mathrm{d}R_N}{\mathrm{d}t} = \underbrace{\omega_{Ps} \cdot P_{s,N}}_{part.trans.P_s \to R} + \underbrace{\omega_{Pl} \cdot P_{l,N}}_{part.trans.P_l \to R} - \underbrace{\xi_{R,N} \cdot R_N}_{direct\ remin.} \quad (2.8)$$

All other formulations like zooplankton require more complicated grazing kinetics with extra parameter sets.

Dissolved Inorganic Nitrogen equation

The dissolved inorganic nitrogen pool of the subtropical ocean is dominated by ammonia (NH_4^+). Nitrate (NO_3^-) is only detectable below the euphotic zone. In my model these two inorganic nutrients contribute to the DIN pool. It is assumed that all losses from the phytoplankton and recycling compartment are ammonia. Both the increased nitrate level in the deepest sample and the remineralised ammonia is treated as one nitrogen pool.

The state equation of dissolved inorganic nitrogen is:

$$\frac{\mathrm{d}N}{\mathrm{d}t} = \underbrace{\xi_{Ps,N} \cdot P_{s,N}}_{remin.\ P_s} + \underbrace{\xi_{Pl,N} \cdot P_{l,N}}_{remin.\ P_l} + \underbrace{\xi_{R,N} \cdot R_N}_{remin.\ R} - \underbrace{\mu_{Ps}(I,N) \cdot P_{s,N}}_{P_s\ growth} - \underbrace{\mu_{Pl}(I,N) \cdot P_{l,N}}_{P_l\ growth} \quad (2.9)$$

Carbon uptake equations

The carbon pool was designed to simulate the carbon uptake and turnover of the small phytoplankton, the large phytoplankton and the recycling pool. The uptake kinetics are linked to the nitrogen uptake through the Redfield factor (r_f). The carbon remineralisation parameters are independent of the nitrogen turnover. All model formulations describing carbon uptake and turnover processes are labeled with the index C_a for assimilated carbon, although especially values of the carbon state variables from the second half of the experiment better describe the absolute carbon turnover than the assimilated carbon. The according equations for the carbon state variables are:

Phytoplankton (small):

$$\frac{\mathrm{d}P_{s,C_a}}{\mathrm{d}t} = r_f \cdot \mu_{Ps}(I,N) \cdot P_{s,N} - \xi_{Ps,C_a} \cdot P_{s,C_a} - r_f \cdot \omega_{Ps} \cdot P_{s,N} \tag{2.10}$$

Phytoplankton (large):

$$\frac{\mathrm{d}P_{l,C_a}}{\mathrm{d}t} = r_f \cdot \mu_{Pl}(I,N) \cdot P_{l,N} - \xi_{Pl,C_a} \cdot P_{l,C_a} - r_f \cdot \omega_{Pl} \cdot P_{l,N} \tag{2.11}$$

the remineralisation rate (ξ_{Pl,C_a}) is calculated from:

$$\xi_{Pl,C_a} = \xi_{Ps,C_a} \cdot \left(\frac{mass_{Pl}}{mass_{Ps}}\right)^{\beta_{rs}} \tag{2.12}$$

Recycling pool:

$$\frac{\mathrm{d}R_{C_a}}{\mathrm{d}t} = r_f \cdot \omega_{Ps} \cdot P_{s,N} + r_f \cdot \omega_{Pl} \cdot P_{l,N} - \xi_{R,C_a} \cdot R_{C_a} \tag{2.13}$$

Dissolved Inorganic Carbon:

$$\begin{aligned}\frac{\mathrm{d}C}{\mathrm{d}t} =& \xi_{Ps,C_a} \cdot P_{s,C_a} + \xi_{Pl,C_a} \cdot P_{l,C_a} + \xi_{R,C_a} \cdot R_C - \\ & r_f \cdot \mu_{Ps}(I,N) \cdot P_{s,N} - r_f \cdot \mu_{Pl}(I,N) \cdot P_{l,N}\end{aligned} \tag{2.14}$$

Model Initialisation

Nitrogen compartment The nitrogen compartment was initialised with DIN data from St.159 of the Poseidon 284 cruise. The phytoplankton (small and large) biomass values were computed from the PON measurements. The different biomass fractions corresponding to the model compartments were not directly measured. Before I calculated the phytoplankton fractions, 10% of the total biomass (PON) was assigned to the recycling pool. The remaining 90% of the PON were split into the small and large phytoplankton compartment according to the average PON ratio ($PON(< 5\mu m) \cdot PON(> 5\mu m)^{-1} = 1.8$) that was measured at St.159.

Carbon compartment The initial values of the carbon compartment were artificial, because it should directly simulate the carbon uptake which was derived from the ^{14}C experiment during the cruise. The initial values of phytoplankton (small and large) and of the recycling pool were set to zero for all depths because the assimilated carbon traced by ^{14}C was zero in all biomass fractions at the start of the experiment. The specific setup of the carbon compartment and the initial values lead to errors, because in the natural system even at the beginning of the experiment a loss from all carbon compartments occurs. In the model simulation this is suppressed by the low carbon initial values. From the observation of the ^{14}C experiment and the first model runs it was obvious that this error can be neglected, because the experiments started at sunrise with enhanced carbon assimilation and therefore the loss terms of the model reach their correct values within the first model time steps.

The background dissolved inorganic assimilable carbon was assigned to a value of 2200 mmol DIC $\cdot$ m^{-3}. It was observed how this assimilable DIC is channeled through the modelled food web.

Model optimization

To get appropriate results from the model it is essential to choose the correct parameter set. One way to reduce the potential range of each parameter is to use a systematic optimization procedure which tests randomized sets of parameters for their model output according to observations made onboard. This optimization procedure can be compared to a non-linear regression. These model observation comparisons are done by computing the cost function term (difference between observations and model output) for six variables. From the nitrogen model compartments, the small and large phytoplankton, the recycling pool and the DIN were included. From the carbon model compartments the small phytoplankton and the sum of the large phytoplankton and the recycling pool were used. The model output of 24 and 48 hour time step were used to calculate the cost function. These time steps were used because at these points the assumptions to fix the observations are quite simple. Because the oligotrophic system is very stable I assumed that all nitrogen state variables should be the same at the start and after 24 and 48 hours. In the meantime changes in the state variables can occur, but after 24 hours they should come back to the start values.

The assimilated carbon values should follow the calculated carbon uptake derived from the ^{14}C measurements. For the measurements filters were used as size delimiters. Values for the two size classes were distinguished by parallel filtration with different filter pore sizes (0.2 μm; 5 μm). The 0.2 μm filter values represent the total ^{14}C uptake. The carbon uptake small fraction ($< 5\mu$m) was computed by subtracting the 5μm value from the total. The result was assigned to P_{s,C_a} from the model. The 5μm filter (carbon uptake large fraction) was assigned to the sum of P_{l,C_a} and R_{C_a} from the model.

The single cost funtion term (C_{SV}) for one state variable (SV) results from equation 2.15:

$$C_{SV} = \sum_{depth=1}^{5} \sum_{t=24h}^{48h} \left(\frac{SV_{M,t} - SV_{O,t}}{SV_{O,t}} \right)^2 \cdot s_f \tag{2.15}$$

C_{SV}	Cost function of state variable (SV)
$SV_{M,t}$	State variable output from model at time t
$SV_{O,t}$	State variable observation at time t
s_f	Scaling factor

This cost function term of each state variable or transferred state variable was summed to get the overall cost function value (C_{total}) for one set of parameters:

$$C_{total} = C_{Ps,N} + C_{Pl,N} + C_{R,N} + C_{DIN} + C_{s,C_a} + C_{l,C_a} \tag{2.16}$$

Term C_{s,C_a} represents the cost function term of the carbon assimilation small, and C_{l,C_a} represents the cost function term of the carbon assimilation large fraction.

The scaling factors of the single cost function computation (equation 2.15) were included to pronounce the importance of the carbon turnover processes (see table 2.2):

Table 2.2.: Scaling factors of the cost function equation

Cost function variable	Scaling factor (s_f)
Phytoplankton nitrogen	1
Recycling pool nitrogen	1
Dissolved Inorganic Nitrogen	1
Carbon uptake	5

Optimization procedure The cost function value is computed for 40000 randomized parameter sets in preselected parameter ranges. The a priori bounds of the parameter ranges are given in table 2.3. Best model fits correspond to minima in the cost function values. The first step is to visualize the cost function results for the predefined parameter ranges. Therefore, each parameter axis range was splitted into 100 equal segments. About

400 cost function values should be stored in the optimization matrix for each of these segments, because the 40000 parameter sets were chosen randomly. For each of these segments the minimum cost function value was extracted from these 400 values in the optimization matrix. This mimimum was plotted against the corresponding parameter value (see figure 2.2). When starting an optimization, only few of the parameters showed clear trends in the cost function (strong parameters). For the other parameters no or only weak trends can be extracted from noise. To visualize all trends more clearly the noise was reduced by using a smoothing algorithm spanning over six parameter segments.

Table 2.3.: Parameter ranges at the start of the optimization

Parameter	Minimum	Maximum	unit
μ_{max}	0.01	100	day^{-1}
α	0.01	1	$(\mathrm{Wm}^{-2})^{-1}\mathrm{day}^{-1}$
k_N	0.01	1	mmol N m^{-3}
$\xi_{Ps,N}$	0.01	1	day^{-1}
ξ_{Ps,C_a}	0.01	1	day^{-1}
$\xi_{R,N}$	0.01	1	day^{-1}
$\xi_{R,C}$	0.01	1	day^{-1}
ω_{Ps}	0.01	1	day^{-1}
β_{rs}	-1	0	

Besides the visual control of the optimization the minima were derived numerically from the cost function matrix. For this purpose the parameter values for the lowest, the second lowest, the five lowest and the twenty lowest cost function values were extracted from the cost function matrix. For the five lowest and the twenty lowest cost function values the parameter range was computed. A comparison of the four parameter sets or -ranges allows to determine which parameters converge in the optimization.

Minima extracted from the numerical analysis were compared with the results from the corresponding figures to investigate whether these minima are local or global minima. The global minima were fed into the basic model to analyse the dynamics and state variables of the model. If this analysis resolves inconsistencies in certain state variables, because the assumptions of the optimization were too strict, additional model runs were performed to investigate alternative setups.

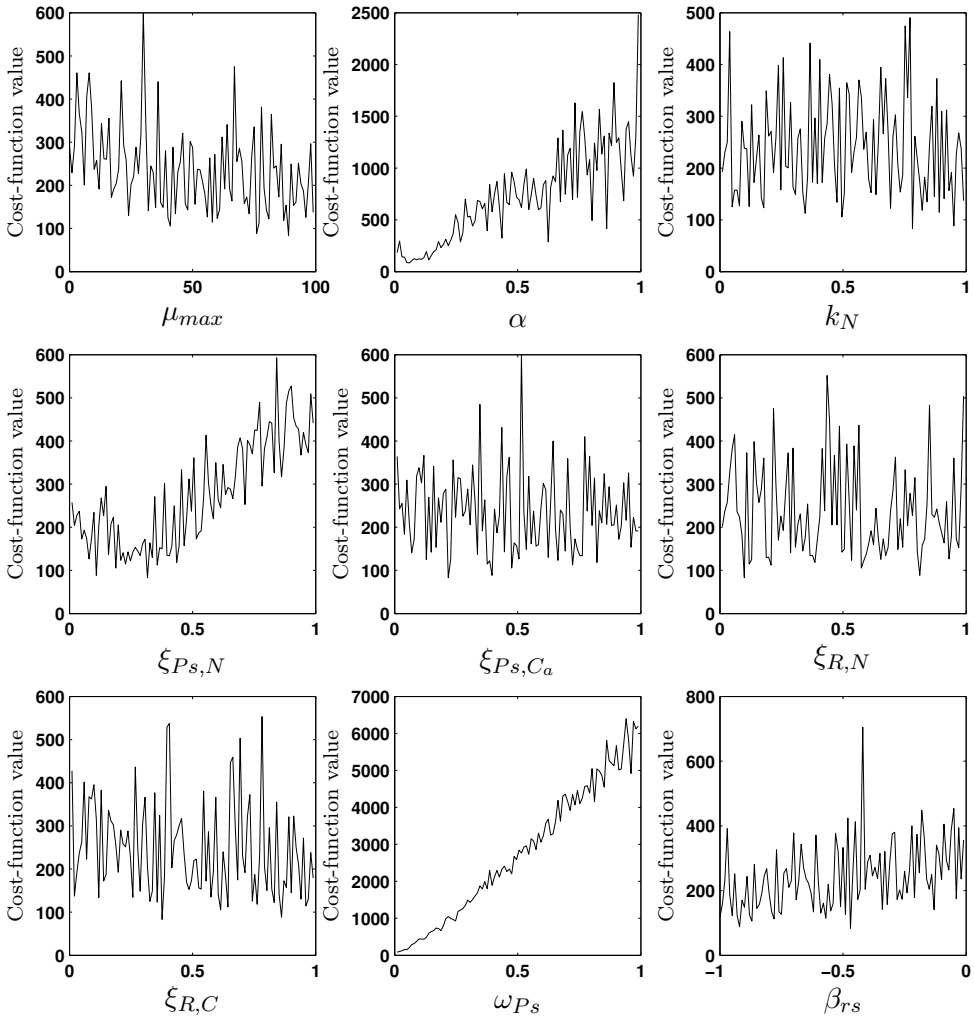

Figure 2.2.: Minimum cost function overview (raw data). The parameter axis range was splitted into 100 equal segments. For each of these segments the minimum cost function value was extracted from the optimization matrix. This mimimum was plotted against the corresponding parameter value

2.4. Results

2.4.1. Optimization

The structure of the cost function is set up to show values near zero if model and observation fit perfectly. The raw data, especially from the first optimization run, show large amplitudes of the cost function for the different parameters (see figure 2.2). The large amplitudes are due to noise in the cost function because of the randomized combination

of parameters. The minimum of the cost function from the first run was near 100, the maximum was near 6000. The maximum values in the cost function are only visible in the parameter which is responsible for these high values. In the first run the transfer rate from phytoplankton to the recycling pool ω_{Ps} showed the most obvious trend and the highest cost function values. The lowest cost function values were achieved for ω_{Ps} values below 0.03. Besides this parameter, α and $\xi_{Ps,N}$ showed remarkable trends with global minima ($\alpha \approx 0.07$; $\xi_{Ps,N} \approx 0.2$). For the other parameters the noise was too high, even when using the smoothed distribution, to obtain any global minima. Therefore, I started a new optimization with reduced parameter ranges. These ranges were extracted from the 20 lowest cost function values as described in material and methods.

The range of the cost function values from the second run was much smaller (60–110). For five of the nine parameters the trend is clearly visible (α, $\xi_{Ps,N}$, ξ_{Ps,C_a}, ω_{Ps}, β_{rs}; see figure 2.3). Three of the remaining four parameters show trends in the smoothed cost function figure, but the ranges of the minima are much wider (μ_{max}, k_N, $\xi_{R,C}$). Only for $\xi_{R,N}$ no trend was visible.

Both α and $\xi_{Ps,N}$ showed a distinct minimum (≈ 0.06 and ≈ 0.2) as mentioned from the first run. For ξ_{Ps,C_a}, ω_{Ps} and β_{rs} no such minimum can be observed. The cost function values decrease steadily for parameter values approaching the lower parameter limit. For ξ_{Ps,C_a} and ω_{Ps} the cost function decreases linearly but for β_{rs} the cost function converges for parameter values lower than -0.6.

I performed a third optimization run to check if smaller parameter ranges would resolve more obvious trends for the remaining four parameters, especially for $\xi_{R,N}$. The results showed only minor changes. Therefore, I decided to perform the basic model analysis based on the second optimization run. The parameter ranges for the lowest cost function values were extracted as described earlier (see table 2.4).

Although in the smoothed figures local minima can be observed, the numerical parameter range analysis often show larger ranges, because single value minima in the optimzation matrix can spread over these local minima. For the determination of the starting parameter set (see table 2.5) of the detailled output analysis I extracted global minima. If these span over a larger range I used the center of these ranges.

Table 2.4.: Parameter ranges of the optimization. The left minima and maxima are from the 5 lowest cost function values. The right minima and maxima are from the 20 lowest cost function values

	based on 5 values		based on 20 values		
parameters	Minimum	Maximum	Minimum	Maximum	Unit
μ_{max}	64.9	96.1	27.8	96.1	day^{-1}
α	0.057	0.067	0.052	0.075	$(Wm^{-2})^{-1}day^{-1}$
k_N	0.075	0.36	0.075	0.72	mmol N m^{-3}
$\xi_{Ps,N}$	0.17	0.25	0.13	0.25	day^{-1}
ξ_{Ps,C_a}	0.078	0.13	0.078	0.3	day^{-1}
$\xi_{R,N}$	0.33	0.86	0.13	0.92	day^{-1}
$\xi_{R,C}$	0.22	0.91	0.22	0.94	day^{-1}
ω_{Ps}	0.01	0.011	0.01	0.014	day^{-1}
β_{rs}	-0.88	-0.64	-0.99	-0.57	

Table 2.5.: Parameter set of basic model analysis extracted from the optimization matrix

Parameter	Value	Unit
μ_{max}	96	day^{-1}
α	0.066	$(Wm^{-2})^{-1}day^{-1}$
k_N	0.075	mmol N m^{-3}
$\xi_{Ps,N}$	0.24	day^{-1}
ξ_{Ps,C_a}	0.12	day^{-1}
$\xi_{R,N}$	0.33	day^{-1}
$\xi_{R,C}$	0.86	day^{-1}
ω_{Ps}	0.011	day^{-1}
β_{rs}	-0.88	

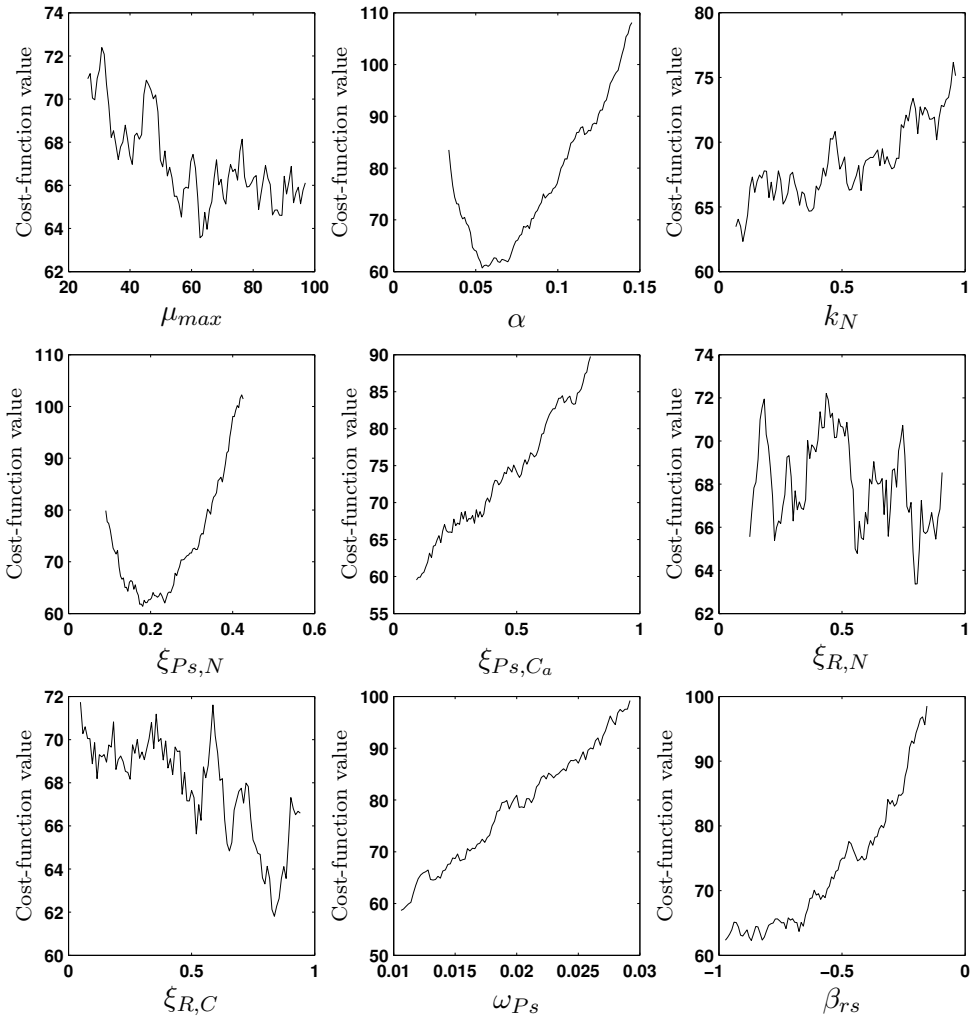

Figure 2.3.: Minimum cost function overview (smoothed). The parameter axis range was splitted into 100 equal segments. For each of these segments the minimum cost function value was extracted from the optimization matrix. This mimimum was plotted against the corresponding parameter value

2.4.2. Basic model analysis

The detailled analysis of model output offers the possibility to check if a model can reproduce general observation patterns and quantities. One of the basic patterns that was quite well reproduced is the daily light induced biomass increase in the small and large phytoplankton (see figure 2.4). One assumption of the optimization was the recurring nitrogen values after 24 and 48 hours. This assumption was not fulfilled for all state variables. Only the large phytoplankton showed this pattern quite well. The small phy-

toplankton decreased in the deep layers. Especially the recycling pool nitrogen decreased rapidly during the first hours of the model experiment in all depth layers. Therefore, I performed additional model runs with stepwise reduction of the recycling pool loss term ($\xi_{R,N}$).

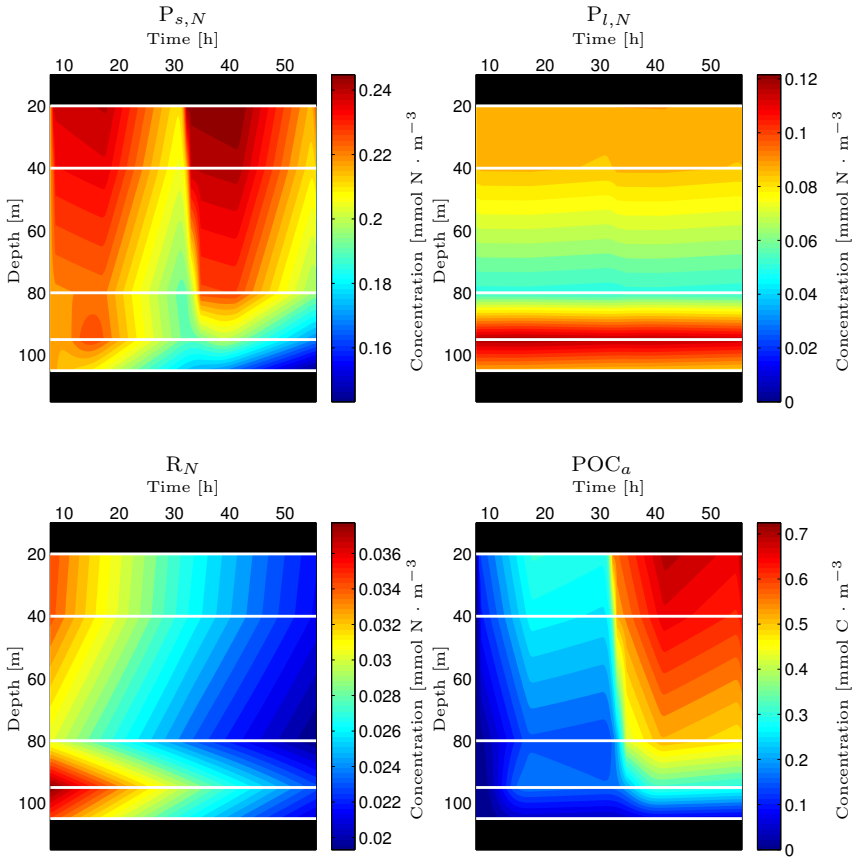

Figure 2.4.: Basic model output; parameterset from table 2.5; Phytoplankton and Recycling Pool state variables over time; POC_a compartment represents the sum of the three particulate carbon pools; white lines indicate modelling depths, intermediate values were linearly interpolated by the graphic routine

Parameter modifications

Much better results were achieved with a $\xi_{R,N}$ value of 0.08. For this model run the recycling pool nitrogen showed nearly the same pattern than the other nitrogen state variables. Besides the reduction in nitrogen loss from the recycling pool the parameter adjustment also reduces the total assimilated carbon. From the first model runs it was

obvious that the total assimilated carbon that was observed in the ^{14}C experiments was not reached by the model. The highest model value of 0.8 only represents 80% of the observed value. An increase of carbon assimilation is only possible by increasing the growth rates or decreasing the loss rates. The maximum growth rate (μ_{max}=96 day^{-1}) is very high. But this maximum growth rate is never achieved. Either nutrient or light limits the growth rate. Therefore, the realised growth rate is more important (see figure 2.5). It is mainly controlled by the low nitrogen values in the upper layer and the low light in the deeper layers.

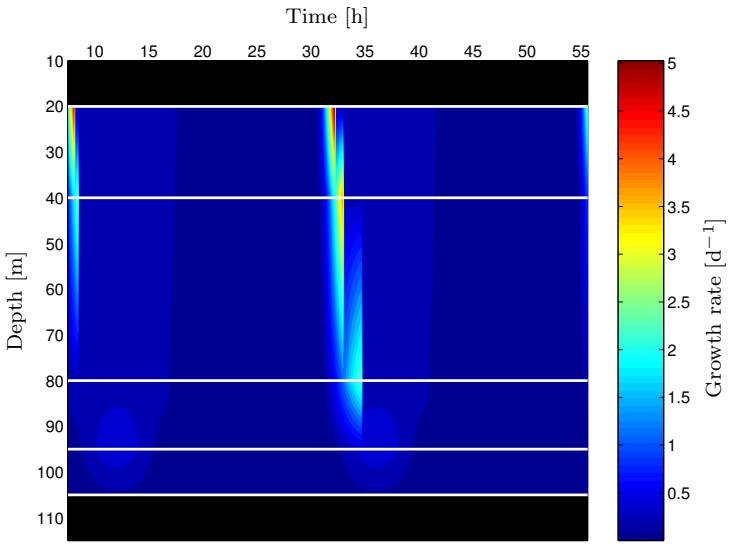

Figure 2.5.: Realised growth rate μ_r for the model run with the basic parameter set (see table 2.5); white lines indicate modelled depths, intermediate values were linearly interpolated

The structure of the realised growth rate followed the assumptions from ressource distribution. But the absolute value was much too high (5 day^{-1}). In the literature maximum values of 3 day^{-1} were published. Therefore, I decided to reduce the maximum growth rate μ_{max} stepwise. Appropriate realised growth rate ($\mu_r \leq 2$) values were reached for μ_{max} values below 5 day^{-1}. When reaching such realistic growth rates the assimilated carbon is further decreased to 0.55 mmol C $\cdot$ m^{-3}. Above I mentioned that an increase in the maximum growth rate can eliminate the bias in the assimilated carbon results. But because of the unrealistically high growth rates a further reduction of the assimilated carbon must be tolerated. Because the growth in the model is mainly fueled by nitrogen

and the surrounding nitrogen is depleted, an increase in phytoplankton nitrogen loss $\xi_{Ps,N}$ could lead to an increased carbon assimilation. I stepwise increased the $\xi_{Ps,N}$ value to 0.5 day^{-1} with a maintained μ_{max} value of 5 day^{-1}. The resulting carbon assimilation is very close to the observed 1 mmol C $\cdot$ m^{-3}. The maximum realised growth rate for this parameterset was 3.4 day^{-1}. After the modifications the output of the final model run fits the assumptions and data from the ship experiments much better (see figure 2.6).

Final model output

The picture of the state variables was much more consistent with the data after the modifications. Both small and large phytoplankton nitrogen ($P_{s,N}, P_{l,N}$) showed typical daily progress in the upper layers, with maximum values (0.23, 0.09 mmol N $\cdot$ m^{-3}) at noon. The decrease at night was about 22% of the maximum values for $P_{s,N}$ and about 10% for $P_{l,N}$. Only slight net growth could be observed for the deep layers. The high loss rates, especially for the small phytoplankton, led to a 30% decrease in biomass for the deep layers. The continuous negative trend seemed to become flattened, but a possible steady state could not be observed in the 48 h experiment. Loss for the larger phytoplankton only achieved maximal values of approximately 5%. The recycling compartment started with values of 0.0345 mmol N $\cdot$ m^{-3} in the upper layer and 0.038 mmol N $\cdot$ m^{-3} in the deeper layer. For all layers a slight decrease (3-5%) could be observed. The overall loss in nitrogen in all compartments leaded to a corresponding increase of dissolved inorganic nitrogen, especially in the deep layers ($\approx$32%). During the night an increase in the upper layers could also be observed (from 0.02 to $\approx$0.05 more than 100%). This elevated dissolved inorganic nitrogen was completely eliminated during the day.

Patterns of the assimilated carbon followed the observations very closely. The maximum uptake per day was nearly equal for both days (0.5 mmol C $\cdot$ m^{-3}). During the night a slight decrease occured (0.05 mmol C $\cdot$ m^{-3}).

Allometry

The rates of the larger phytoplankton were computed from previously derived rates of the smaller phytoplankton by appliing the allometric scaling. Therefore, changes in the allometric coefficient only affect the state variables of the large phytoplankton. The

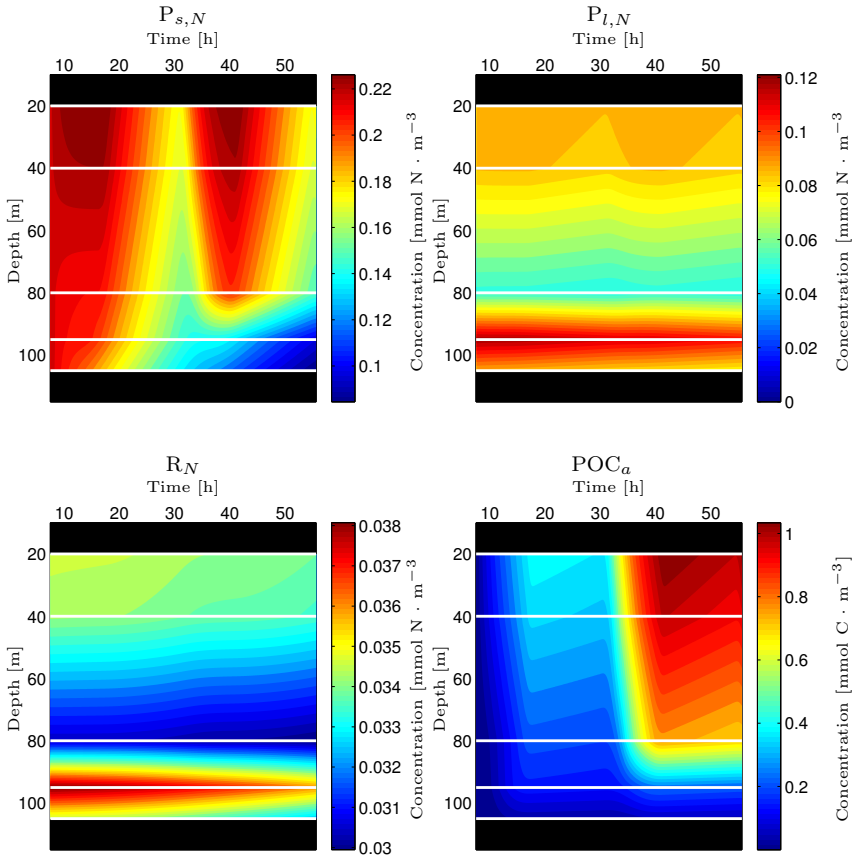

Figure 2.6.: Final model output; parameterset from table 2.5 with modifications: μ_{max}=5, $\xi_{Ps,N}$=0.5 and $\xi_{R,N}$=0.08; Phytoplankton and Recycling Pool state variables over time; $P_{s,N}$: small phytoplankton nitrogen; $P_{l,N}$: large phytoplankton nitrogen; R_N: recycling pool nitrogen ; POC_a compartment represents the sum of the three particulate assimilated carbon pools; white lines indicate modelling depths, intermediate values were linearly interpolated by the graphic routine

results presented above are based on an allometric coefficient (β_{rs}) of -0.88. This low coefficient suppressed nearly all daily patterns in the large phytoplankton nitrogen. The color resolution of figure 2.6 only revealed daily increase and decrease for the 40m depth level.

Besides the absolute values of the assimilated carbon, the splitting of the value into the small and large plankton fraction is crucial for these modelling experiments. Observations of station 159 from the Poseidon cruise 284 showed an increasing carbon assimilation ratio ($C_{up;small} \cdot {C_{up;large}}^{-1}$) with depth (7.3 (20m) to 17.5 (105m)). The range of these observations correspond to the values found in the model although the depth distribution was different (see figure 2.7). An increase of β_{rs} to -0.5 did not change the corresponding total carbon uptake, but the carbon assimilation ratio was decreased to 5.5–7.

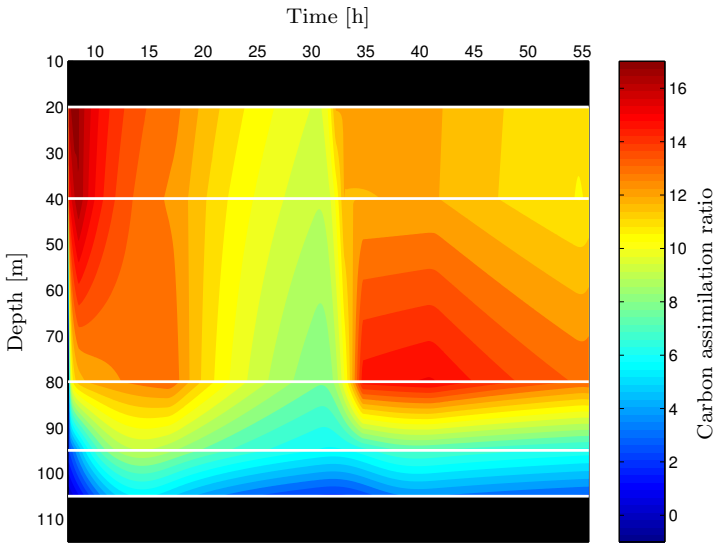

Figure 2.7.: Carbon assimilation ratio $C_{up;small} \cdot {C_{up;large}}^{-1}$ from a model run using the modified parameter set with β_{rs}=-0.88

2.5. Discussion

2.5.1. Optimization

The dynamics of modelling approaches depend to a high degree on the preselected parameter values. One approach choosing the best parameter value is to search a predefined

multidimensional parameter space for minima of the model-observation difference (residuals). There are two ways to search these minima. Several techniques (adjoint method (Schartau et al. (2001), genetic algorithm (Schartau and Oschlies (2003))) search the parameter space for minima of the residuals in a directed way using special functions. My approach scans the entire parameter space and visualizes the model data misfit. The perceptability of the resulting cost function trends depends on the total number of optimization runs, because they determine the error amplitude for the parameter segments. For the weak parameters the cost function trend can be masked by this error amplitude. For $\xi_{R,N}$ no trend can be extracted, because the maximum cost function trend amplitude (2) was equal to the error amplitude. Even a further reduction of the other parameter boundaries did not reveal any trend. An increase of the optimization runs is not practicable, because a necessary exponential increase of runs will also increase computation time exponentially (22h for 40000 runs).

2.5.2. Parameter values

The numerical analysis of the cost function matrix revealed certain ranges for all parameters. For the detailled analysis I chose the parameter set as described above. Within this section I want to discuss the parameter ranges which are derived from the five smallest cost function values (see table 2.4).

Modified parameters

The first model run with parameter values derived from the optimization revealed too high losses in the recycling pool nitrogen state variable ($\xi_{R,N}$=0.33 day^{-1}) and an unrealistically high realised growth rate (μ_r=5 day^{-1}). The reason for these wrong parameter values is the coupling of the nitrogen and carbon assimilation. The influence of a deviation from this tight coupling is discussed in chapter 2.5.3. On the one hand the optimization is set up to maintain the nitrogen pools, and on the other hand dissolved nitrogen is needed to fuel the high carbon uptake values. The optimization solves the counteracting assumptions by remineralising as much nitrogen as possible and by assuming unrealistic growth rates. I compensated these difficulties by loosening the assumptions. First I decreased $\xi_{R,N}$ to 0.08 day^{-1}, a value that corresponds to literature (Evans and Garcon (1997):0.03-

0.21 for zooplankton and 0.1-0.4 for detritus, Hurtt and Armstrong (1996): case 1(less realistic) 0.397; case 2(more realistic) 0.056, Hurtt and Armstrong (1999): 0.05-0.06). The next step was to reduce the maximum growth rate μ_{max} to 5 day^{-1}. This resulted in a realised growth rate (μ_r) of about 1.45 day^{-1}, a value that corresponds to the maximum values published by Hurtt and Armstrong (1996) (0.48-1.2) and which are twice the values published by Bissett et al. (1994) (0.63-0.9). All these modifications resulted in halved total carbon uptake (0.5 mmol C $\cdot$ m^{-3}), because the nitrogen supply was too low (0.038 mmol N $\cdot$ m^{-3}). An increase of $\xi_{Ps,N}$ to 0.5 day^{-1} doubled the nitrogen supply and therefore the carbon uptake. Other modelling studies revealed phytoplankton loss values below 0.1 day^{-1} (Evans and Garcon (1997),Schartau and Oschlies (2003)). Besides the increase in carbon uptake the maximum realised growth rate was further increased ($\mu_r \approx$2 day^{-1}) to the two- to threefold of the literature values.

Unmodified parameters

The initial slope of the P-I curve α was 0.05-0.07 (W m^{-2})$^{-1}$ d^{-1}, which matches the classical assumed values of 0.025 of Fasham et al. (1990). This parameter range is also revealed by Evans (1999) and Fennel et al. (2001). Higher values of α were published for some data-assimilation approaches (Schartau and Oschlies (2003): 0.25, Hurtt and Armstrong (1999)), but the authors stated that these high values resulted from assimilating data of an early spring bloom at Ocean-Weather-Ship India under low light conditions. The low α value of my model experiment is necessary to reduce carbon assimilation in the deep layers. The observations showed carbon uptake of about 15% for the deep layers compared with the upper layers. The computation of the light field which is fed into the growth equations was run without cloud attenuation. All growth is therefore computed under maximum light conditions. When including cloud attenuation, the α value will be increased slightly.

The half saturation constant of the nitrogen uptake k_N was 0.07-0.36 mmol N m^{-3}. This range fits well to literature values (Fasham et al. (1990): 0.5, Evans and Garcon (1997): 0.01-1.5, Hurtt and Armstrong (1996): 0.0024-0.0102, Hurtt and Armstrong (1999): 0.23-0.92, Schartau and Oschlies (2003): 0.7). From this parameter range I chose a value (0.1) at the lower boundary, because the cost function distribution (see figure 2.3) showed a

slight trend towards the lower boundary. This low value is necessary to permit the high growth rates which have to be achieved.

The particle loss coefficient ω_{Ps}, which is responsible for fluxes from phytoplankton to the recycling pool, was estimated to be 0.011 d^{-1}. The range of this parameter was very narrow, and the cost function increased remarkably at values above 0.03. My results correspond to the values published by Evans and Garcon (1997) (0.015-0.5 PHY→DET fluxes) and Hurtt and Armstrong (1999) (0.056-0.073). The higher values of Hurtt and Armstrong (1996) (0.43-1.13) are not explained in their article. Low ω_{Ps} values in my experiment conserve the carbon and the nitrogen distribution of the different state variables. Higher values will remarkably increase recycling pool nitrogen values, because this transfer is directly fueled by much higher nitrogen values of the small phytoplankton state variable. The same is valid for the assimilated carbon state variables.

The two carbon remineralisation coefficients ξ_{Ps,C_a} and ξ_{R,C_a} were introduced to offer the possibility that the model can leave the Redfield conditions. The values of the parameters (ξ_{Ps,C_a}=0.07-0.13 d^{-1}, ξ_{R,C_a}=0.22-0.91 d^{-1}) are quite contrarily. The low ξ_{Ps,C_a} value was liable to retain the assimilated carbon of the small particles to reach the high observation values. The much lower carbon observations for the larger particles could be reached without retaining the carbon. Therefore, the ξ_{R,C_a} value was responsible for conserving the carbon assimilation difference of small and large particles.

Allometric coefficient

The allometric coeffcient β_{rs} of my model is responsible for scaling the rate processes of the small and large phytoplankton state variables. Its value was estimated to be in the range of -0.88 to -0.64. Model tests with an increased allometric coefficient of -0.5 showed decreased carbon uptake ratios.

Values derived from single-species growth experiments revealed allometric coefficients of -0.1 to -0.3 (Banse (1976), Schlesinger and Molot (1981), Sommer (1989), summarized in Moloney and Field (1989) and Chrisholm (1992)). Only under light limiting conditions lower allometric coefficients can be achieved (Finkel (2001): -0.45, summarized in Raven and Kübler (2002)). Banse (1976) suggested that the environemental conditions can have a notable influence on the allometric coefficients.

The value of the allometric coefficient depends on the mass ratio and the rate ratio of the small and large phytoplankton. In my model experiment only the carbon assimilation was simulated. Therefore I concentrate on the carbon assimilation as a source for the low allometric coefficient . The observed carbon mass ratio (small $\cdot$ large^{-1}) of the two phytoplankton size classes was much lower (1.8) than the carbon assimilation ratio (≈ 8). These large differences can only be achieved by a low allometric coefficient (like in this case) or by using asymetric allometric scaling coefficients for uptake and loss rates (Laws, 1975). As mentioned above, the carbon assimilation directly influences the resulting allometric coefficient. Additionally the nitrogen turnover also influences the results of the optimization routine.

To get an insight of the influence of the carbon processes, I computed the allometric coefficient β_{rs} from carbon uptake of the 24 hour ^{14}C incubation and biomass data from the cruise. From the size fractionated carbon assimilation and the size fractionated POC data the specific carbon assimilation (C_{spec}) was calculated for the two size classes. A modified version of equation 2.4

$$\beta_{rs} = \frac{\log\left(\frac{C_{spec,low}}{C_{spec,high}}\right)}{\log(massratio)} \tag{2.17}$$

was used to compute β_{rs} for three profiles from the cruise (see figure 2.8).

Here, I focus on the values of station 159. The values of the upper three depths range from -0.75 at the subsurface to -0.45 at the deep chlorophyll maximum. This way of computing β_{rs} values assumes an instantaneous carbon assimilation within 24 hours. Therefore, these values mark the upper boundary that can be expected. Additional biological processes tend to further decrease the allometric coefficient (β_{rs}). The best model cost function values are achieved for β_{rs} values below -0.6. It seems that not only the carbon, but also the nitrogen distribution or the model structure contributes to the slightly lower allometric coefficient.

The absolute value of the allometric coefficient depends on the specific mass ratio (see equation 2.4). A value of 10 was assigned to the mass ratio. The larger size class was defined by using a 5μm pore size filter. This results in a size class which is missing an upper limit. Therefore the mass ratio I assumed could be even higher.

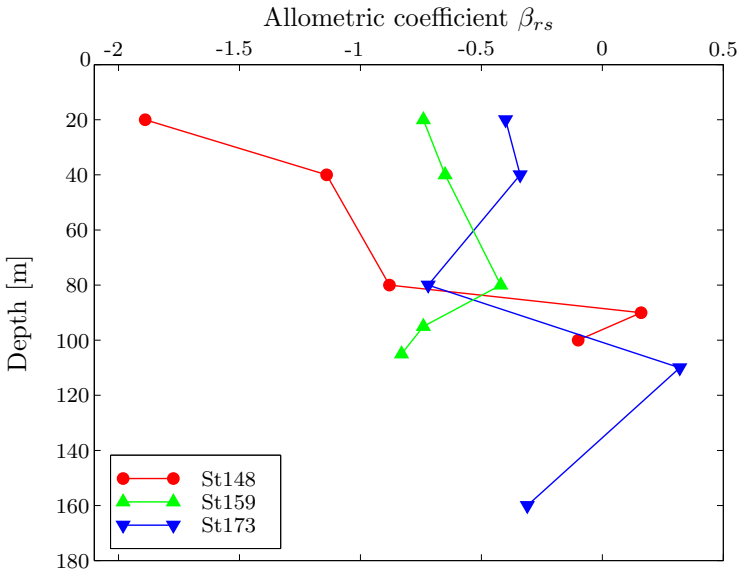

Figure 2.8.: Allometric coefficient β_{rs} computed from cruise carbon assimilation and POC data; values below 80m are uncertain, because carbon assimilation was low

A conversion of equation 2.4 allows to compute β_{rs} values for other mass ratios (see equation 2.18).

$$\beta_{rs,2} = \beta_{rs,1} \cdot \frac{\log(mass\ ratio_1)}{\log(mass\ ratio_2)} \tag{2.18}$$

Possible assumptions of the size ranges of the major primary producers could be 0.6-5μm of the small phytoplankton and 5-10μm of the large phytoplankton. These ranges result in mean cell sizes of 1.73 and 7μm. The corresponding mass ratio, assuming equal carbon to volume ratios, would be 66. Recalculating the boundaries of the allometric coefficient β_{rs} (-0.88/-0.6) from my optimization using a mass ratio of 66 leads to new β_{rs} boundaries of -0.48/-0.32. This range fits in the values published by Schlesinger and Molot (1981) and Finkel (2001).

The model structure I presented here is quite simple. Especially for the oligotrophic conditions of the subtropical gyre a remarkable influence of bacteria and DOC can be assumed. Bacteria growing on the DOC loss from the algae can contribute to the carbon tunover I measured. Assuming the same scaling for the DOC loss as for the growth rate, the addition of bacteria will decrease the allometric coefficient even further, because the

extra losses which would be included have to be compensated by an increased average algae growth rate to match the overal carbon turnover rates. When higher DOC losses from larger cells are assumed, the growth rates must also be enhanced. In this case, the allometric coefficient will increase, because carbon is transferred from the large to the small carbon pool. From the present data I can not distinguish these assumptions.

2.5.3. Model results

The model structure I developed is quite simple but it fits the carbon assimilation data quite reasonably. The results from the first model analysis run revealed that especially the nitrogen processes are not well representedin the model. This misfit can result from timing displacement or wrong model formulations. In this case both processes influence the model results. I have shown that parameter modifications can result in reasonable model output for most of the state variables. The remineralisation is one crucial process in the model, because the model carbon uptake relies on the available dissolved inorganic nitrogen. During the night the remineralized nitrogen accumulates in the DIN compartment, because no dark nutrient uptake into internal nutrient pools of the phytoplankton was assumed. This accumulated nitrogen is assimilated by the phytoplankton within the first hours after sunrise. This assimilation has to occur before the optimization routine samples the model. Therefore, an addition of model structure (internal pools) or timing compensation can eliminate difficulties of the remineralisation process.

An increased value of the remineralisation directly or indirectly decreases all three particulate nitrogen state variables. The phytoplankton loss is due to direct loss, where the loss of the recycling pool is mainly caused by the decrease of the small phytoplankton and therefore reduced uptake values. As mentioned before, the high remineralisation is necessary to fuel the high carbon uptake. In my model formulation I used a fixed carbon:nitrogen assimilation ratio of r_f=6.625 (Redfield factor). An increase of this factor or a decoupling would result in a lower remineralisation rate, because less nitrogen is needed to achieve the observed carbon assimilation values. Results from Goldman et al. (1979) not only promote higher carbon to nitrogen values under nutrient limiting conditions, but they also suggested that C:N ratios should not be used as conversion factors. Therefore, a decoupling of the carbon and nitrogen turnover in the model might be quite useful.

POC/PON measurements from the reference station also showed increased C:N values for the smaller size class (C:N:6.6-8). The surface values for the larger size class were estimated to be 9, in the deeper layers C:N decreased to values of about 5-6. I assume that this decrease was due to a larger fraction of degraded detritus in the deeper layers. A comparison of the nitrogen and carbon remineralisation parameters indicates that more carbon was retained in or at the cells, especially in the smaller size class. In the natural system such carbon accumulation must be counteracted by extra carbon losses, for example to the DOC pool.

The carbon assimilation values of the model fit the observations accurately. The complete dataset (6, 12, 24, 48h incubations) of the carbon assimilation experiment onboard showed a slight decrease during night which is due to respiration. Even this decrease in the observations could be resolved by the model.

2.5.4. Summary and conclusion

In this study I set up a model framework to investigate the carbon turnover processes observed in ^{14}C incubation experiments. Within this general topic I focused on the influence of size class processes on carbon turnover in the oligotrophic Atlantic Ocean. Even quite simple models with three compartments (NPR) could adequately fit size fractionated carbon assimilation data. But there were still deficiencies especially in the nitrogen part of the model. High nitrogen losses which were necessary to fuel the high carbon assimilation data may result from the strict coupling of nitrogen and carbon uptake via the Redfield factor. A decoupling might result in more realistic nitrogen and carbon turnover processes.

The size distribution and the size fractionated carbon was only adequatly simulated with an allometric coefficient of about -0.88 (-0.48 for a mass ratio of 66). An increase of the allometric coefficient to -0.5 (-0.27 for a mass ratio of 66) leaded to lower carbon uptake ratios than observed from the ship experiment. The results corresponded to the assumptions that limiting conditions can enhance allometric relationships. Because the findings of the parameter optimization strongly depended on the model structure, the results can only be interpreted in this context. A simplified approach assuming instantaneous carbon uptake into the two phytoplankton size classes revealed allometric

coefficients in the range of -2 to -0.5, which were pretty close to the allometric coefficients of the model.

The results of my model approach correspond to the conclusions of other authors that size related processes are much more common and that including size relationships into biogeochemical models can significantly enhance model usability (Michaels and Silver (1988), Moloney and Field (1991), Boyd and Newton (1995), Hurtt and Armstrong (1996), Boyd and Newton (1999), Hurtt and Armstrong (1999), Baird et al. (2003)).

3. Allometric coefficients for metabolic rate processes in phytoplankton

3.1. Introduction

The term allometry describes the dependency of a parameter (bodylength, metabolic rate) on the size (body mass) of an individual. Here, I focus on metabolism - body mass relationships. A linear correlation is the most simple relationship (some snails, insects Schmidt-Nielsen (1972)). In this case oxygen consumption or food ingestion is doubled in species with doubled individual biomass. Drug resistence experiments with mammals revealed a more complex relationship (see equation 3.1; Kleiber (1932)):

$$rate = a \cdot mass^{\beta_r} \tag{3.1}$$

In this equation a represents a species or group dependent normalization factor, and β_r represents the allometric coefficent. Kleiber (1932) was the first to suggest an allometric coefficent of 0.75 for metabolic and growth rates. Individuals with doubled biomass do not have doubled metabolic rate as predicted from a linear relationship. Their metabolic rate is reduced to the 1.68 fold. For the specific metabolic rate this allometric coefficient converts to -0.25. Allometric relationship analysis conducted with size ranges of more than 15 orders of magnitude show this "three quarter power law" quite consistently (Brody et al. (1934) -0.266, Fenchel (1974) -0.25). First explanations of this stable coefficient assumed a strong influence of body surface to body volume ratios. But this assumption will lead to an allometric coefficient of -0.33. A theoretical model explains this "three quarter power law" by using similarity analysis of dimensionless physical units (Peters, 1983). Another model uses fractal-like branching theory of ressource distribution networks in the organisms to

explain the allometric coefficient (West et al. (1997), West et al. (1999), West et al. (2002)). All these explanations can not account for the range of allometric coefficients observed in phytoplankton studies (-0.5 Finkel (2001) to -0.1 Sommer (1989)). Most studies are based on the maximum growth rate (μ_{max}) which is achieved under ideal growth conditions (nutrient and light saturation). In these studies the allometric coefficients range from -0.25 to -0.1. The low values published by Schlesinger and Molot (1981), Finkel and Irwin (2000), Finkel (2001) and reviewed by Raven and Kübler (2002)) are all achieved under light limiting conditions. Banse (1976) postulated that the environmental conditions have a strong effect on the allometric relationship.

One goal of these allometric relationship studies is to find universal mathematical formulations and parameters which can be used to predict metabolic processes by biomass. With these prediction functions dynamic processes of food web components can be resolved by the biomass distribution which is much easier to acquire (Peters, 1986). When coupling measured biomass distribution with production data derived from these functions even fish production can be predicted for certain areas (Sheldon et al., 1977). For these large scale predictions it is necessary to have profound knowledge about the interactions of environmental conditions and allometric scaling.

For phytoplankton biotic and abiotic interactions are very important. Therefore, I decided to measure metabolic rates in natural, undisturbed phytoplankton communities. The incubation step used by most authors to adapt the cells to specific conditions was skipped in these experiments. To acquire the metabolic turnover processes within minutes I used a metabolically active fluorochrome which was detected by flow cytometry. A derivate of the fluorochrome fluorescein diacetate was used for the measurement. Unspecific intracellular esterases split off the acetate molecules, resulting in a bright green fluorescence (fluorescein). This fluorochrome was first used to separate active from inactive bacteria in soil (Schnürer and Rosswall, 1982) and water (Holzapfel-Pschorn et al., 1987). Later it was shown for phytoplankton that the turnover of the FDA fluorochrome is linearly correlated to carbon turnover measured by ^{14}C-bicarbonate (Dorsey et al., 1989). Based on this publication I assumed that this method can provide estimates of metabolic carbon turnover for different phytoplankton size classes within the same sample. The allometric relationship could be resolved for single samples if they consist of

enough species to compute a reasonable regression. Because this method does not fix or integrate any environmental conditions, the natural variability of allometric relationships can be observed.

3.2. Material and methods

In the experiments metabolic processes of single phytoplankton cells were assessed by flow cytometry. The flow cytometer measures optical properties of each cell (scatter and fluorescence). Therefore, the metabolic processes have to be converted into optical signals. This is done by introducing a metabolic reactive fluorochrome into the cells. The developing fluorescence is monitored over several minutes. The ideal fluorochrome additions were established in experiments with culture phytoplankton. Details of these tests are described in appendix A on page 101. After fixing the setup, metabolic turnover of natural phytoplankton communities was measured.

3.2.1. Flow cytometry

In our laboratory we use a Becton Dickinson FACS Calibur flow cytometer for phytoplankton studies. The cytometer is equipped with two lasers (blue-green(488nm) and red(655nm)) and six detectors. In my study I used the blue green laser and the FSC (Front scatter), SSC (Side Scatter), FL1 (green fluorescence) and FL3 (red fluorescence) detectors. The scatter signals are used for size estimation and species identification in combination with the red fluorescence (FL3 = Chlorophyll; see figure 3.2). The green fluorescence (FL1) shows naturally occuring fluorescence because of plasma ingredients and the fluorescence of the marker fluorochrome that was added.

3.2.2. Fluorochrome

The fluorochrome should visualize metabolic processes and it should be a proxy for the intracellular carbon turnover. Dorsey et al. (1989) and Jochem (1999) showed that fluorescein diacetate (FDA) might serve as such a fluorochrome. The fluorochrome (FDA) penetrates into the cell where unspecific esterases splitt off the diacetate molecules. The fluorescence of the remaining fluorescein molecule is increased by a factor of 100 in com-

parison to the FDA molecule. All studies with FDA showed one problem. The turnover product fluorescein leaks through the cell membrane. Therefore, the fluorescence is not stable and the error of the results increases with time. Molecular Probes developed the fluorochrome Celltracker CMFDA to overcome this problem. The molecule is developed for long term cell labelling over several generations. The molecule consists of reactive groups that bind to internal cell structures after the diacetate is split off.

3.2.3. Phytoplankton

The first experiments were conducted to specify the ideal fluorochrome setup. These experiments were performed using culture phytoplankton. Five species were used: *Isochrysis* sp. , *Pseudopedinella* sp. , *Rhodomonas* sp. , *Synechococcus* sp. , *Teleaulax* sp. .

The natural surface samples were taken from the pier of the Institute of Marine Research in Kiel between September 2002 and June 2003. They were transferred to the laboratory within 5 minutes and measured, according to the procedure described in the next section.

3.2.4. Experimental procedure

The basic procedure for all the experiments consists of adding 5μl of a fluorochrome solution to 2 ml of a water sample and to follow the developing green fluorescence for about ten minutes in the flow cytometer. All samples were prefiltered through a 50μm filter to prevent the flow cytometer flow cell from being clogged up by larger particles. For the culture phytoplankton experiments I used several fluorochrome concentrations to check the saturating values of the fluorochrome (further details see A on page 101). From these experiments I decided to use a final concentration of Celltracker CMFDA of 2.5 $\mu g \cdot ml^{-1}$ for the natural community experiments.

3.2.5. Data processing

Allometry, in this case, describes metabolic rate processes as a function of body mass. Metabolic turnover processes convert non-fluorescent substrate into a brightly fluorescent green product. This development is monitored with the flow cytometer. The data are stored in special files (FCS *Flow Cytometry Standard* 2.0) for each individual sample.

These sample files were analysed with the software WINMDI 2.8.

The analysis starts with displaying the green fluorescence versus time in a regular dotplot (see figure 3.1) for one single phytoplankton species. In this plot outliers are eliminated. From this "cleaned" plot the green fluorescence and time data are exported for each single cell. These data were fitted (least square regression) to a standard saturation curve:

$$green\ fluorescence[arbitrary\ units;\ channel] = y0 + \frac{B_u \cdot S_i \cdot Time}{B_u + S_i \cdot Time} \tag{3.2}$$

$y0$	deviation from zero
B_u	upper boundary
S_i	initial slope

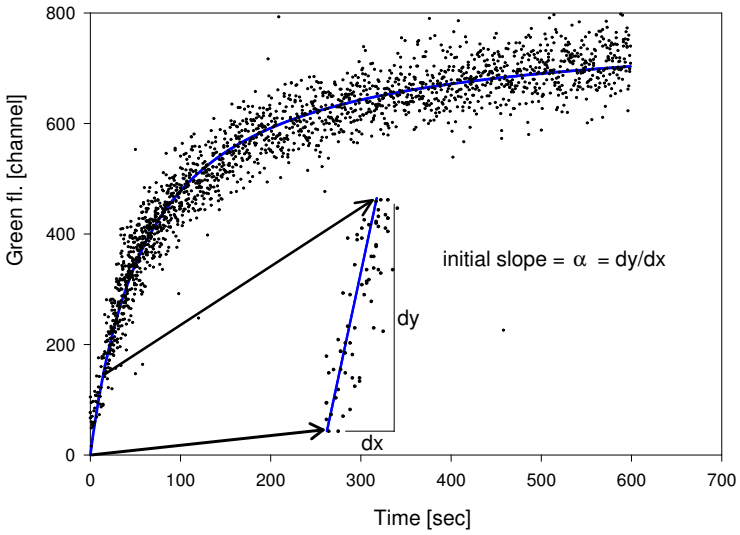

Figure 3.1.: Sample dotplot with saturation curve

Usually enzyme kinetic curves are linear in short term monitoring. The raw data (green fluorescence) show this linear behaviour. But because the scatter and fluorescence distribution of phytoplankton cells is too wide, all scatter and fluorescence parameters are acquired in log mode. Therefore, the y-axis in figure 3.2 on page 80 ranges from 10^1–10^4. This log transformation converts the linear fluorescence increase in the raw data

into a saturation curve. The saturation curve in figure 3.1 does not have a log y-axis. This axis and the left side of equation 3.2 show the green fluorescence in channel format. This channel format results from machine specific data handling. Each parameter axis is divided into 1024 linearly distributed channels. When measuring in linear mode (*time*), these channel represent the raw data. But when measuring in log mode (*fluorescence and scatter*), the raw data are converted into channels following equation 3.3:

$$\text{channel} = 256 \cdot \log(\text{raw data}) \tag{3.3}$$

The software WINMDI only exports these channel data for each cell. The analysis of the raw data is more difficult, because some species do not show the typical linear enzyme kinetics but a more curved progression either at the end or at the beginning. An analysis of such data with the recommended linear regression resulted in too low slopes. The regression analysis of the channeled data is more robust, because the initial slope of the fitted curve do not primarily rely on the saturation part of the curve. Therefore, I used the channel data for the metabolic turnover analysis. For the allometric relationship the initial slope (S_i) of the saturation curve represents the metabolic turnover over time. A numerical test showed that the initial slope of the channel data I used can be transferred into raw data initial slope by multiplying with 2.5881. This linear conversion has no effect on the allometric coefficient.

The mass (basis of the allometric function) of the respective cells was not measured directly. I used two assumptions to calculate the mass. First, the cells are assumed to have a constant mass to biovolume conversion factor. In this case, the allometric coefficient is independent of either using mass or biovolume. Second, all cells are assumed to be spheres and therefore the biovolume can be approximated from the maximum cell size (d) by computing:

$$biovolume = \frac{4}{3} \cdot \pi \cdot \left(\frac{d}{2}\right)^3 \tag{3.4}$$

Maximum cell size was estimated from the FSC (Front Scatter) of the flow cytometer. Most authors use a relative conversion based on the size of calibration beads. For this analysis a size calibration of the flow cytometer was performed using culture phytoplankton. The cells were measured microscopically (cell dimensions) and with the flow

cytometer (FSC, SSC). From the microscope data the biovolume was estimated. I performed regressions for maximum cell size, mean cell size and biovolume to Front Scatter and Side Scatter. The regression of maximum cell size versus Front Scatter median showed the best fit. In the size range of 1.5μm to 30μm, the maximum cell size can be computed from the linear regression:

$$\text{maximum cell size} = y0 + c_f \cdot \text{FSC median} \tag{3.5}$$

Coefficient	Value	Standard Error	p-value
r^2	0.9996		<0.0001
y0	1.4101	0.0834	<0.0001
c_f	0.0049	0.0000	<0.0001

All allometric coefficients that are presented from my data are based on the biovolume of the organisms. A conversion to a biomass based allometric coefficient will decrease the coefficient slightly Banse (1976). The metabolic turnover rates (fluorescence initial increase) and the biovolume were log transformed and fitted into a linear regression. This linear regression ($log(Rate) = log(a) + \beta_r \cdot log(biovolume)$) represents the logarithmic allometric equation with the allometric coefficient (β_r) as slope. The log transformation also transforms (decreases) the errors and therefore the r^2 values of the transformed fit are higher.

Experiments with culture phytoplankton

The culture experiments were used to fix the saturating fluorochrome substrate concentration. The regression analysis described above was performed for up to eight substrate fluorochrome concentration levels. For each phytoplankton species the rate derived from the regression is plotted against the fluorochrome concentration of this specific assay. The resulting Michaelis Menten type kinetic curve is fitted to equation 3.6.

$$turnover\ rate = y0 + \frac{T_{max} \cdot S_i \cdot [fluorochrome]}{T_{max} + S_i \cdot [fluorochrome]} \tag{3.6}$$

$y0$	y-axis section
T_{max}	maximum turnover rate
S_i	initial slope
$[fluorochrome]$	fluorochrome concentration

Curves for the different species are shown in figure A.2 and A.3 on page 104. The maximum turnover rates (T_{max}) from the regressions and the biovolumes of the culture species are fitted into the allometric relationship analysis. The culture experiments serve as an external data point to have a reference for the allometric coefficients derived from the natural samples.

Experiments with natural phytoplankton communities

Samples from the culture experiments consisted of only one species. Natural samples from the IFM Kiel pier instead consisted of up to eight species, which could be analysed by the flow cytometer setup. Therefore, the dotplot time versus FL1 (green fluorescence ;CMFDA turnover) shows a mixture of fluorescence development curves. Each curve represents the fluorescence development for one species. To resolve the species dependent curve for export, I used a special feature of the software. In general, species are defined in the FSC (size) versus Fl3 (red fluorescence) dotplots by surrounding the corresponding cell cloud with region borders (see figure 3.2).

After defining the regions a second dotplot is opened with time versus green fluorescence (FL1) data. The software offers the possiblity to include logical gates to show only cells of one region. The result is a dotplot with one kinetic curve belonging to one specified region (species). The logical gates are set one after the other for each region observed in the FSC/FL3 dotplot, and the data (time/FL1) of the corresponding cells are exported and treated like described in section 3.2.5.

Allometric coefficient conversion

Authors usually present the allometric coefficient for the specific rate R_s:

$$R_s = \frac{rate}{biovolume} = a \cdot biovolume^{\beta_{rs}} \tag{3.7}$$

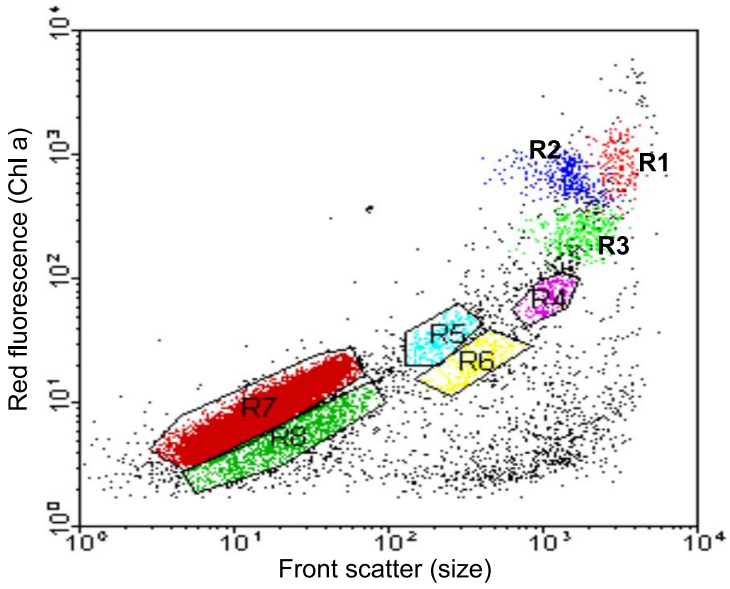

Figure 3.2.: Sample dotplot with eight regions marking different phytoplankton groups (R1-R8)

Correlations of specific rate-biovolume data contain the problem of producing spurious correlations (Berges, 1997), because the x-axis is also included in the y-axis. Therefore, I followed the recommendation of Berges (1997) to perform the regressions with the rate data and to convert the allometric coefficients ($\beta_{rs} = \beta_r - 1$) only for those data which showed significant regressions.

3.2.6. Comments to the method

Cell density

One of the most important parts of this method is the accurate measurement and analysis of the time versus green fluorescence turnover regression. It is necessary to analyse enough cells, especially at the inital part of the curve. The number of cells analysed per time is based on the flow velocity of the flow cytometer and the cell density of the species in the sample. The flow velocity of the sample is limited technically to a maximum value of 180 $\mu l \cdot min$. Therefore, the cell density should not be lower than 50 cells $\cdot$ ml^{-1} for one species. In cultures this density was always reached but in natural samples especially the larger cells could occur in lower cell densities. These could not be analysed with this

method (machine setup). Therefore, cell density can limit the number of species passed to the allometry regression.

pH sensitivity

The fluorescence intensity of all fluorochromes depends on the chemical structure of the molecule. The two order of magnitude increase in fluorescence by splitting off the acetates from the Celltracker CMFDA is an example of this phenomenon. The chemical structure of some fluorochromes is also sensitive to medium conditions. The fluorescence of my turnover reaction product, fluorescein, shows a pH sensitivity in the near neutral pH range. The highest fluorescence is achieved at a pH of about 9. It is not clear to what extent the results of the turnover reaction are influenced by the internal pH of the measured cells. I assumed that all occuring pH differences in the cells are not size dependent and therefore will only increase the error of the allometric relationship. Further considerations are not possible because of the rare information in the literature.

3.3. Results

3.3.1. Culture phytoplankton

Maximum metabolic turnover rates (T_{max}; fluorescence development) for each of the five species were calculated fom the Celltracker CMFDA adjustment experiments. The increase of the turnover velocity with increasing substrate concentration followed the typical Michaelis Menten kinetics for most of the species very accurately (see r^2 values in table 3.1). T_{max} values were significant for all species but *Teleaulax* sp. . Although it was not significant I decided to use the value for the allometric analysis, because the maximum turnover was quite stable over a wide range of fluorochrome concentrations (see figure A.2 on page 103). .

A comparison of the size data for all species revealed that the size (FSC values) for *Pseudopedinella* sp. must be wrong, because it should be smaller than *Synechococcus* sp. . It was not possible to fix the source of this error by remeasuring the samples. Therefore, *Pseudopedinella* sp. was excluded from the allometric relationship analysis (marked red in figure 3.3).

Larger cells show a higher absolute maximum turnover rate (T_{max}) than the smaller cells. This pattern corresponds to literature data for several rates and taxonomic groups. A clear linear correlation is displayed by the log(biovolume)-log(rate) data (see figure 3.3). The regression is highly significant, though only four data points are used (r^2=0.95; p=0.03). The slope of the regression (allometric coefficient β_r) was 0.48 which is much lower than the general assumed literature value of 0.75.

3.3.2. Natural phytoplankton community

Phytoplankton composition

The natural phytoplankton community at the IFM institute pier (Kieler Förde) consists of several phytoplankton taxonomic and size groups changing their dominance over the year. However, prefiltration of the samples excluded the larger and chain forming species from the samples. The spectrum I analysed reached from small procaryotic phytoplankton (*Synechococcus* sp.) to autotrophic flagellates with sizes of up to 30μm. Unicellular diatoms which would pass the prefiltration were not abundant enough in the samples. Picoeucaryotic flagellates had the highest cell densities in all samples. Cryptophytes were present with one species in autumn and early spring and with two species in late spring. The analysed phytoplankton was completed by different chlorophyte and haptophyte flagellates.

Table 3.1.: Regression parameters of substrate saturation curves of culture phytoplankton using a modified Michaelis Menten kinetic curve; r^2=goodness of fit, p=significance of the regression, S_i=initial slope, T_{max}= maximum turnover rate; *ns* marking a non significant and * a significant regression coefficient

Species	r^2	p	S_i	T_{max}
Synechococcus sp.	0.9999	0.0179	35.64 (*)	3.05 (*)
Isochrysis sp.	0.994	0.0769	239.43 (*ns*)	5.38 (*)
Pseudopedinella sp.	0.997	0.0469	127.6 (*ns*)	10.37 (*)
Rhodomonas sp.	0.997	0.0461	113.39 (*ns*)	10.98 (*)
Teleaulax sp.	0.898	0.3191	2209 (*ns*)	25.39 (*ns*)

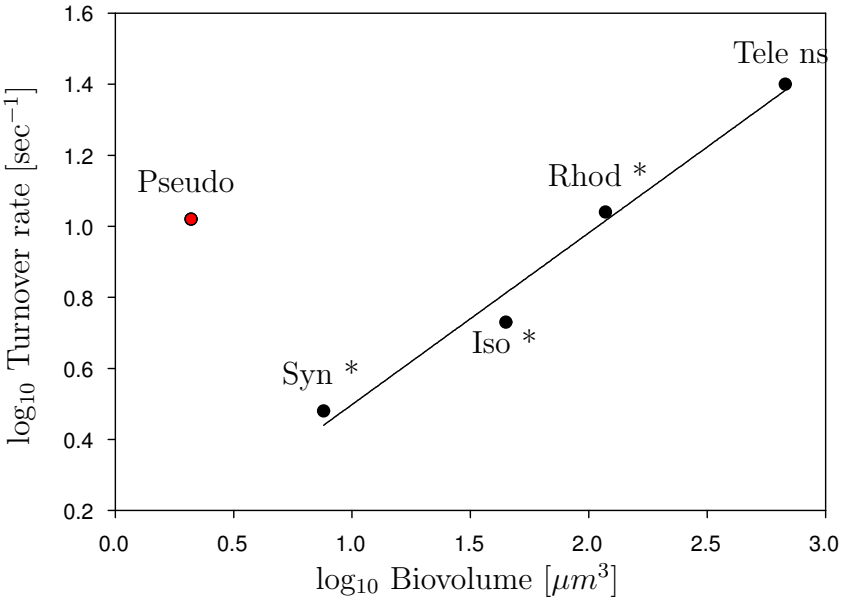

Figure 3.3.: Allometric relationship of single species culture experiments, using T_{max} from modified substrate saturation Michaelis Menten regressions (see equation 3.6); Iso=*Isochrysis* sp., Pseudo=*Pseudopedinella* sp., Rhod=*Rhodomonas* sp., Syn=*Synechococcus* sp., Tele=*Teleaulax* sp., ; *=significant, ns=not significant T_{max} in the regression

Allometric relationship

All groups described were analysed for their metabolic rates and biovolumes. Only the procaryote *Synechococcus* sp. showed very little responses to fluorochrome additions. The regression analysis of *Synechococcus* sp. showed no significant initial slope which could be used for the allometric relationship. Therefore, *Synechococcus* sp. was excluded from analysis.

Single day overview During the period from September 2001 until June 2003 I performed experiments at ten days. Three of these ten days were not further processed, because the samples included not enough groups to get a reasonable regression of metabolic rate versus size (volume). The remaining seven regressions are included in figure 3.4.

The cell size of the phytoplankton groups which were included in the regression analysis was in the range of 1 to 16μm maximum cell length. This range was only achieved at one

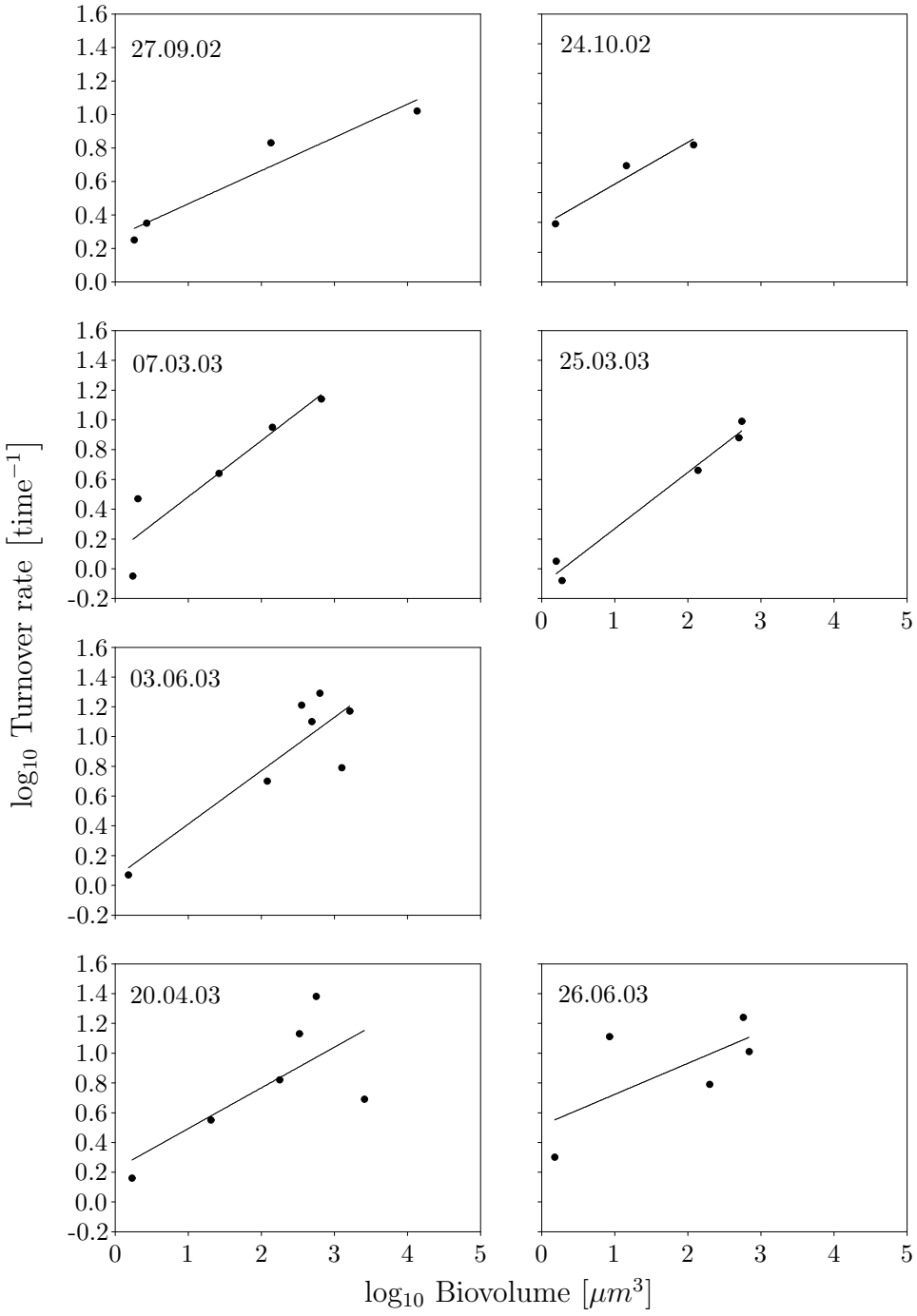

Figure 3.4.: Overview of allometric regressions of seven days from September 02 to June 03; the five upper figures have significant slopes, the two lower figures do not have significant slopes

day (27.09.2002). The typical range was 1 to 6μm. Converting these sizes into biovolume or biomass, the results include a size range of up to four orders of magnitude but more

often three orders of magnitude (see x-axis in figure 3.4).

The upper five regressions in figure 3.4 were all significant(p: 0.001–0.035) and the goodness of fit was very high (r^2: 0.85–0.98). For the lower two regressions the spreading and the scarcity of the data led to lower r^2 values (0.5) and to non-significant slopes, although there is a clear trend in both cases. In September and Oktober 2002 the slopes of the linear regressions (allometric coefficient β_r) were 0.2 and 0.24. In the following spring experiments the slopes increased to 0.38 in March and 0.36 in June (see figure 3.5). Both non-significantslopes were lower (0.27 for April and 0.21 for late June).

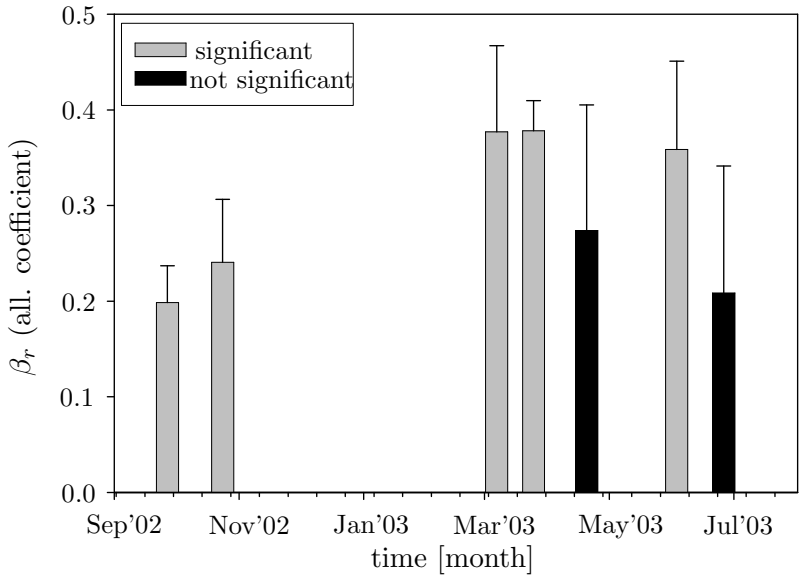

Figure 3.5.: Allometric coefficients overview; error bars showing the standard error

General allometric relationship The previous analysis shows the results for each measurement day seperately. To get a general overview, all data points from figure 3.4 were combined in one regression analysis. The fluorescence increase per time spreads over a remarkable range for one specific phytoplankton size class (see figure 3.6). Even so the increase in turnover rate over a size range of four orders of magnitudes is still obvious. Variability in the turnover rates is explained by the size by 69.7%. Regression and slope (β_r=0.29) are highly significant($p \leq 0.0001$).

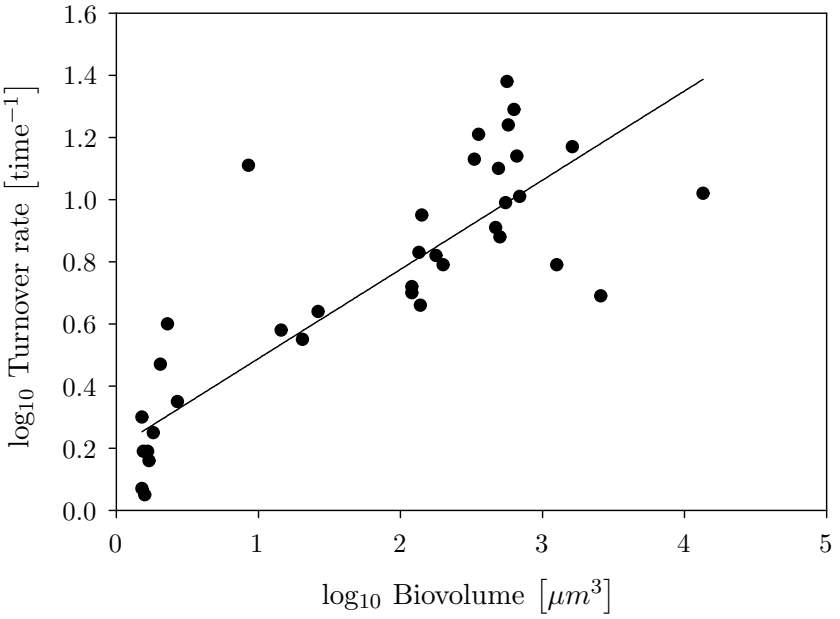

Figure 3.6.: General allometric regression with datapoints of seven experiments from September 2002 until June 2003

3.4. Discussion

3.4.1. Methodological considerations

In the past the data for analysing allometric coefficients resulted from culture experiments or from short or long term incubations of natural phytoplankton. This is necessary when the allometric relationship of the maximum growth rate or the metabolic rates under saturation conditions are investigated. The cells must be adapted to the new conditions. Especially for growth analysis through cell number changes it is necessary to perform experiments which last for days. The method I present here has the advantage that it is possible to analyse field samples within minutes without severe changes in the community and the corresponding changes in rate processes and interactions. The method delivers single cell data and is as group selective as the cell counting method. This is an advantage over tracer studies in which groups are integrated over distinct size classes.

3.4.2. Allometric relationship

The existence and expression of allometric relationships in phytoplankton metabolism is a controversially discussed topic in plankton research. The general allometric coefficient of the specific rate (β_{rs}=-0.25) found over size ranges of 21 orders of magnitude (Kleiber (1932), Schmidt-Nielsen (1972), Peters (1983), West et al. (1997), Beuchat (1997)) is not yet fixed for phytoplankton (Chrisholm, 1992). Allometric coefficients of phytoplankton range from -0.5 (Finkel (2001), reviewed by Raven and Kübler (2002)) to -0.1 (Banse (1976), Sommer (1989); overview see table 3.2). The data used to evaluate these allometric coefficients are based on incubations experiments with cultures and natural phytoplankton. My culture experiments derived an allometric coefficient (β_{rs}=-0.52) at the lower boundary of this range. In general, lower allometric coefficients can result from light limitation because of the package effect (Finkel, 2001) or from nutrient limitation (Chrisholm (1992)). In my experiment light and nutrients should not be limiting. Possible explanations of this low coefficient are derived from the method or the size range of the species that are used. All my experiments are based on the linear relation of FDA turnover to ^{14}C uptake published by Dorsey et al. (1989). This linear relation leads to direct comparability of the fluorescence turnover experiments with other metabolic experiments and the derived allometric coefficients. Deviations from this linearity can result in an amplification of the allometric relationship. There is no evidence from the literature for such a deviation from linearity. An amplification of the allometric relationship can also result from detecting unbalanced turnover processes. This behaviour is observed for short term (several hours) nutrient and carbon uptake experiments. The balanced uptake and turnover which is necessary to maintain a constant biomass composition might only be detectable by long term (integrating) observations. Results from a side-experiment show that for two out of six species the fluorescence turnover is almost linearly correlated to growth rate measured by cell counting. Therefore, the fluorescence method seems to detect balanced metabolic processes, assuming that cell growth should always be balanced under saturating conditions. This experiment was not included into this chapter because the growth conditions were not ideal.

The reduced size range is the favourite explanation for the low allometric coefficient of the culture experiments. Data from general allometric analysis (β_{rs}=-0.25) spreading over

more than 20 orders of magnitude show much more diverse allometric coefficients when the size range is reduced (Gilloly pers. comm.). In the literature dealing with allometric coefficients for phytoplankton the size range covers six orders of magnitude. My culture experiment just covers three orders of magnitude. But further work has to be done to verify these findings and explanation.

Table 3.2.: Allometric coefficients of metabolic processes of plankton organisms

	organism	unit	β_{rs}	reference
Growth				
	phytopl.	μ_{max}	-0.08	Sommer (1989)
	phytopl.	$div. \cdot day^{-1}$	-0.108	Laws (1975) (biovolume)
	phytopl.	$div. \cdot day^{-1}$	-0.11	Banse (1976)
	diatoms	$div. \cdot day^{-1}$	-0.1128	Blasco et al. (1982) (biovolume)
	phytopl.	$div. \cdot hour^{-1}$	-0.32	Schlesinger and Molot (1981)
Respiration				
	Daphnia		-0.15	Lampert (1977)
	phytopl.	$pgC \cdot (h \cdot cell)^{-1}$	-0.28	Finkel (2001)
	plankton		-0.309	Ikeda (1970)
	phytopl.	$pgC \cdot (h \cdot cell)^{-1}$	-0.31	Laws (1975)
Photosynthesis				
	diatoms	$mgC \cdot h^{-1}$	-0.44	Finkel (2001)
Nutrient uptake				
	algae	$\mu gN \cdot (gDW \cdot h)^{-1}$	-0.203	Hein et al. (1995)

The allometric coefficient for all field samples is further reduced (β_{rs}=-0.71) in comparison to the culture experiments. The method of the measurements was identical. Therefore, I assume that the lower allometric coeffcient is derived from differences in biotic and abiotic conditions of the examined system. First, the nutrients are much lower in the natural system. Smaller species can take up nutrients better because of their higher surface to volume ratio. Under nutrient limited conditions smaller cells can maintain their maximal growth rates much longer without becoming diffusion limited. The larger cells can only reach a small percentage of their maximal growth rates because diffusion can no longer supply the necessary nutrients (Chrisholm (1992), Raven (1986)). So the allometric coefficient decreases under low nutrient conditions. These effects should increase if the phytoplankton species have to compete for nutrients, as in natural systems. The smaller

cells take up the nutrients faster and therefore they reduce the ambient nutrient concentrations for their larger competitors. Both, the direct and indirect nutrient effect can be observed in the single day regression overview. In spring with highest nutrient concentrations the allometric coefficients were higher than for the nutrient depleted conditions in autumn.

Raven and Kübler (2002) and Finkel (2001) postulated that the ambient light field should have a strong influence on the allometric relationship. Under low light conditions phytoplankton increase their chlorophyll. This increase leads to a stronger package effect (self shading) in larger species. Therefore, light harvesting and growth efficiency are greatly reduced in larger cells and the resulting allometric coefficient decreases. My experiments do not reveal this light effect. A strong light effect will result in low allometric coefficients in winter, increased but equal allometric coefficients in spring and autumn and maximum values in summer. My data show a difference in autumn and spring that better corresponds to the ambient nutrient concentrations. An interactive effect of nutrients and light can be assumed because the allometric coefficients are still high at the beginning of June, when nutrient depletion already started. But the nutrient effect seems to be much stronger than the light effect.

For all allometric relationships presented here, biovolume served as measure of size. The conversion to cell carbon as the allometric basis decreases the allometric coefficients slightly (Banse, 1976). Therefore, all trends presented in this chapter even become increased.

3.4.3. Summary and conclusion

Research on allometric relationships is performed to develop numerical prediction frameworks. These frameworks can be used to predict difficult to measure turnover processes by easy to measure size distributions.

For ecologists, differences between taxa or functional groups are important. These differences are represented by the factor a in the allometric equation. The data presented in this chapter can not resolve this parameter because the conversion factors from fluorescence turnover to carbon turnover are not known. Therefore, an absolute prediction of the metabolic turnover from size measurement is not possible at present. What can

be predicted from the data in these experiment is the relative metabolic rate of a certain size class from the known rate of another size class. These relative turnover processes are important for the determination of sinking rates (Kriest and Evans, 1999), Grazing (Katechakis et al., 2002) or productivity analysis. The size distribution and the according turnover is one major factor controlling the relative amounts of new and regenerated production (f-ratio). Both passages have different ecological efficencies. Enhanced regenerated production fueled by fast ammonium regeneration and assimilation includes more trophic steps and therefore the secondary and export production is reduced. These tight connections show that it is crucial to know which size class contributes to production at which time. My data indicate that even in the Baltic size scaling of metabolic processes is important. The overall allometric coefficient for the natural samples was always lower than for the culture organisms ($\Delta\beta_{rs}$=-0.19). A comparison of the different allometric coefficients from a nine month period showed that the size scaling seems to be related to the ressource conditions of the environment (nutrients and light). The pronounced allometric scaling results in much higher relative metabolism of the smaller size classes than formerly expected. This higher metabolism of smaller cells can lead to higher DON and DOC concentration because of the higher loss rates of smaller algae. Therefore, the whole ecosystem is further shifted towards the smaller size classes.

The incorporation of size scaled auto- and heterotrophs into ecological and biogeochemical studies can help to resolve observed differences from different ecosystems. The method presented here can help to get an insight on the size scaling of metabolic turnover in natural communities. Further experiments have to be conducted to understand the applicability of the derived allometric coefficients and to understand the influence of the background conditions on the allometric scaling.

Bibliography

Alves M L G R and de Verdière A C. 1999. Instability dynamics of a subtropical jet and applications to Azores Fronts Current System: Eddy-Driven mean flow. *J. Phys. Oceanogr.*, **29**: 837–864.

Asper V L, Deuser W G, Knauer G A and Lohrenz S E. 1992. Rapid coupling of sinking particle fluxes between surface and deep ocean waters. *Nature*, **357**: 670–672.

Baird M E, Oke P R, Suthers I M and Middleton J H. 2003. A size-based plankton population model in an idealized 2-D ocean basin. *J. of Mar. Syst.*, **preprint**.

Banse K. 1976. Rates of growth, respiration and photosynthesis of unicellular algae as related to cell size – a review. *J. Phycol.*, **12**: 135–140.

Beers J R, Reid M H and Stewart G L. 1975. Microplankton of the North Pacific central gyre. Population structure and abundances, June 1973. *Int. Rev. ges. Hydrobiol.*, **60**: 707–737.

Berger W H, Smetacek V S and Wefer G. 1989. *Productivity of the ocean*, chap. Ocean productivity and paleoproductivity- an overview:, 1–34. Wiley and Sons, New York.

Berges J A. 1997. Ratios, regression statistics, and spurious correlations. *Limnol. Oceanogr.*, **42**(5): 1006–1007.

Betzer P R, Showers W J, Laws E A, Winn C D, DiTullio G R and Kroopnick. 1984. Primary production and particle flux on a transect of the equator at 153W in the Pacific Ocean. *Deep-Sea Res.*, **31**: 1–11.

Beuchat C. 1997. Allometric scaling laws in biology. *Science*, **278**: 371–.

Bissett W P, Meyers M B, Walsh J J and Muller-Karger F E. 1994. The effects of temporal variability of mixed layer depth on primary productivity around bermuda. *J. Geophys. Res.*, **99**(C4): 7359–7553.

Blasco D, Packard T T and Garfield P C. 1982. Size dependence of growth rate, respiratory electron transport system activity, and chemical composition in marine diatoms in the laboratory. *J. Phycol.*, **18**: 58–63.

Boyd P and Newton P. 1995. Evidence of the potential influence of planktonic community structure on the interannual variability of particulate organic carbon flux. *Deep-Sea Res. I*, **42**(5): 619–639.

Boyd P W and Newton P P. 1999. Does planktonic community structure determine downward particulate organic carbon flux in different oceanic provinces? *Deep-Sea Res. I*, **46**: 63–91.

Brock T D. 1981. Calculating solar radiation for ecological studies. *Ecol. Model.*, **14**: 1–19.

Brody S, Proctor R C and Ashworth U S. 1934. Basal metabolism, endogenous nitrogen, creatine and neutral sulphur excretions as functions of body weight. *Mo. Agric. Exp. Sta. Res. Bull.*, **220**: 40 p.

Brown J, Colling A, Park D, Phillips J, Rothery D and Wright J. 1989. *Ocean circulation*. Pergamon Press, Oxford.

Bury S J, Boyd P W, Preston T, Savidge G and Owens N J P. 2001. Size-fractionated primary production and nitrogen uptake during a North Atlantic phytoplankton bloom: implications for carbon estimates. *Deep-Sea Res. I*, **48**: 689–720.

Capone D G and Carpenter E J. 1999. *Nitrogen fixation by marine cyanobacteria: historical and global perspectives*, vol. 19 of *Bulletin de l´Institut océanographique, Monaco*, 235–256. Monaco, Musée Océanographique.

Chrisholm S W. 1992. *Primary Productivity and Biogeochemical Cycles in the Sea*, chap. Phytoplankton Size, 213–237. Plenum Press.

Cullen J J and Eppley R W. 1981. Chlorophyll maximum layers of the Southern California Bight and possible mechanisms of their formation and maintenance. *Oceanol. Acta*, **4**: 23–32

DeNiro M J and Epstein S. 1981. Influence of diet on the distribution of nitrogen isotopes in animals. *Geoch. Cosmoch. Acta*, **45**: 341–351.

Dietrich G, Kalle K, Krauss W and Siedler G. 1975. *Allgemeine Meereskunde*. Gebrüder Bornträger, Berlin.

Dorsey J, Yentsch C M, Mayo S and McKenna C. 1989. Rapid analytical technique for the assessment of cell metabolic activity in marine microalgae. *Cytometry*, **10**: 622–628.

Eppley R W and Peterson B J. 1979. Particulate organic matter flux and planktonic new production in the deep ocean. *Nature*, **282**: 677–680.

Eppley R W and Sharp J H. 1975. Photosynthetic measurements in the central North Pacific: The dark loss of carbon in 24-h incubations. *Limnol. Oceanogr.*, **20**(6): 981–987.

Evans G T. 1999. The role of local models and data sets in the Joint Global Ocean Flux Study. *Deep-Sea Res. I*, **46**: 1369–1389.

Evans G T and Garcon V C. 1997. One-dimensional models of water column biogeochemistry. Workshop Report 23, JGOFS Project Office, Bergen.

Falkowski P G, Barber R T and Smetacek V. 1998. Biogeochemical controls and feedbacks on ocean primary productivity. *Science*, **281**: 200–206.

Fasham M J R, Ducklow H W and McKelvie S M. 1990. A nitrogen-based model of plankton dynamics in the oceanic mixed layer. *J. Mar. Res.*, **48**: 591–639.

Fenchel T. 1974. Intrinsic rate of natural increase: The relationship with body size. *Oecologia*, **14**: 317–326.

Fennel K, Losch M, Schröter J and Wenzel M. 2001. Testing a marine ecosystem model: Sensitivity analysis and parameter optimization. *J. Mar. Syst.*, **28**: 45–63.

Fernández E, Marañón E, Morán X A G and Serret P. 2003. Potential causes for the unequal contribution of picophytoplankton to total biomass and productivity in oligotrophic waters. *Mar. Ecol. Prog. Ser.*, **254**: 101–109.

Finkel Z V. 2001. Light absorption and size scaling of light-limited metabolism in marine diatoms. *Limnol. Oceanogr.*, **46**(1): 86–94.

Finkel Z V and Irwin A J. 2000. Modeling size-dependent photosynthesis: light absorption and the allometric rule. *J. Theor. Biol.*, **204**: 361–369.

Fry B. 1988. Food web structure on Georges Bank from stable C, N and S isotopic composition. *Limnol. Oceanogr.*, **33**: 1182–1190.

Goldman J C, McCarthy J J and Peavey D G. 1979. Growth rate influence on the chemical composition of phytoplankton in oceanic waters. *Nature*, **279**: 210–215.

Grande K D, Williams P J, Marra J, Purdie D A, Heinemann K, Eppley R W and Bender M L. 1989. Primary production in the North Pacific gyre: a comparison of rates determined by the ^{14}C, O_2 concentration and ^{18}O methods. *Deep-Sea Res.*, **36**(11): 1621–1634.

Grasshoff K, Ehrhardt M and Kremling K. 1983. *Methods of seawater analysis*. Verlag Chemie, Weinheim.

Hansson S, Hobbie J E, Elmgren R, Larsson U, Fry B and Johansson S. 1997. The stable nitrogen isotope ratio as a marker of food-web interactions and fish migration. *Ecology*, **78**(7): 2249–2257.

Healey F P. 1985. Interacting effects of light and nutrient limitation on the growth rate of *Synechococcus linearis* (Cyanophyceae). *J. Phycol.*, **21**: 134–146.

Hein M, Foldager Pedersen M and Sand-Jensen K. 1995. Size-dependent nitrogen uptake in micro- and macroalgae. *Mar. Ecol. Prog. Ser.*, **118**: 247–253.

Holzapfel-Pschorn A, Obst U and Haberer K. 1987. Sensitive method for the determination of microbial activities in water samples using fluorigenic substrates. *Fresenius Z. Analyt. Chem.*, **327**: 521–523.

Hurtt G C and Armstrong R A. 1996. A pelagic ecosystem model calibrated with BATS data. *Deep-Sea Res. II*, **43**(2–3): 653–683.

Hurtt G C and Armstrong R A. 1999. A pelagic ecosystem model calibrated with BATS and OWSI data. *Deep-Sea Res. I*, **46**: 27–61.

Ikeda T. 1970. Relationship between respiration rate and body size in marine plankton animals as a function of the habitat temperature. *Bull. Fac. Fish. Hokkaido Univ.*, **21**: 91–112.

Jochem F. 1990. Zur Struktur und Dynamik autotropher Ultraplankton-Gemeinschaften in marinen Warmwasser-ökosystemen. *Ber. Inst. Meereskunde*, **195**: 220pp.

Jochem F J. 1999. Dark survival strategies in marine phytoplankton assessed by cytometric measurement of metabolic activity with fluorescein diacetate. *Mar. Biol.*, **135**: 721–728.

Jochem F J and Zeitschel B. 1993. Productivity regime and phytoplankton size structure in the tropical and subtropical North Atlantic in spring 1989. *Deep-Sea Res. II*, **40**: 495–519.

Joint I R and Pomroy A J. 1983. Production of picoplankton and small nanoplankton in the Celtic Sea. *Mar. Biol.*, **77**: 19–27.

Karl D. 1997. The role of nitrogen fixation in biogeochemical cycling in the subtropical North Pacific Ocean. *Nature*, **388**: 533–538.

Karl D M, Björkman K M, Dore J E, Fujieki L, Hebel D V, Houlihan T, Letelier R M and Tupas L M. 2001. Ecological nitrogen-to-phosphorus stoichiometry at Station ALOHA. *Deep-Sea Res. II*, **48**: 1529–1566.

Katechakis A, Stibor H, Sommer U and Hansen T. 2002. Changes in the phytoplankton community and microbial food web of Blanes Bay (Catalan Sea, NW Mediterranean) under prolonged grazing pressure by doliolids (Tunicata), cladocerans or copepods (Crustacea). *Mar. Ecol. Prog. Ser.*, **234**: 55–69.

Kimor B, Berman T and Schneller A. 1987. Phytoplankton assemblages in the deep chlorophyll layers off Mediterranean coast of Israel. *J. Pl. Res.*, **9**: 433–443.

Kleiber M. 1932. Body size and metabolism. *Hilgardia*, **6**: 315–353.

Klein B and Siedler G. 1989. On the origin of the Azores Current. *J. Geophys. Res.*, **94**: 6159–6168.

Kriest I and Evans G T. 1999. Representing phytoplankton aggregates in biogeochemical models. *Deep-Sea Res. I*, **46**: 1841–1859.

Lampert W. 1977. Studies on the carbon balance of *Daphnia pulex* (de Geer) as related to environmental conditions 2. The dependence of carbon assimilation on animal size, temperature, food concentration and diet species. *Arch. Hydrobiol. Suppl.*, **48**: 310–335.

Laws E A. 1975. The importance of respiration losses in controlling the size distribution of marine phytoplankton. *Ecology*, **56**: 419–426.

Lochte K, Ducklow H W, Fasham M J R and Stienen C. 1993. Plankton succession and carbon cycling at 47^{o}N 20^{o}W during the JGOFS North Atlantic Bloom Experiment. *Deep-Sea Res. II*, **40**(1/2): 91–114.

Lohrenz S, Knauer G A, Asper V L, Tuel M, Michaels A F and Knap A H. 1992. Seasonal variability in primary production and particle flux in the northwestern Sargasso Sea. *Deep-Sea Res.*, **39**: 1373–1391.

Marañón E, Holligan P M, Varela M, Mouriño B and Bale A J. 2001. Basin-scale variability of phytoplankton biomass, production and growth in the Atlantic Ocean. *Deep-Sea Res. I*, **47**: 825–857.

Markager S. 1997. Dark uptake of inorganic ^{14}C in oligotrophic oceanic waters. *J. Plankton Res.*, **20**(9): 1813–1836.

Martin J H, Knauer G A, Karl D M and Broenkow W W. 1987. Vertex: Carbon cycling in the northeast Pacific. *Deep-Sea Res.*, **34**: 267–285.

McCave I N. 1984. Size spectra and aggregation of suspended particles in the deep ocean. *Deep-Sea Res.*, **31**: 329–352.

Michaels A F and Silver M W. 1988. Primary production, sinking fluxes and the microbial food web. *Deep-Sea Res.*, **35**(4): 473–490.

Moloney C L and Field J G. 1989. General allometric equations for rates of nutrient uptake, ingestion and respiration in plankton organisms. *Limnol. Oceanogr.*, **34**(7): 1290–1299.

Moloney C L and Field J G. 1991. The size-based dynamics of plankton food webs. I. A simulation model of carbon and nitrogen flows. *J. Plankton Res.*, **13**(5): 1003–1038.

Monod J. 1950. La technique de culture continue, théorie et applications. *Ann. Inst. Pasteur, Paris*, **79**: 390–410.

Oschlies A. 2002. Nutrient supply to the surface waters of the North Atlantic - a model study. *J. Geophys. Res.*, **107**(C5): 3046.

Oschlies A and Garcon V. 1998. Eddy-induced enhancement of primary production in a model of the North Atlantic Ocean. *Nature*, **394**(6690): 266–269.

Owens N J P. 1987. Natural variations in ^{15}N in the marine environment. *Adv. Mar. Biol.*, **24**: 389–451.

Peters R H. 1983. *The ecological implications of body size*. Cambridge University Press.

Peters R H. 1986. The role of prediction in limnology. *Limnol. Oceanogr.*, **31**: 1143–1160.

Rau G H, Teyssie J L, Rassoulzadegan F and Fowler S W. 1990. ^{13}C:^{12}C and ^{15}N:^{14}N variations among size-fractionated marine particles: implications for their origin and trophic relationship. *Mar. Ecol. Prog. Ser.*, **59**: 33–38.

Raven J A. 1986. Physiological consequences of extremely small size for autotrophic organisms in the sea. *Can. Bull. Fish. Aqu. Sci.*, **214**: 1–70.

Raven J A. 1999. Picoplankton. *Progr. Phycol. Res.*, **13**: 33–106.

Raven J A and Kübler J E. 2002. New light on the scaling of metabolic rate with the size of algae. *J. Phycol.*, **38**: 11–16.

Roman M R, Caron D A, Kremer P, Lessard E J, Madin L P, Malone J M T C abd Napp, Peele E R and Youngbluth M J. 1995. Spatial and temporal

changes in the partitioning of organic carbon in the plankton community of the Sargasso Sea off Bermuda. *Deep-Sea Res. I*, **42**(6): 973–992.

Sarmiento J L and Siegenthaler U. 1992. *Primary productivity and biogeochemical cycles in the sea*, chap. New production and global carbon cycle, 317–332. Plenum, New York.

Sarmiento J L and Toggweiler J R. 1984. A new model for the role of the oceans in determining atmospheric pCO_2. *Nature*, **308**: 621–624.

Schartau M and Oschlies A. 2003. Simultaneous data-based optimization of a 1D-ecosystem model at three locations in the North Atlantic: Part I–Method and parameter estimates. *J. Mar Res.*, **61**: 765–793.

Schartau M, Oschlies A and Willebrand J. 2001. Parameter estimates of a zero-dimensional ecosystem model applying the adjoint method. *Deep-Sea Res. II*, **48**: 1769–1800.

Schlesinger D A and Molot L A. 1981. Specific growth rates of freshwater algae in relation to cell size and light intensity. *Ca. J. Fish- Aquat. Sci.*, **38**: 1052–1058.

Schmidt-Nielsen K. 1972. *How animals work*, chap. Body size and problems of scaling, 85–96. Cambridge University Press.

Schnürer J and Rosswall T. 1982. Fluorescein diacetate hydrolysis as a measure of total microbial activity in soil and litter. *Appl. Environ. Microbiol.*, **43**: 1256–1261.

Sheldon B F and Sutcliffe W H J. 1978. Generation time of 3h for Sargasso Sea microplankton determined by ATP analysis. *Limnol. Oceanogr.*, **23**: 1051–1054.

Sheldon R W, Sutcliffe Jr W H and Paranjape M A. 1977. Structure of pelagic food chain and relationship between plankton and fish production. *J. Fish. Res. Board Can.*, **34**: 2344–2353.

Siegenthaler U and Sarmiento J L. 1993. Atmospheric carbon dioxide and the ocean. *Nature*, **365**: 119–125.

Smith E L. 1936. Photosynthesis in relation to light and carbon dioxide. *Proc. Nat. Acad. Sci.*, **22**: 1–22.

Sommer F. 2003. A comparison of the impact of major mesozooplankton taxa on marine, brackish and freshwater phytoplankton during summer. Rep. 329, Institut für Meereskunde, Kiel.

Sommer U. 1989. Maximal growth rates of Antarctic phytoplankton: Only weak dependence on cell size. *Limnol. Oceanogr.*, **34**(6): 1109–1112.

Sommer U. 1998. *Biologische Meereskunde*. Springer, Berlin.

Steemann Nielsen E. 1952. The use of radioactive carbon (^{14}C) for measuring organic production in the sea. *J. Cons. Intern. Explor. Mer*, **18**: 281–299.

Sterner R W and Elser J J. 2002. *Ecological Stoichiometry: The biology of elements from molecules to the biosphere*. Princeton University Press, Princeton.

Süss E. 1980. Particulate organic carbon flux in the oceans - surface productivity and oxygen utilization. *Nature*, **288**: 260–263.

Sy A. 1988. Investigation of large-scale circulation patterns in the central North Atlantic: The North Atlantic Current, the Azores Current, and the Mediterranean water plume in the area of the Mid-Atlantic Ridge. *Deep-Sea Res. I*, **35**: 383–413.

Tagushi S, DiTullio G R and Laws E A. 1988. Physiological characteristics and production of mixed layer and chlorophyll maximum phytoplankton populations in the Caribbean Sea and western Atlantic Ocean. *Deep-Sea Res.*, **35**: 1363–1377.

Volk T and Hoffert M I. 1985. Ocean carbon pumps: Analysis of relative strengths and efficiencies in ocean-driven atmospheric CO_2 changes. *Geophys. Monogr.*, **32**: 99–110.

Wada E, Terazaki M, Kabaya Y and Nemoto T. 1987. ^{15}N and ^{13}C in the Antarctic Ocean with emphasis on the biogeochemical structure of the food web. *Deep-Sea Res.*, **34**(5/6): 829–841.

Wasmund N, Voss M and Lochte K. 2001. Evidence of nitrogen fixation by non-heterocystous cyanobacteria in the Baltic Sea and recalculation of a budget of nitrogen fixation. *Mar. Eco. Prog. Ser.*, **214**: 1–14.

West G B, Brown J H and Enquist B J. 1997. A general model for the origin of allometric scaling laws in biology. *Science*, **276**: 122–126.

West G B, Brown J H and Enquist B J. 1999. The fourth dimension of life: fractal geometry and allometric scaling of organisms. *Science*, **284**: 1677–1679.

West G B, Woodruff W H and Brown J H. 2002. Allometric scaling of metabolic rate from molecules and mitochondria to cells and mammals. *PNAS*, **99**(1): 2473–2478.

Zehr J P, Carpenter E J and Villareal T A. 2000. New perspectives on nitrogen-fixing microorganisms in tropical and subtropical oceans. *Trends Microbiol.*, **8**: 68–73.

Zehr J P, Mellon M T and Zani S. 1998. New nitrogen fixing microorganisms detected in oligotrophic oceans by the amplification of nitrogenase (nifh) genes. *Appl. Environ. Microbiol.*, **64**: 3444–3450.

Zehr J P, Waterbury J B, Turner P J, Montoya J P, Omoregie E, Steward G F, Hansen A and Karl D M. 2001. Unicellular cyanobacteria fix N_2 in the subtropical North Pacific Ocean. *Nature*, **412**: 635–638.

A. Celltracker CMFDA adjustement

The described tests of the fluorochrome, solvent (DMSO=dimethylsulfoxid) and the fluorochrome concentration were performed, because no method for using Celltracker CMFDA were published. For the experiments I used the following cultures: *Isochrysis* sp. , *Pseudopedinella* sp. , *Rhodomonas* sp. , *Synechococcus* sp. and *Teleaulax* sp. . All experiments were conducted three to ten days after the addition of new media. They were grown at sunlight under identical conditions.

A.1. DMSO amount

Because DMSO (dimethylsulfoxid), the fluorochrome solvent, is often used as a cell permeabilizer we first tested the amount of DMSO which is tolerable without severe damage or irritation of the cells. As you can see in figure A.1 higher amounts of DMSO not only resulted in a decrease of the size of the cells but also in a wider spreading over the size axis. Based on these data we decided to use a DMSO amount of 2.5μl per ml sample.

A.2. Celltracker CMFDA concentration

After these tests we set up a concentration gradient of Celltracker CMFDA to test for substrate saturation of the different species. As a stock solution 1mg fluorochrome powder was dissolved in 500μl DMSO. This stock solution was diluted in eight steps. Table A.1 shows the tested fluorochrome concentration for each phytoplankton species.

From these solutions I added 5μl to a 2ml sample and followed the resulting green fluorescence for about ten minutes. For each species the fluorescence development over time data were extracted like described in section 3.2.5. The resulting initial slope (a

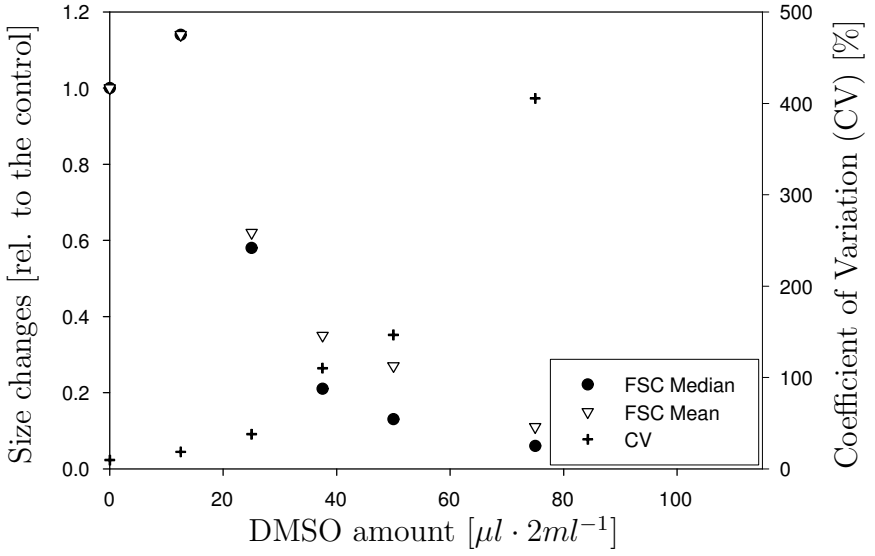

Figure A.1.: Dimethylsulfoxid (DMSO) induced cell damages; cell size (FSC median, FSC mean); cell variability (CV (coeffcient of variation) of FSC median)

measure of the metabolic rate) was plotted against the fluorochrome concentration (see figures A.2 and A.3.

Because I used single species cultures the dotplots consisted of only one region from which the fluorescence development over time data were exported. The regression and the analysis was computed like discribed in section 3.2.5. The resulting initial slope (a measure of the metabolic rate) was plotted against the fluorochrome concentration (see figures A.2 and A.3). These figures represent Michaelis Menten enzyme kinetic curves. From these figures I derived two information. First, I extracted the substrate concentration

Table A.1.: Endconcentration step combinations for the five culture species

Species	Concentration $\left[\frac{\mu g}{ml}\right]$							
	5	2.5	1	0.5	0.2	0.05	0.005	0.0005
Rhodomonas sp.	x	x	x	x	x	x	x	x
Isochrysis sp.				x		x	x	x
Pseudopedinella sp.				x		x	x	x
Synechococcus sp.				x		x	x	x
Teleaulax sp.				x		x	x	x

at which there was no further increase in the turnover rate. For all species this point was reached at an end concentration of about $1\mu g{\cdot}ml^{-1}$. Therefore I decided to use a concentration of $2.5\mu g{\cdot}ml^{-1}$ Celltracker CMFDA for the remaining experiments of the allometric relationship analysis.

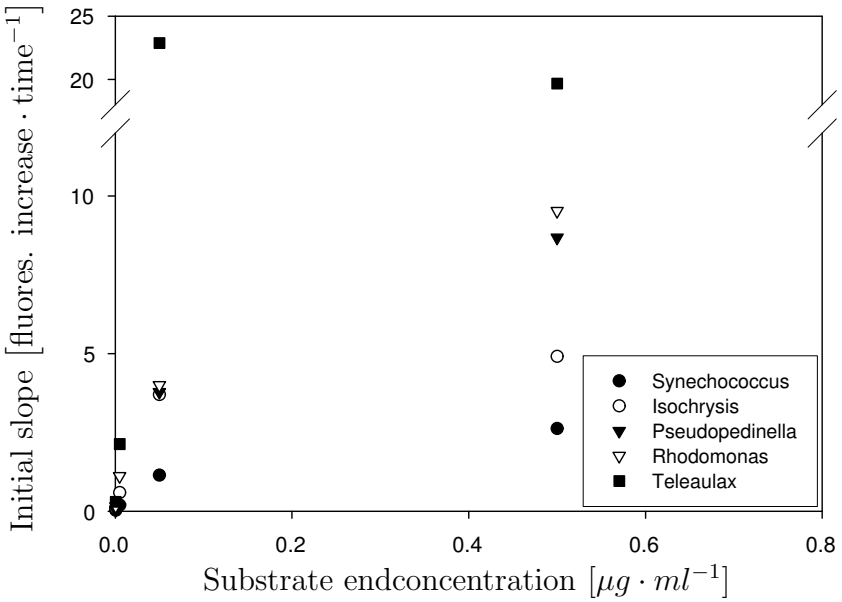

Figure A.2.: Substrate saturation curves for culture phytoplankton

The second parameter that was extracted from the culture experiments was the maximum turnover rate coefficient T_{max}. To extract this information from the data I fitted a Michaelis Menten type regression (see equation 3.6) to the data. Additonally I extracted the size of each species from the flow cytometry data (conversion of the FSC data). The resulting allometric relationship analysis was performed to have a reference besides the natural community data. For the results see section 3.2.5 on page 78.

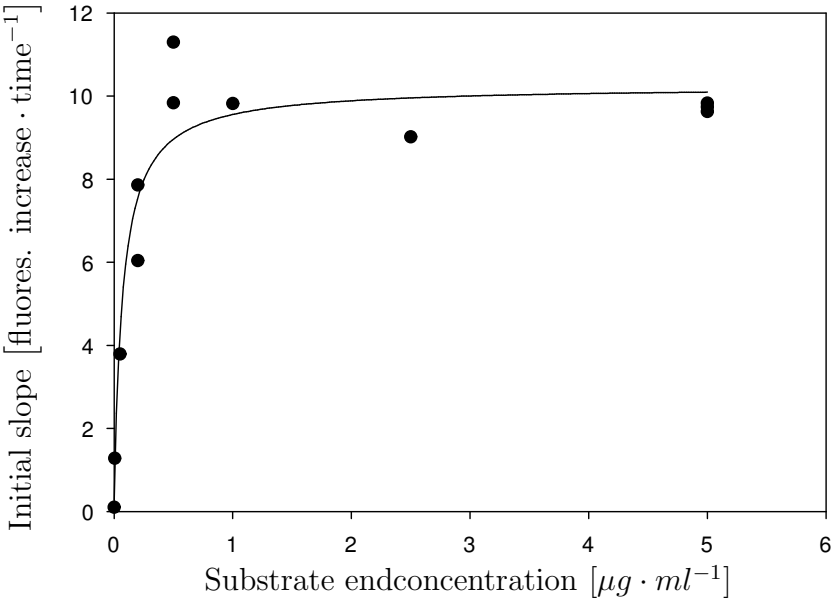

Figure A.3.: Substrate saturation curve for *Rhodomonas* sp. ; data from day seven and ten after the addition of new media to the batchculture

List of abbreviations

log	logarithm base 10
δ^{15}N	ratio of ^{15}N:^{14}N according to standard
POM	Particulate Organic Matter
POC	Particulate Organic Carbon
PON	Particulate Organic Nitrogen
DIN	Dissolved Inorganic Nitrogen
DON	Dissolved Organic Nitrogen
C:N	Carbon to nitrogen ratio
DCM	Deep Chlorophyll Maximum
JGOFS	Joint Global Ocean Flux Study
BATS	Bermuda Atlantic Time series Study

Acknowledgements

I would like to greatly thank Ulrich Sommer and Andreas Oschlies, the supervisors of this thesis, for their scientific and organisational support and particularly for their patience and commitment during the writing process. Many thanks to the administrative personnel of the formerly Institute of Marine Research Kiel, Gerd Kortum, Harald Vogt, Ursula Frank-Scholtz and Barbara Moll for their help with the logistics of the cruises and their help arranging the background logistics of my employment. I am grateful to the board of directors of the institute and to the german JGOFS project of the Bundesministerium für Bildung und Forschung for their employment and their financial support of my thesis. I would like to thank the SeaWiFS Project (Code 970.2) and the Goddard Earth Sciences Data and Information Services Center/Distributed Active Archive Center (Code 902) at the Goddard Space Flight Center, Greenbelt, MD 20771, for the production and distribution of the sea surface chlorophyll data and pictures, respectively. These activities are sponsored by NASA's Earth Science Enterprise. Many thanks to the crew of the research vessel Poseidon for their help and the great logistics in challenging situations. I am grateful to Paul Kähler for the numerous discussions and for arranging the cruises. Many thanks to all members of the cruises for their help. Special thanks to Heiner Dietze, Stefan Siebert, Eike Breitbarth and Kerstin Nachtigall for providing background data and information and for their helpful discussions. I am grateful to Thomas Hansen, Robert Ptacnik, Frank Sommer and Steffi Moorthi for their help and their scientific and nonscientific comments ('darf ich mal den Blutdruck messen'). Many thanks to the members of the department 'Experimental Ecology I' for creating a great working ambience.

Many thanks to all people from my congregation and especially to Oliver Baro, Klaus Beith, Dietmar Bluhm, Horst Dochhan, Christoph Gänzle, Thomas Mayer, Erhard Menzel, Dieter Pietsch, Joachim Ratzko, Andreas Rother, Daniel Rottmann and Stuart Timm for their love and prayer and for listening what God wants to tell me especially during the writing process. Many thanks to my parents for their love, patience and for making my degree possible. Special thanks to my wife Verena for her love, numerous prayer, encouragments, consideration and all the help during the years of my PhD.

Finally I want to thank Jesus Christ for his exceeding love and passion and many thanks to the Holy Spirit for his friendship, power, guidance and encouragements.